UNIVERSIDADE DE LISBOA

FACULDADE DE CIÊNCIAS

DEPARTAMENTO DE FÍSICA

CONTRIBUTION TO FUNDAMENTAL ASPECTS OF BIOPHYSICS, RADIOBIOLOGY, AND MODELING OF CELLULAR RESPONSE TO LOW RADIATION DOSES

ANA LÚCIA VITAL BELCHIOR

DOUTORAMENTO EM ENGENHARIA BIOMÉDICA E BIOFÍSICA

2013

UNIVERSIDADE DE LISBOA
FACULDADE DE CIÊNCIAS
DEPARTAMENTO DE FÍSICA

CONTRIBUTION TO FUNDAMENTAL ASPECTS OF BIOPHYSICS, RADIOBIOLOGY, AND MODELING OF CELLULAR RESPONSE TO LOW RADIATION DOSES

ANA LÚCIA VITAL BELCHIOR

Tese orientada pelo Professor Doutor José Pedro Trancoso Miragaia Vaz e pelo Professor Doutor Pedro Miguel Dinis de Almeida, especialmente elaborada para a obtenção do grau de doutor em Engenharia Biomédica e Biofísica

DOUTORAMENTO EM ENGENHARIA BIOMÉDICA E BIOFÍSICA

2013

ABSTRACT

This thesis aims at studying the direct and bystander effects (observations in which effects of ionizing radiation arise in non-irradiated cells) induced by alpha-particle irradiation, using a Po-210 source, in a human lung adenocarcinoma cells (A549), and at investigating and providing a contribution to the clarification of the protective or potentially detrimental effects of low-dose exposures (< 100 mGy). Besides addressing and analyzing the toxic effects of α-radiation on the A549 cell line the studies undertaken may contribute toward the goal of improving the effectiveness of targeted therapies, with alpha-radiation, such as radioimmunotherapy or Boron Neutron Capture Therapy (BNCT). The work performed consisted, at first, of a dosimetric study in order to determine the average local dose in a cell monolayer, encompassed by experimental and computational studies, followed by a biological study of the direct and bystander effects of α-radiation exposure. The averaged dose rate at the cell monolayer was calculated; through the Linear-Energy-Transfer (LET) value measured using a Passivated Implanted Planar Silicon (PIPS) detector, to be 25 mGy/min. To study the cellular response at low-dose exposures, several studies were conducted using the A549 cell line and a ^{210}Po α-source. Initially, the effects of directly irradiated A549 cells were analyzed through the micronucleus and clonogenic assay. Then, the time and dose dependence of directly and bystander effects in the region of very low doses, was investigated through micronucleus and clonogenic assay. The study encompassed three different cell culture conditions: i) a culture of irradiated cells, ii) a medium transfer culture with non-irradiated cells and iii) a culture with irradiated cells after centrifugation. A dependence on dose and time was observed in both directly irradiated and bystander cells. Taking the advantage of the *in situ* γ-H2AX technique, the way how the *bystander signals* released after low-doses of α-radiation are influenced by the number of irradiated cells was studied. Evidence that bystander signals can easily spread through the culture medium was observed. Moreover, the neighboring of irradiated cells differ with the number of irradiated cells, i.e. with a higher number of cells being irradiated, the cellular damage in bystander areas seems to increase. Finally, the gene expression, in GADD45A, BCL2A1 and PTGS2 genes, was assessed with the qRT-PCR technique. This study revealed that all genes are expressed both in directly irradiated and bystander cells, except PTGS2. Moreover, the differences between gene expression levels in both irradiated and bystander cells, for the same dose value, suggest that the mechanisms underlying the response of both types of cells to radiation are different from each other.

Summarizing, our results emphasize that the risks attributable to low doses encompass a complex cellular response. The observed hyper-radiosensitivity, time and dose-dependence of the bystander effects and gene expression profiles and the easily spread of bystander signals over the cell culture, raise important questions about the potentially detrimental effects resulting from low dose exposures, which are not included in a simple linear extrapolation from higher dose effects.

KEY WORDS: Bystander effects, low-dose risks, high-LET radiation, dose/dosimetry, A549 cells

RESUMO

Esta tese aborda o estudo dos efeitos biológicos, induzidos por exposição a radiação-alfa (α), em células tumorais de pulmão humano (linha celular A549). Foram quantificados os efeitos biológicos em células diretamente irradiadas e em células *bystander* (efeitos biológicos observados em células não expostas diretamente à radiação), com o objetivo de aprofundar o conhecimento acerca dos efeitos possivelmente protetores ou potencialmente prejudiciais de uma exposição a baixas doses de radiação (<100 mGy). O trabalho desenvolvido nesta tese permite, não só, analisar o efeito tóxico induzido pela radiação em células epiteliais (primeira linha de defesa do organismo) como também contribuir para o estudo da utilização de radiação-α em terapias como a radioimunoterapia ou a terapia por captura de neutrões com boro.

Este trabalho consiste, em primeiro lugar, num estudo de dosimetria, com o objetivo de determinar a dose média absorvida por uma monocamada celular, utilizando uma metodologia experimental e uma computacional, seguido de um estudo biológico dos efeitos diretos e dos efeitos *bystander* induzidos na linha celular A549 após exposição a baixas doses de radiação-α. A taxa média de dose medida na monocamada celular, através do valor da transferência linear de energia (LET) medido por um detector PIPS (*Passivated Implanted Planar Silicon*), foi de 25 mGy/min. Com o objetivo de quantificar a resposta celular induzida por baixas doses de radiação foram realizados vários estudos, utilizando a linha celular A549 e uma fonte de radiação-α de ^{210}Po. No primeiro estudo, foi quantificada a lesão e a sobrevivência celular em células diretamente irradiadas, através do ensaio de micronúcleos e clonogénico, respetivamente. Em seguida, investigou-se a dependência, com o tempo de incubação e diferentes valores de dose, da lesão e sobrevivência celular na região de doses muito baixas (<mGy 100). O estudo inclui três culturas celulares distintas: uma cultura de células irradiadas, uma cultura de células não-irradiadas em contacto com o meio proveniente das células irradiadas e uma cultura com células irradiadas após centrifugação. Foi observada uma dependência, nas três culturas descritas, com o tempo e os valores de dose absorvida. Utilizando a vantagem da técnica γ-H2AX que permite uma quantificação da lesão celular *in situ* estudou-se a forma como os *sinais de bystander* se propagam através do meio de cultura influenciados por um diferente número de células irradiadas, após uma exposição a baixas doses de radiação-α. Foram observadas evidências de que os *sinais de bystander* podem facilmente propagar-se no meio de cultura. Além disso, verificou-se igualmente que o número de células irradiadas faz com que a lesão celular induzida nas células *bystander* seja diferente. Finalmente, avaliámos a expressão genética, nos genes GADD45A, BCL2A1 e PTGS2 utilizando a técnica de qRT-PCR. Este estudo revelou que somente os genes GADD45A e BCL2A1 são expressos em células diretamente irradiadas e em células *bystander*. As diferenças observadas na expressão genética nas células diretamente irradiadas e em células *bystander,* para um determinado valor de dose, sugerem diferentes mecanismos na resposta à radiação. Quando a resposta de ambos os genes é estudada em função dos valores de dose, é observada uma expressão não-linear com a dose, em ambas as condições, isto é, em células diretamente irradiadas e em células *bystander*.

Em suma, os resultados apresentados nesta tese evidenciam que os riscos da exposição atribuídos a baixas doses de radiação constituem uma resposta celular complexa. Os fenómenos observados, tais como, a híper-radiosensibilidade, a dependência temporal e com a dose dos efeitos de *bystander* e dos níveis de expressão genética e a facilidade de propagação dos sinais emitidos pelas células irradiadas ao longo da cultura celular, levantam questões importantes acerca dos efeitos potencialmente prejudicais associados à exposição a baixas doses de radiação. Assim, o trabalho descrito nesta tese sugere que os riscos associados a baixas doses de radiação não podem ser simplesmente extrapolados dos observados para a altas doses de radiação.

PALAVRAS CHAVE: Efeitos de *bystander*, risco, baixas doses de radiação, radiação de alto-LET, dosimetria, células A549.

ACKNOWLEDGMENTS

First and foremost I want to thank my supervisors Professor Pedro Vaz and Professor Pedro Almeida. Their criticism joined with the fruitful discussions over the years made this work possible. Also their friendship and complete availability were paramount for the progress of my work. A special word to Professor Pedro Vaz. I work with him, since I'm at ITN, and without any doubts all that I learned with him were pivotal to the progress and enrichment of my scientific outcome. By the way, sorry for my contribution to the increase of your gray hair!

My next acknowledgment goes to Professor Luis Peralta, Professor Sebastião Rodrigues, Doctor Imre Balashazy and Doctor Marta Gromicho without whom this work would not have been possible. Thanks for opening me "your labs", but especially for your friendship and completely availability.

I also want to thank all my colleagues from the UPSR who welcomed me with open arms when, in the middle of my PhD, I moved here. A special thanks goes to Doctor Margarida Goulart for her strong criticism allied with her ability to give me an intensive course from the basics to the ultimate goals of Radiobiology. Thanks MG!

A special word to Doctor Maria Luísa Botelho. When I first came to ITN, at 2005, fortunately I worked, for 4 years, in the Group of radiation technologies: processes and products, headed by Doctor Luisa Botelho. Without any doubts all that I learned with her were pivotal to the progress and enrichment of my scientific outcome and most of all for my multi-disciplinary way to solve any problem, always with the fingers crossed scientifically.

And because, a group of excellence, besides a good leader, is composed of excellent people, my next acknowledgment goes to my *babes* for the eternity, Helena Marcos, Rita Melo, Sandra Cabo Verde and Telma Silva. Thanks for your support, friendship and for transform a bad day onto a beautiful day over the last 8 years and some months.

I also want to thank my colleagues from the Group of Dosimetry and Radiobiology, Ana Catarina Antunes, Catarina Figueira, Filipa Costa, Joana Bento, Mariana Batista, Mónica Mendes, Octávia Monteiro Gil, Pedro Teles, Raul Luis, Salvatore, Silvia Barros, Vanda Martins and Yuriy Romanets, for them support and friendship.

Some of you, Salvatore, Mariana, Mónica and Filipa, who have heard my "corridor "speeches very carefully, thanks for that moments…
A special thanks to Yuriy Romanets. He is a great friend always available to help in everything. Definitively a friend for the eternity…
A special thanks to Pedro Teles. I want to thank him for his friendship, support, but mostly for our discussions… I should say that I prefer those which end on a fight! Thanks for make each day a challenging one… hmm, not so challenging, because, I am graduated in Physics!
The last but not the least, I want to express my gratitude to a special friend, more than a cabinet colleague. During the last years, she accompanied, not only me, but also, for 9 months, Rodrigo with a great, great love and care. Thanks, CF!

I gratefully acknowledge Fundação para a Ciência e Tecnologia for the PhD grant No. SFRH / BD / 42172 / 2007, to ITN and to IBEB for hosting and funding, which make this work possible.

I want to thank all the unconditional support of my all family during this enriching but hard period. A special thanks for my sweet parents who always support me and teach me to fight for my aims. I also want to thank my husband, Pedro, for him unconditionally support, personal and scientific, friendship, care and love during the last years.

To the two most important persons in my life, Francisco and Rodrigo, I just want to thank for making me each day unique and special. I love you guys.

Lisbon, December 2013
Ana Belchior

To Pedro, Francisco and Rodrigo

CONTENTS

ABSTRACT ..... **V**

RESUMO ..... **VII**

ACKNOWLEDGMENTS ..... **IX**

LIST OF ACRONYMS ..... **XIX**

LIST OF FIGURES ..... **XXI**

CHAPTER 1 - INTRODUCTION **1**

1.1 THE MOTIVATION – STUDY OF THE BIOLOGICAL EFFECTS OF IONIZING RADIATION **1**

1.2 THE BYSTANDER EFFECTS **3**

1.2.1 Gap-junction intercelular communication 4

1.2.2 Medium transfer technique 5

1.3 THE STUDIES UNDERTAKEN **6**

1.3.1 Dose and time dependence of targeted and untargeted effects 6

1.3.2 Does the number of irradiated cells affect the spatial distribution of bystander effects? 7

1.3.3 Bystander effects and gene expression 8

1.4 THE CELL LINE **9**

1.5 THE α-RADIATION SOURCE 9

1.6 ORGANIZATION 11

CHAPTER 2 - BIOMARKERS OF RADIATION EXPOSURE AND EFFECTS 13

2.1 INTRODUCTION 13

2.2 BIOMARKER OF RADIATION EXPOSURE 14

2.2.1 The cell cycle 15

2.2.2 DNA damage response 16

2.2.2.1 DNA damage signaling 18

2.2.2.1.1 DNA single- strand breaks (SSBs) 18

2.2.2.1.2 DNA double- strand breaks (DSBs) 19

2.2.2.1.3 DNA alteration of bases 19

2.2.2.1.4 DNA disruption of the sugar-phosphate backbone 20

2.3 BIOMARKERS OF DNA DAMAGE 20

2.3.1 The cytokinesis blocked micronuclei assay 21

2.3.2 The γ-H2AX assay 22

2.3.3 The clonogenic assay 25

2.3.4 Laboratory and experimental procedures 26

2.3.4.1 The cytokinesis blocked micronuclei assay 26

2.3.4.2 The γ-H2AX assay 26

2.3.4.3 The clonogenic assay 27

CHAPTER 3 - INTERACTION OF HEAVY CHARGED PARTICLES WITH MATTER 29

3.1 INTRODUCTION 29

3.2 ENERGY LOSS OF CHARGED PARTICLES 31

3.2.1 Interaction between charged particles and the electrons of the medium 33

3.2.2 Momentum Transfer from the incident charged particle to orbital electrons 34

3.2.2.1 Collisional Stopping Power 35
3.2.3 The Bethe-Bloch formula for stopping power 36
3.2.4 Maximum energy transfer in a single collision 37
3.2.5 Minimum energy transfer in a single collision 38
3.3 SLOWING DOWN OF CHARGED PARTICLES 38
3.3.1 Linear-energy transfer (LET) 39
3.3.2 Range 41
CHAPTER 4 - DOSIMETRY OF AN α-PARTICLE DEVICE FOR IN VITRO CELLS IRRADIATION 43
4.1 INTRODUCTION 43
4.2 MATERIALS & METHODS 44
4.2.1 The α-particle irradiator setup 44
4.2.2 Monte Carlo modeling and simulation of the experimental setup 45
4.2.2.1 SRIM 46
4.2.2.1.1 Structure of the program 46
4.2.2.2 MCNPX 47
4.2.2.2.1 Transport and interaction physics 47
4.2.2.2.1.1 Charged Particle Transport 47
4.2.2.2.1.2 Data Libraries 48
4.2.2.2.2 Structure of the *input file* 48
4.2.2.2.2.1 The definition of the geometry 50
4.2.2.2.2.2 The definition of the materials 50
4.2.2.2.2.3 The Source definition card: SDEF card 50
4.2.2.2.2.4 The tallies 51
4.2.2.2.2.4.1 The *tally* F8 51
4.2.3 Dosimetry experiments 52
4.2.3.1 Alpha-particle energy spectra 52
4.2.3.1.1 Energy to LET conversion 52

4.2.3.1.2Dose calculation....53

4.3 RESULTS....53

4.3.1 The simulation results....53

4.3.1.1 Results from SRIM....53

4.3.1.2 Results from MCNPX....54

4.3.1.2.1 Modeling and simulation of the response of the Sil(Li) detector....54

4.3.1.2.2 Modeling and simulation of the experimental setup....56

4.3.2 The dosimetry measurements....57

4.3.2.1 Energy and flux measurements of the ^{210}Po source....57

4.3.2.2 Alpha-particle energy and LET spectra at the cell irradiation position....58

4.3.2.3 Dose calculation....61

4.4 DISCUSSION....61

CHAPTER 5 - DOSE AND TIME DEPENDENCE OF TARGETED AND UNTARGETED EFFECTS AFTER A-PARTICLE IRRADIATION OF HUMAN LUNG CANCER CELLS....63

5.1 INTRODUCTION....63

5.2 MATERIALS & METHODS....65

5.2.1 Cells directly irradiated....65

5.2.2 Medium transfer study....65

5.2.3 Statistical analysis....67

5.3 RESULTS & DISCUSSION....67

5.3.1 Radiation-induced cellular effects immediately after irradiation....67

5.3.2 Radiation and bystander-induced cellular damage (2 and 6 days after irradiation)....69

5.3.2.1 Survival Fraction....69

5.3.2.2 Micronuclei frequency – Early cellular damage....73

5.3.2.3 Micronuclei frequency – Delayed cellular damage....74

5.3.2.4 Micronuclei distribution 75

5.4 CONCLUSIONS 77

CHAPTER 6 - INFLUENCE OF THE NUMBER OF IRRADIATED CELLS IN THE SPATIAL DISTRIBUTION OF BYSTANDER EFFECTS 81

6.1 INTRODUCTION 81

6.2 MATERIALS & METHODS 82

6.2.1 Cell culture and irradiation 82

6.2.2 Immunofluorescence staining 83

6.2.3 Treatment with Lindane or dimethyl sulfoxide 83

6.2.4 Statistical analysis 84

6.3 RESULTS 84

6.3.1 Induction of DSB in irradiated cells 84

6.3.2 Induction of DSB in bystander cells 87

6.3.2.1 Bystander I 89

6.3.2.1.1 Role of the gap-junctional intercellular communication (GJIC) 91

6.3.2.2 Bystander II 93

6.4 CONCLUSIONS 96

CHAPTER 7 - GENE-EXPRESSION IN DIRECTLY IRRADIATED AND BYSTANDER A549 CELLS AFTER EXPOSURE TO LOW DOSES OF α-RADIATION 99

7.1 INTRODUCTION 99

7.1.1 The RNA isolation and cDNA synthesis 103

7.1.2 Principle of the quantitative real-time PCR 105

7.2 MATERIALS & METHODS 108

7.2.1 Cell culture and exposure 108

7.2.2 Medium transfer technique....108
7.2.3 RNA isolation and cDNA generation....108
7.2.4 Quantitative Real-Time PCR (qRT-PCR)....110
7.2.5 Statistical Analysis....110

7.3 RESULTS....110

7.3.1 Directly irradiated cells....111
7.3.2 Bystander cells....116
7.3.3 Directly irradiated and Bystander cells....121
7.3.3.1 GADD45A gene profile expression....121
7.3.3.2 BCL2A1 gene profile expression....122

7.4 DISCUSSION AND CONCLUSIONS....124

CHAPTER 8 - CONCLUSIONS AND FUTURE WORK....127

8.1 CONCLUSIONS....127

8.2 FUTURE WORK....131

BIBIOLOGRAPHY....133

RESEARCH PROTOCOLS....145

PROTOCOL I - CYTOKINESIS-BLOCKED MICRONUCLEI ASSAY....147

PROTOCOL II – γ – H2AX ASSAY....149

PROTOCOL III – CLONOGENIC ASSAY....151

PROTOCOL IV - RNA ISOLATION....153

PROTOCOL V – cDNA SYNTHESIS....155

LIST OF ACRONYMS

BSA - Bovine Serum Albumin

CBMA – Cytokinesis Blocked Micronuclei Assay

cDNA – Complementary DeoxyriboNucleic Acid

DDR – DNA Damage Response

DMEM – Dulbecco's Modified Eagle Medium

DNA – DeoxyriboNucleic Acid

DSB – Double Strand Break

FBS – Fetal Bovine Serum

GJIC - Gap Junction-mediated Intercellular Communication

HLEG – High Level and Expert Group

IR – Ionizing Radiation

LET – Linear Energy Transfer

LNT – Linear no-Threshold model

MCNPX – Monte Carlo N-Particle eXtended (simulation code)

NF-kB – Nuclear Factor-kappa B

PBS – Phosphate-Buffered Saline

PCR – Polymerase Chain Reaction

PE - Plating Efficiency

RBE – Relative Biological Effectiveness

RIBE – Radiation-induced bystander effects

RNA – RiboNucleic Acid

ROS - Reactive Oxygen Species

RT-PCR – Real-Time Polymerase Chain Reaction

SF – Survival Fraction

SRIM – The Stopping and Range of Ions in Matter (simulation code)

SSB – Single Strand Break

TRIM – TRansport of Ions in Matter (simulation code)

LIST OF FIGURES

Figure 1: Indicative research directions to address issues on the shape of dose response relationship and tissue sensitivities for cancer [Report of HLEG, 2009]. 2

Figure 2: Gap junctions are hexameric hemichannels of connexin proteins that are inserted into the plasma membrane and allow for direct exchange of cytosolic contents among adjacent cells. [Extracted from Trauner and Jansen, 2003] 5

Figure 3: The medium-transfer technique to study the bystander effects. First, the cells are irradiated, then the culture medium is removed and filtered and finally is added to a non-irradiated culture. 5

Figure 4: Track length of alpha-particles, beta-particles, and Auger electrons relative to the cell diameter. *Extracted from* [Pouget et al., 2011]. 10

Figure 5: The DNA molecule. *Adapted from* McGrawHill education website (https://catalogs.mhhe.com/mhhe/home.do) 14

Figure 6: Phases of the cell cycle 16

Figure 7: A view of the general outline of the DNA damage response pathway. DSBs are recognized by the MRN complex [Petrini and Stracker, 2003]. MRN recruits proteins of the phosphatidylinositol 3-kinase like preotein kinase (PIKKs) family – ATM, ATR that encode DSB-inducible protein kinases. The consequent cellular responses include cell cycle arrest, apoptosis and DSB repair. [Nagaria *et al.*, 2013]. 17

Figure 8: Proposed model for an IR – induced signaling pathway 18

Figure 9: Induction of DSBs by IR. At the end of radiation tracks, the energetic electrons deposit their energy raising multiple ionizations (clustering), which in turn induce complex DNA damage. The principal concern of ionization cluster is that IR interacts with the molecule of DNA at several locations, within the cell area. This interaction leads to i)

promptly DSBs when two SSB occur in DNA, ii) SSB after sugar lesions within clustered-damaged sites after chemical processing and iii) SSB after BER by leading breaks in DNA after replication. *Figure extracted* from Mladenov *et al.*, 2011. 19

Figure 10: Schematic view of the micronucleus formation process. The upper process describes the normal cellular division, in which a cell divides into two separate daughter cells, each containing one nucleus. By adding cytochalasin B, an inhibitor of actins, the cell is blocked from the cell division after the completion of nuclear division. The resulting cell called a binucleated (BN) cell contains two nucleus. When a fragment of DNA is broken due to damage, one or more micronuclei (MN) appear within the binucleated cell. 21

Figure 11: Images obtained during the MN quantification performed in this work. (a) binucleated cell and (b) a binucleated cell with 2 micronuclei.....22

Figure 12: H2AX in the context of chromatin. (A) Organization of DNA in chromatin. (B) Schematic representation of the core histones (C) A model of the nucleosome core particle showing DNA interactions with core histones. The DNA entry and exit points are localized at the H2A/H2B dimer. [Extracted from Kinner *et al.*, 2008] 23

Figure 13: γ-H2AX foci formation. Immediately after a DSB, the phosphorylated form of H2AX is formed γ-H2AX, being accumulated at sites of DNA DSB. If the DNA repair machinery is no efficient, the DNA does not repair and an accumulation of foci is observed in the nuclei. Figure adapted from: *Efficient DNA Repair: A Cell's Fountain of Youth?*.....24

Figure 14: Representative image of DSBs positive cells obtained in this work; non-irradiated (A) and irradiated cells with 100 mGy (B). 25

Figure 15: Clonogenic assay for cells growing in monolayer. Cells are trypsinized, counted, and diluted. The colonies are fixed and stained when they reach at least 50 cells each.....25

Figure 16: Cultures of colonies obtained during this work with clonogenic assay; (a) 0 mGy, (b) 5 mGy and (c) 100 mGy. 26

Figure 17: Direct and Indirect effects of IR in DNA. The creation of a OH^- ion is depicted, as an example of indirect effects.....30

Figure 18: Sequence of events after radiation energy absorption. 30

Figure 19: Ionization event. If the energy transferred to an atom, due to coulomb forces exerted when a charged particle passes near the electric field generated by the atom's electrons and protons, exceeds the electron's energy binding, the result is an ion-pair (i.e. an ejected electron and a positively charged atom). If the energy of the ejected electron is sufficient enough, a secondary electron, named delta ray, could be produced. Thus, further ionizations are produced by secondary ionizations events. Figure extracted from [Bushberg *et al.*, 2012] 32

Figure 20: Excitation event (left), an electron (represented in green) is transferred to a higher energy level. De-excitation event (right), occurs when the electron returns to a lower energy level emitting either electromagnetic radiation or an Auger electron. Figure extracted from [Bushberg *et al.*, 2012]. 33

Figure 21: Parameters for a charged particle (mass M, charge ze and velocity V) collision with an electron (mass m and charge –e) where *a* is the classical radius of the atom and *b* is the classical impact parameter. *Adapted from* Turner, 2007 33

Figure 22: Annular cylinder of length dx. The cylinder's axis is aligned with the trajectory of the heavy charged particle. Extracted from [Turner *et al.*, 2007]. 35

Figure 23: Variation of relative biologic effectiveness (RBE) with linear energy transfer (LET) in tissue. It can be inferred that high-LET particles, such as α-particles, protons and neutrons, cause a higher damage to the crossing tissues. 40

Figure 24: Patterns of DNA damage caused by different types of radiation. a) Low-LET radiation produces sparse ionizations and excitations within DNA along a track, resulting in individual DNA lesions that are easily repairable. b) Cascades of Auger electrons (with intermediate LET). c) α-particles with high LET produce densely localized ionizations and excitations along a linear track, resulting in locally, and multiple damaged sites that are poorly repairable. Extracted from [Pouget *et al.*, 2011] 41

Figure 25: Energy loss of an α-particle with 4 MeV of energy reaching a layer of air. Results obtained with SRIM, 2008. 41

Figure 26: The range of 3 and 6 MeV α-particles in air. Doubling the energy of the incident particles allow the particles to travel a higher distance in air. In this simulation, the range

differs by a factor of 3. Results obtained using the state-of-the-art computer program SRIM. 42

Figure 27: Irradiation device (up), cross – section of the exposure device (down). 45

Figure 28: Input file structure 48

Figure 29: Example of a particle´s trajectory in a cell. In this, the particle experiences a set of interactions, resulting in several tracks, before leaving the cell. The track length estimator tally scores a different value of energy for each track. The resulting energy, using the pulse height tally, is the accounting of all energies (entering and leaving the cells) involved, i.e., in this example, the resulting energy is equal to $E_{in1} + E_{in2} – E_{out1}$.At the end of history, the account in each cell is dividing by the source weight determining in which energy bin the score is put in. *Adapted from* [RSICC, 2006]. 52

Figure 30: Study of the LET as a function of incidence angles of the alpha particles in the cell monolayer. Note that, 0° of incidence means the beam is perpendicular to the target. ...54

Figure 31: Schematic representation of the configuration used to model the response of the Si(Li) detector with MCNPX. All the components are cylindrical in shape. Dimensions are not to scale. 55

Figure 32: Comparison between the measured alpha-particles energy and the MCNPX simulation. 55

Figure 33: Results obtained by MCNPX for the dependence of LET values with the water monolayer depth.....56

Figure 34: Energy spectra of ^{232}U and ^{210}Po. The dash curve corresponds to the energy peaks used to perform the calibration. The peak energies used in the calibration are the following: ^{212}Po– 8.785 MeV, ^{216}Po - 6.777 MeV, ^{220}Rn - 6.287 MeV and ^{224}Ra – 5.684 MeV 58

Figure 35 – Energy spectrum at cell position.....59

Figure 36: Schematic view of the parameters included on the input file.....60

Figure 37: LET spectrum at cell position 60

Figure 38: Medium transfer study for 1 Gy of exposure; the same methodology was used for the others values of dose. In group I irradiated cells were cultured with fresh medium after

exposure to the aforementioned radiation doses. In group II, non-irradiated cells received irradiated medium. Finally, group III corresponds to irradiated cells cultured after centrifugation with supplemented fresh medium. 66

Figure 39: Dose response curve. Number of MN in 1000 BN cells (mean ± SEM) of 3 independent experiments. By analyzing the results, it can be summed up that there is a significant increase of MN per 1000 BN cells when the result of each dose is compared with the control (non-irradiated cells). This indicates that the cellular damage increase with dose values, as each MN represents a specific lesion. 68

Figure 40: MN distribution in BN cells. 1 MN, 2 MN, 3 MN and >3 MN means that BN cells contain one, two, three and more than three MN. The obtained results show that genetic lesion results essentially in BN cells with only one MN. As dose values increase, the frequency of 2 MN becomes more evident. By the appearance of more than one MN, one can predict that higher doses are more damaged to the cell. 68

Figure 41: Survival fraction (SF), obtained by clonogenic assay, for each group, i.e. I, II and III. The results represent the mean of three independent experiments ± standard error of the mean (SEM). Note: The lines are purely eye guided. 71

Figure 42: Survival fraction (SF), obtained by clonogenic assay, at day 2 (a) and at day 6 (b). The results represent the mean of three independent experiments ± standard error of the mean (SEM). At both time points and for all groups, survival is significantly reduced compared to its own controls. The only exception is observed for Group III at day 2, at 10 mGy, being the survival fraction similar to unirradiated control ($p=0.84$). In the media transfer experiment, group II a lower survival fraction is observed at 10 mGy, which corroborates with the HRS observed, by means of MN assay, at this dose value. Note: The lines are purely eye guided. 72

Figure 43: Number of MN per 1000 BN cells for each value of dose; 5, 10 50, 100, 500 and 1000 mGy at day 2 after irradiation for groups I to III. The non-irradiated cell cultures are marked as 0 mGy. Data represent means of 3 independent experiments, ± SEM. Note: the lines are purely eye guided. 73

Figure 44: Number of MN, 6 days after irradiation for groups I to III, per 1000 BN cells for each value of dose, i.e., 5, 10, 50, 100, 500 and 1000 mGy (a). (b) refers to a detailed view for

lower doses. The non-irradiated cell cultures are marked as 0 mGy. Data represent means of 3 independent experiments, ± SEM. In all groups, radiation significantly increased the number of MN when compared with its own controls ($p<0.05$), with exception in group III for 5 mGy where the increasing of MN was almost the same ($p=0.68$). Similarly to earlier effects, the trend to reach a plateau after 10 mGy for group II is observed. Note: the lines are purely eye guided. 74

Figure 45: Schematic view of the culture dish for irradiation. The dimensions are in cm and not at scale. The cell dish has 3.5 cm of diameter and depending on the experiment (A) or (B); approximately, 98 or 92% of this area was shielded by aluminum foils, respectively. The unshielded area was exposed to 5, 10, 50 and 100 mGy of α–particles emitted by a ^{210}Po source. Immediately after-irradiation the γ-H2AX assay was performed. 83

Figure 46: Induction of DSBs in irradiated cells, by means of foci number, after 5, 10, 50 and 100 mGy of α-radiation. Data were collected from three independent experiments. Error bars represents the SEM. The statistical significance between each dose value, for both irradiated area A and B, and matched controls, i.e. 0 mGy, is $p<0.005$. 85

Figure 47: Distribution of foci number per cell for all dose values; left and right panels show the distribution of foci number in the irradiated areas – A and B, respectively. The histograms show cells presenting 0 to 45 γ-H2AX foci per nucleus. Data were collected from three independent experiments. Different scales were used for a better visualization. 86

Figure 48: Average number of foci per cell in the experiment A (up) and B (down) with a lower and a higher number of irradiated cells, respectively. Irradiated area – A and irradiated area B refers to the irradiated areas, Bystander I – A and Bystander I - B, the closest to the irradiated cells, refers to the first non-irradiated area and bystander II – A and Bystander II - B to the second non-irradiated area. Data were collected from three independent experiments. Error bars represents the SEM. Note: The lines are purely to guide the eye. ...87

Figure 49: Induction of DSBs in the "Bbystander I-A" and "Bystander I-B" areas corresponding to non-irradiated cells in the areas nearest to the irradiated cells, in case of a lower and a higher number of irradiated cells, respectively. Data were collected from three independent experiments. Error bars represents the SEM. * $p< 0.005$ represents the statistically significance between each group and its own controls. 89

Figure 50: Distribution of foci number per cell for all dose values; left and right panels show the distribution of foci number in the Bystander I areas – A and B, respectively. The histograms show cells presenting 0 to 45 γ-H2AX foci per nucleus. Data were collected from three independent experiments. Different scales were used for a better visualization. 90

Figure 51: Average number of foci per cell of bystander cells with or without treatment with Lindane or DMSO. The data are plotted with the averaged values ± SEM of three independent experiments. * $p< 0.005$, ** $p<0.02$, *** $p<0.01$, $^{+}$ $p<0.1$ and $^{++}$ $p<0.05$ represents the statistically significance between each group and its own controls The statistical analysis, per dose value, of the data obtained for the three independent treatments was performed by ANOVA analysis. 92

Figure 52: Induction of DSBs in the "Bystander II-A" and "Bystander II-B" areas, corresponding to non-irradiated cells in the areas more distant of the irradiated cells, in case of a lower (experiment A) and a higher number (experiment B) of irradiated cells, respectively. Data were collected from three independent experiments. Error bars represents the SEM and * $p< 0.005$. 93

Figure 53: Distribution of foci number per cell for all dose values; left and right panels show the distribution of foci number in the Bystander II areas – A and B, respectively. The histograms show cells presenting 0 to 45 γ-H2AX foci per nucleus. Data were collected from three independent experiments. Different scales were used for a better visualization. 94

Figure 54: Induction of DSBs in "Bystander II – A" and "Bystander III – B" areas. "Bystander II – A" and "Bystander III – B" refers to non-irradiated cells, corresponding to a lower and a higher number of irradiated cells, respectively, but at the same distance from the irradiated cells. Data were collected from three independent experiments. Error bars represents the SEM and * $p< 0.005$. 95

Figure 55: Cross-talking between apoptosis and NF-kB signaling. Figure extracted from Sun and Karin [Sun and Karin, 2008]. 101

Figure 56: The intrinsic and extrinsic pathways in apoptosis. Apoptosis can be induced by cell surface receptors, extrinsic pathway, such as FAS and TNFR1 and by intrinsic pathway due to the exposure to various stress stimuli. Stress stimuli that induce apoptosis include

DNA damage by IR, aberrant signals from cell surface receptors and production of ROS, among others. Figure extracted from Youle [Youle *et al.*, 2008].....102

Figure 57: A schematic view of cDNA synthesis. (a) RNA template. Before the synthesis of cDNA, total or mRNA must be extracted from the biological sample. (b) To generate cDNA molecule by an enzyme reverse transcriptase (RT), a primer must be annealed to the template of RNA. This is the starting point for DNA synthesis. (c) The action of the enzyme RT beginning at the primer annealing site. (d) the first cDNA strand created. (e) Removal of RNA by RNAse H. After this step, the single-stranded cDNA is ready to be used for amplification by PCR. Figure adapted from Kendall and Riley [Kendall and Riley, 2000]...104

Figure 58: The 3 steps of PCR; denaturation, annealing and extension.....106

Figure 59: Model of a single-sample amplification plot, showing parameters used to a quantitative analysis.. Normalized reporter (Rn) is the ratio of the fluorescence emitted by the reporter dye and the passive reference dye. ΔRn is calculated by subtracting the baseline line value to the Rn values. All PCR measurements should have a No Template Control (NTC), without cDNA template, in order to verify the amplification quality. Figure extracted from: http://www.ncbi.nlm.nih.gov/projects/genome/probe/doc/TechQPCR.shtml.....107

Figure 60: Medium transfer study for an exposure of 100 mGy; the same methodology was used for the others dose values. In group I irradiated cells were cultured with fresh medium after exposure to the aforementioned radiation doses. In group II, non-irradiated cells received irradiated medium. 108

Figure 61: Illustration of the cDNA protocol.....109

Figure 62: Relative gene expression levels after direct radiation. Quantitative real-time RT-PCR was used to quantify the expression of the GADD45A and BCL2A1 genes 4h after irradiation of A549 cells. Gene expression was normalized to GAPDH and is relative to the expression of 0 mGy. The presented data corresponds to the mean and the standard deviation of two independent experiences. The *p*-values represent the statistical analysis between each dose values and the control, i.e. 0 mGy. 115

Figure 63: Relative gene expression levels for bystander cells. Quantitative real-time RT-PCR was used to quantify the expression of GADD45A and BCL2A1 genes 4h after irradiation of A549 cells. Gene expression was normalized to GAPDH and is relative to the expression of

0 mGy. The presented data is the mean and the standard deviation of two independent experiences. The *p*-values represent the statistical analysis between each dose values and the control, i.e. 0 mGy. 120

Figure 64: Relative gene expression of GADD45A in directly irradiated and bystander cells, 4h after irradiation of A549 cells for different dose values. The gene expression was normalized to GAPDH and is relative to the expression of 0 mGy. The data displayed corresponds to the mean and the standard deviation of two independent experiences.....122

Figure 65: Relative gene expression of BCL2A1 in directly irradiated and bystander cells, 4h after irradiation of A549 cells. The gene expression was normalized to GAPDH and is relative to the expression of 0 mGy. The data displayed corresponds to the mean and the standard deviation of two independent experiences 123

Figure 66: Different effects that can be observable when a single cell is irradiated. 128

LIST OF TABLES

Table 1: DNA structural modifications caused by a genotoxic agent (physical or chemical). 15

Table 2 – Type of *tallies* that can be used in MCNPX. 51

Table 3: Values of SF, obtained by clonogenic assay, at day 2 after irradiation. The results represent the mean of three independent experiments ± standard error of the mean (SEM). 70

Table 4: Values of SF, obtained by clonogenic assay, at day 6 after irradiation. The results represent the mean of three independent experiments ± standard error of the mean (SEM). 70

Table 5: The distribution and yield of MN in the aforementioned groups and dose values, 2 days after irradiation 75

Table 6: The distribution and yield of MN in the aforementioned groups and dose values, 6 days after irradiation. 76

Table 7: PCR reaction volume. 110

Table 8: Ct values for the 1st independent experience. Using the GAPDH as the endogenous control, the $2^{-\delta Ct}$ values were obtained for both genes, GADD45A and BCL2A1, for different dose values. 112

Table 9: Ct values for the 2nd independent experience. Using the GAPDH as the endogenous control, the $2^{-\delta Ct}$ values were obtained for both genes, GADD45A and BCL2A1, for different dose values. 113

Table 10: Ct values for the 3rd independent experience. Using the GAPDH as the endogenous control, the $2^{-\delta Ct}$ values were obtained for both genes, GADD45A and BCL2A1, for different dose values. 114

Table 11: Values of $2^{-\delta Ct}$ for both genes, considered for further studies, after take out the outliers.....115

Table 12: Ct values for the 1st independent experience. Using the GAPDH as the endogenous control, the $2^{-\delta Ct}$ values were obtained for both genes, GADD45A and BCL2A1, for different dose values, for bystander cells.....117

Table 13: : Ct values for the 2nd independent experience. Using the GAPDH as the endogenous control, the $2^{-\Delta\Delta Ct}$ values were obtained to both genes, GADD45A and BCL2A1, at different dose values, for bystander cells.....118

Table 14: Ct values for the 3rd independent experience. Using the GAPDH as the endogenous control, the $2^{-\delta Ct}$ values were obtained for both genes, GADD45A and BCL2A1, for different dose values, for bystander cells.....119

Table 15: Values of $2^{-\delta Ct}$ for both genes, considered for further studies, after take out the outliers.....120

Table 16: Required volume of Lysis buffer (Extracted from the PureLink® RNA Mini Kit manual).....153

Table 17: Volume required per reaction of each components. * Quantity Sufficient.....155

CHAPTER 1

INTRODUCTION

1.1 The motivation – study of the biological effects of ionizing radiation

Understanding the mechanisms of interaction of ionizing radiation (IR) with biological systems has been driven by two main factors: the need to assess the risks and detrimental effects for human health from accidental, anthropogenic (in medical and industrial, lifestyle, etc. applications) or natural exposures to IR and the IR´s role as a carcinogen. No one questions the lethality of excessive exposure to ionizing radiation or the carcinogenic effects of high doses of radiation, but a detailed and accurate understanding of the mechanisms explaining the way how these effects are mediated remains unclear. Of particular relevance, in low doses radiation exposures the understandings of the mechanisms that lead to biological effects are not clearly understood [Little, 2010]. Recently, an European High Level and Expert Group (HLEG) [Report of HLEG, 2009] was established in order to define research topics and programs paving the way for a more accurate risk assessment in low dose radiation exposures. In this report, it can be read that, during the last decades, a decline in the available expertise on radiobiology and radiotoxicology was observed [Report of HLEG, 2009]. The major concerns to this group are the considerable uncertainties and divergent views about the health effects arising from low dose radiation exposures.

The complexity of the triggered biological responses after low dose exposures shifts the prediction of radiation risk assessment models to a long-term goal. **Figure 1** shows the

strategy of the HLEG to assess the shape of dose-response relationships and tissue sensitivity in the case of cancer.

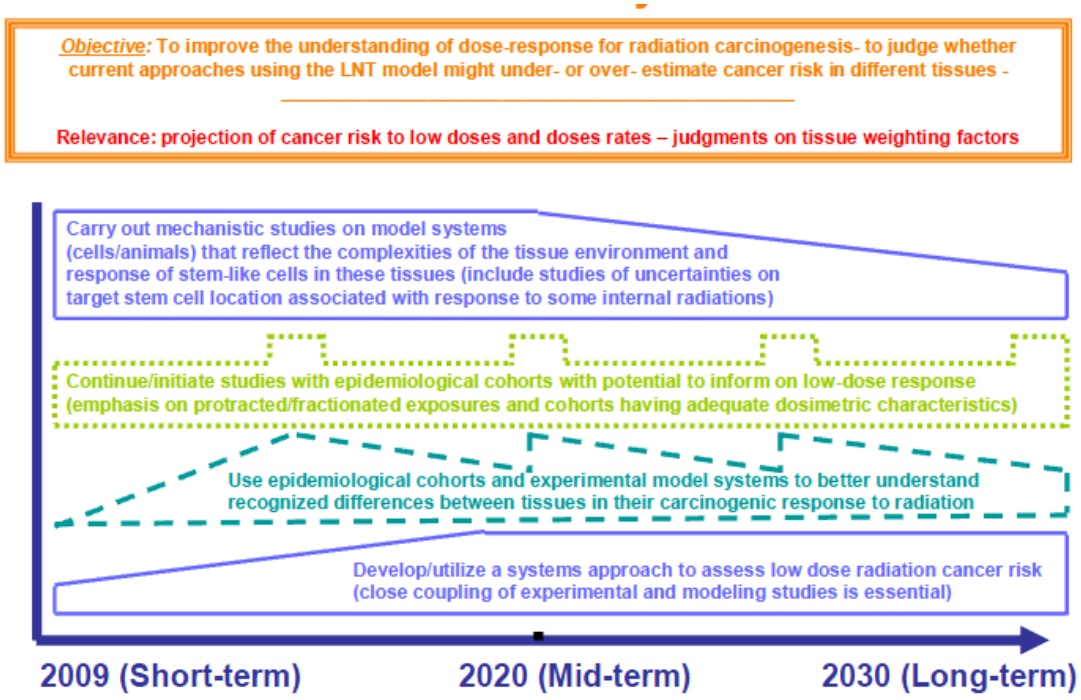

Figure 1: Indicative research directions to address issues on the shape of dose response relationship and tissue sensitivities for cancer [Report of HLEG, 2009].

Besides the influence of the tissue variability on the dose response, other issues are addressed in the report namely the individual variability and sensitivity (as a function of age, sex, gender, genetic factors, etc.), the radiation quality, internal exposures, and non-cancer effects.

One of the most common approaches to model risk versus dose is the linear no-threshold (LNT) model [Tubiana *et al.*, 2006; Brenner and Sachs 2010]. Its epidemiological basis makes it the current approach for the establishment of an "anchor point", which is subsequently used for linear extrapolation to the low dose range. However, the epidemiological data, mainly from accidental exposures with doses in the range of 0.2 to 2.5 Sv, are much higher when compared with the worldwide annual exposures to natural radiation sources estimated in the range of 1 to 10 mSv/year, with 2.4 mSv being at present the estimated world average dose [UNSCEAR, 2000]. For this reason it is currently accepted that this LNT model must be revised, due to the uncertainty on the shape of the risk versus dose- relationship (derived from epidemiological studies) below 100 mGy and on the cellular mechanisms that determine the response, including the role of bystander effects and radiation sensitivity.

Bearing in mind all the uncertainties in the low dose range, considering the cellular response, and assuming that these dose values could have a pivotal impact in the human health, **the main focus of the work developed in this thesis was devoted to the study of the direct and bystander effects induced by absorbed doses lower than 100 mGy**.

The **radiation-induced bystander effect** (RIBE) has been described as an occurrence of a biological effect in non-irradiated cells as a result of exposure of other cells to IR [Shao *et al.*, 2004, Suzuki *et al.*, 2004, Sawant *et al.*, 2001]. The major consequences of these effects on the evaluation of low dose risks are addressed to some questions, for which current scientific knowledge has no answers: i) what is the nature of the bystander signals emitted to unexposed cells, ii) could the dose absorbed by tissues be higher than we thought? iii) is there a threshold for these bystander effects to occur? and iv) could these bystander effects be manipulated to increase the death of tumor cells?.

1.2 The bystander effects

The major adverse consequences of radiation exposures are attributed to DNA damage in irradiated cells that have not been correctly restored by metabolic repair processes. However, this has been challenged by observations in which effects of ionizing radiation arise in non-irradiated cells [Shao *et al.*, 2004, Suzuki *et al.*, 2004, Sawant *et al.*, 2001].
These, so called, bystander effects are demonstrated by cell culture medium transfer [Grifalconi *et al.*, 2007, Mothersill *et al.*, 2001 and Mothersill *et al.*, 1998] or in cells that have communicated with irradiated cells [Azzam *et al.*, 2003 and Hu *et al.*, 2006]. Although, several studies show the existence of RIBE the understanding of the mechanisms that lead to these biological effects are not yet understood. It is most likely that multiple mechanisms are involved in bystander effects. The majority of the published studies focused in *in vitro* studies concentrated on the factors released by the irradiated cells that will trigger a cellular damage in the recipient cells. There are few published studies *in vivo* bystander effects but the complexity of the chain of events is such that it is very difficult to point a cause-effect relationship. So, it is easier to design an experiment with cells *in vitro* and conclude about the obtained results more accurately. However, this is a limitation, since it does not express the whole body response but only an isolated response of a specific cell line to a specific dose value. It must be recognized however that the results *in vitro* are the precursory results for possible effects that could occur *in vivo*.

The major adverse consequence observed in non-irradiated cells, bystander cells, is attributed to the oxidative stress effect induced by reactive oxygen species (ROS) [Azzam *et al.*, 2003]. Additionally, some studies showed that irradiated cells may release soluble factors which are toxic to non-irradiated cells into the medium [Yang *et al.*, 2005]. Differences in DNA damage quantification, among various cell types, can be explained by the different metabolic repair processes, suggesting a fundamental role of the DNA in inducing bystander effects [Nagasawa *et al.*, 2003]. Grifalconi *et al.* (2007) demonstrated that TK6 cells, when exposed to

0.5 – 1 Gy of γ-rays, release into the cell culture medium soluble molecules which maintain cell mortality high in bystander cells for at least 48h. Other study performed by Bowler *et al.* (2006) showed the appearance of delayed aberrations (genomic instability) induced by medium transfer technique in bystander culture, for irradiation doses ranging from 0.1 to 2 Gy. Evidences of these effects in different cell lines have been reported within a few hours post-irradiation as increasing micronuclei formation [Saho *et al.*, 2004, and Belchior *et al.*, 2011] and chromatid aberrations [Suzuki *et al.*, 2004] and at delayed times after irradiation as increased mutation frequency [Nagasawa *et al.*, 1999 and Dahle *et al.*, 2005], delayed reproductive cell death, or chromosomal instability [Hall *et al.*, 2003].

Summarizing, the published studies about bystander effects lead us to verify that;

- the bystander effect is dependent on the cell line used,
- the bystander effect is quantified using the same biomarkers of directly irradiated cells,
- the bystander effects could lead to cell death, implying a severe damage to the cell,
- the bystander effects are more relevant at low doses and have the highest expression at 0.5 Gy being insignificant for high dose values,
- the bystander effects were observed even if only a single cell was irradiated (using a microbeam),
- the bystander effects are observable by cellular medium transfer to non-irradiated cells or by gap-junctional intercellular communication and finally,
- the bystander signals appear to be a consequence of the reactive oxygen species released in the culture medium and of growth factors leading to different proteins regulation.

1.2.1 Gap-junction intercelular communication

Cells can communicate with each other through the gap junction-mediated intercellular communication (GJIC) (see
Figure 2). Connexin proteins, which make up the gap junctions, pass ions and small metabolites between cells that are in contact (like confluent cells). The role of GJIC was first reported by Azzam et al. [Azzam *et al.*, 1998] who investigated the response of confluent cultures of primary human diploid fibroblast exposed to very low fluences of alpha-particles. They observed an increase in the protein levels p53 and p21, a protein involved in cell cycle checkpoint signaling.

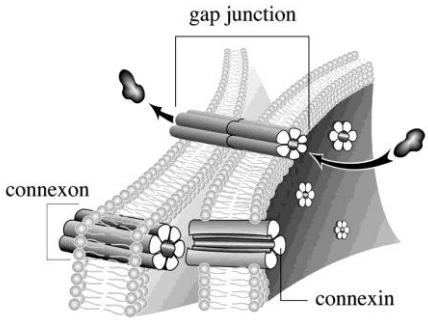

Figure 2: Gap junctions are hexameric hemichannels of connexin proteins that are inserted into the plasma membrane and allow for direct exchange of cytosolic contents among adjacent cells. [Extracted from Trauner and Jansen, 2003]

In this thesis, the role of GJIC was studied in the areas closest to irradiation cells, described in chapter 6.

1.2.2 Medium transfer technique

In addition to intercellular communication, bystander effects can be observed by the medium-transfer technique. When using this technique, cells are irradiated, and the medium from irradiated cells is removed and filtered, being afterwards added to a culture of non-irradiated cells, and finally the bystander effects are assayed (see Figure 3).

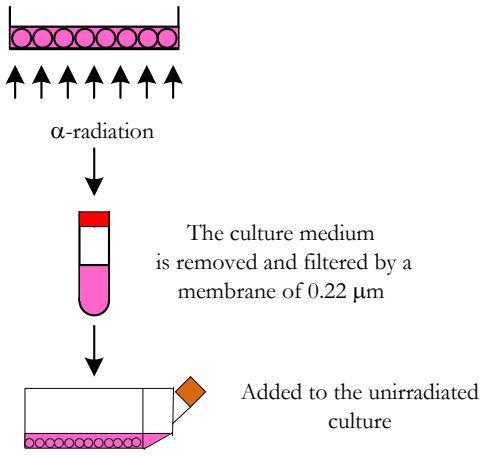

Figure 3: The medium-transfer technique to study the bystander effects. First, the cells are irradiated, then the culture medium is removed and filtered and finally is added to a non-irradiated culture.

1.3 The studies undertaken

The following sub-sections describe the proposed radiobiology studies in order to contribute with some additional data for the better understanding of the bystander effects induced by low-dose values. However, although not described in the sequence, an extensive dosimetric study was performed in order to evaluate the dose delivered in the cellular monolayer. For that, a set of measurements and simulation studies were developed and are described in chapter 4.

1.3.1 Dose and time dependence of targeted and untargeted effects

From the literature, it is believed that different biological responses, induced by radiation exposure, are triggered for each cell type. The same trend is observed for RIBE, in other words, different biological effects, in non-directly irradiated cells, are observed depending on cell type.

This first study is focused on the evaluation, for the first time, of the bystander effects induced in the A549 cell line (described in the sequence - section 1.4) exposed to low doses of α-particle radiation.
The proposed work contributes the better understanding of the dose and time dependence, with respect to the uncertainty of the cellular response to radiation. The matrix of experiments used in this study allowed addressing some relevant questions, such as:

- Does low dose α-particle radiation induce cellular damage in the cell line A549, in both directly irradiated and bystander cells?
- Does the cellular damage induced in directly irradiated and bystander cells persist in time?
- What is the shape of the dose-response curve at this range of doses, i.e. < 100 mGy?

The **dose dependence study** aims at understanding the behavior of the dose response curve in the low dose range. This is important not only to verify the linearity (or non-linearity) of the dose response, but also to study one important topic associated with low doses exposure; the hyper-radiosensitivity. Low dose hyper-radiosensitivity (HRS) is characterized by an increasing sensitivity to low doses of radiation. Consequently, it could represent either a higher risk to the health, by low-dose exposures, or an important applicability on radiation-treatments. In relation to the low-dose risk assessment, the hyper-radiosensitivity is one of the driving forces of the studies performed nowadays. One of the most important outcomes related with this phenomenon is the non-linearity of the dose-response curve. On the other hand, the hyper-radiosensitivity effect may have an important application in radiation-treatments. A higher cellular sensitivity at low doses may imply an increasing cell death, which in turn could be used to decrease the overall dose on the radiation-treatments.

The **time dependence study** aims at evaluating, after verifying that the cellular lesion exists, if the damage persists on time, i.e. the genomic instability. **RIBE** is characterized by the appearance of delayed effects in the progeny of irradiated cells, including delayed chromosomal aberrations and gene mutations, reduced plating efficiency and delayed cell death. The RIBE assumes high importance at low doses, because its contribution for the overall damage imparted by radiation in cells (and tissues) must be taken into account. On one hand, this effect could be used in order to increase the cell death or, in the opposite site, must be quantified to understand for how long after an exposure the damage induced must be quantified. In terms of bystander effects, the genomic instability, if expressed, confers the importance of these effects in terms of low-dose risk assessment.

1.3.2 Does the number of irradiated cells affect the spatial distribution of bystander effects?

The studies undertaken in this section, aim at assessing, (after the study of bystander effects in the A549 cell line), how the number of irradiated cells influences the spatial distribution of the bystander effects. In particular, the work presented in this section shows the cellular damage quantification in the unexposed areas surrounding the irradiated ones, by using an *in situ* technique.

The presented in this section work tries to help answering the following questions:

- Does the number of irradiated cells affect the bystander response?
- How far could the bystander signals be propagated within the cell culture?
- Can the number of irradiated cells be related with the propagation of these signals?

Data obtained in this work is very important. In terms of low-dose risk assessment what we know is that the observed bystander effects raise doubts about the deterministic "hit-model" due to the existence of cellular damage in not-directly exposed cells. Moreover, some studies, including ours, show that the bystander effects can spread easily in the culture medium. The impact of this in terms of low-dose risk assessment is huge. Because it pinpoints that, not only the local closest to the irradiated area is affected by radiation, but also the surrounding areas more distant from the local of irradiation. One of the main outcomes of this study is to understand how far in the cellular culture the damage can be quantified. These findings have a key impact not only in terms of radiological protection but also in radiation-treatments.
Moreover, other important issue related to bystander effects is their relation (or dependence) with the number of irradiated cells. So far, the studies available in the literature establish that some *signals* are emitted from irradiated cells to non-irradiated ones, inducing damage in the last ones, but no information is available about the type, origin or nature of such *signals*. Our

study, although does not disclose the nature of these *signals*, allows however to assess their impact on the areas surrounding the irradiated ones. Knowing the influence of the number of irradiated cells, i.e. of the number of *signals* transmitted, on distribution of the bystander effects is of paramount importance in order to understand the *real* impact of the bystander effects on the low-dose risk assessment. As an example, it is known that the inhalation of Radon gas causes the energy deposition of radiation-particles in lung epithelial cells and this exposure translates into a certain risk. From what we know, until now, this risk will increase with the number of deposited particles. However, this increased risk may not be linear, because, from the literature [Balásházy *et al.*, 2002] it is known that the deposition of particles in inhomogeneous, created hot-spots in certain regions of the bronchial tree structure.

1.3.3 Bystander effects and gene expression

It has been established that *signals* from irradiated cells travel through culture medium and GJIC to produce changes in gene expression [Zhou et al., 2005 and Ghandi Hi et al., 2008]. Some authors [Mothersill and Seymour, 1998a; Wolff, 1998; Joiner *et al.*, 2001; Amundson *et al.*, 2001] claim that additionally to the observation of DNA repair mechanisms, cellular death and/or bystander effects, several others factors, such as genomic instability, adaptive response, low-dose hyper-radiosensitivity, delayed reproductive death and the induction of genes by radiation effects, have challenged what we know about the radiation induced cellular damage.
Ghandi [Ghandi et al., 2008] and Chauhan [Chauhan et al, 2012] showed, in a global gene expression, that a peak of gene expression is observed at four hours after exposure. For this reason, in this study the measurement of gene expression of directly and bystander cells was performed 4 hours after irradiation.
Apoptosis is a form of programmed cell death that occurs in multicellular organisms being crucial for tissue homeostasis. This mechanism is a main contributor for the intricacy of cellular response at low doses. Bearing this in mind, the study described in chapter 7 addresses and tries to answer the following questions:

- Do A549 cells show an apoptosis mechanism when exposed to low doses of α-radiation?
- If it occurs, is the apoptosis response the same in both directly irradiated and bystander cells?
- Do A549 cells express the same cellular damage response in directly and bystander cells, followed by a set of dose values lower than 500 mGy?

1.4 The cell line

Human lung adenocarcinoma cells, A549 cell line (kindly provided by University of Porto, Portugal), were chosen as the epithelial cells which respond directly to the toxic agents that are inhaled in the air [Fujii *et al.*, 2001]. Some of the deleterious effects induced in these cells include changes in cell morphology [Bayram *et al.*, 1998], release of inflammatory cytokines [Ohtoshi *et al.*, 1998] and alterations in cellular functions [Stringer and Kobzik 1998]. Since, α-particles were the radiation type used in this work; the epithelial cells are of extreme relevance to evaluate the cellular damage and survival induced at low doses, namely due to natural sources exposures.

1.5 The α-radiation source

Alpha-particles, discovered in 1899 by Ernest Rutherford, are identical to a helium nucleus having two protons and two neutrons. An α-particle is a heavy-charged particle, with a positive charge of +2 from its two protons. Alpha emitting atoms are usually large atoms, i.e. they have high atomic numbers.
There are many α-emitting radioactive elements, either natural or man-made. Some examples of α-emitters include Americium-241, Plutonium-236, Uranium-238, Thorium-232, Raon-222, Polonium-210, among others. Because experiments using α-particles allow obtaining important insights to assess the human-risk resulting from radiation exposure, irradiation devices using some of the aforementioned α-emitters were developed (described in Chapter 4 of this dissertation).

As a doubly charged particle travels through matter alpha-particles deposit energy mostly by excitations and ionizations of atoms. The term LET (acronym for Lineal Energy Transfer) is used to define the amount of energy transferred by these process per unit distance in units of keV/μm. In terms of cellular damage induced by ionizing radiation, the existing difference in LET values among the different radiation types is crucial. High-LET radiation is characterized by causing higher damage to the cells when compared to a Low-LET radiation. This is because high-LET radiation, heavy charged particles, will impart a large portion of their energy in a single electronic collision. Unlike high-LET radiation, low-LET radiation, as photons and electrons, will have a longer path in matter loosing energy continuously.

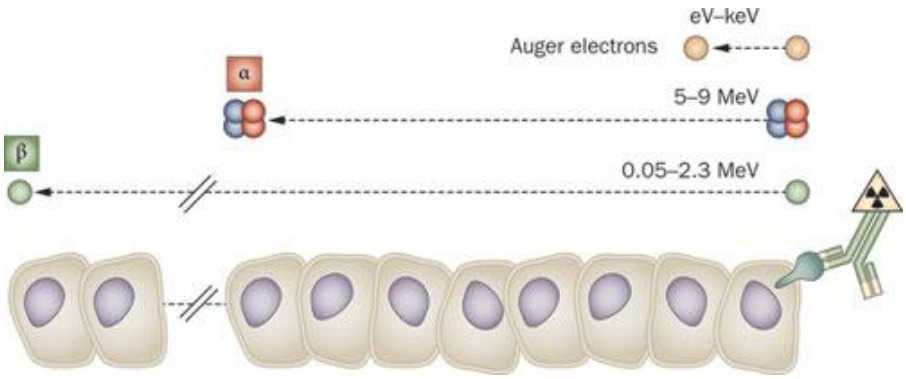

Figure 4: Track length of alpha-particles, beta-particles, and Auger electrons relative to the cell diameter. *Extracted from* [Pouget et al., 2011].

Over the last years, α-particle exposures, associated with occupational exposure (referring to the radiation exposure incurred by a worker) and public exposure has become a prominent public health concern [Wakeford, 2009].

One of the major concerns about the human exposure to natural radiation sources is associated to the radon gas. Most ^{222}Rn gas inhaled is immediately exhaled. However if decay occurs the particles would be deposited onto bronchial epithelial cells. According to the National Research Council (1999) the high density of ionizations than can occur along the path length of α-particles could deliver localized energy of about 10 – 50 cGy. Increasing evidence for a positive correlation between the inhalation of this gas and the development of lung cancer [Darby *et al.*, 2001 and Darby *et al.*, 2005] is the driving force for several ongoing studies.

In this thesis, the α-particle emitter used was the Po-210. To perform the experimental cellular irradiations we used the device developed by Szabo [Szabó *et al.*, 2002], which is described in detailed in section 4.2.1. It must be highlighted that the irradiation device and the α-sources used in this work were kindly provided by Doctor Imre Balashazy from the Hungarian Academy of Sciences.

1.6 Organization

This thesis is organized in 8 chapters. Each chapter can be, in short, summarized as follows:

Chapter 1: Introduction. This chapter describes the motivation for this thesis, the bystander effects and the proposed studies. Moreover, in this, the cell line and the *in vitro* α-particle irradiator is briefly described.

Chapter 2: Biomarkers of radiation exposure and effects. This chapter describes the cellular damage that could be induced by high-LET radiation, and how it can be quantified. The effects observable in the DNA helix are described for directly irradiated and bystander cells. Additionally, it is also performed a description of the cytogenetic assays, used to quantify the cellular damage imparted by α-radiation.

Chapter 3: Interaction of heavy-charged particles with matter. In this chapter, a brief description is made on the energy loss mechanisms for charged particles. Additionally, a special description is provided about the slowing down of charged particles in matter and the concepts use to describe and quantify their effects, namely the linear-energy transfer (LET) and the relative biological effectiveness (RBE).

Chapter 4: Dosimetry of an α-particle device for *in vitro* cells irradiation. This chapter describes the full study regarding the dose rate calculation at the cellular monolayer. Both experimental and simulation procedures and methodologies used are described with great detail, including the simulation codes, SRIM and MCNPX, used in this work. A general discussion of the results obtained is also performed.
The work presented in this chapter was published in the *International journal of low radiation* [Belchior *et al.*, 2010].

Chapter 5: Dose and time dependence of targeted and untargeted effects after α-particle irradiation of human lung cancer cells. In this chapter, the quantification of cellular damage, and its dose and time dependence, is described in both directly irradiated cells and bystander cells. The medium transfer study, methodology used to quantify the bystander effects, is detailed and the results obtained are extensively presented. Moreover, it is presented a general discussion of the results obtained.
The work presented in this chapter was published in *Radiation Measurements* [Belchior *et al.*, 2011] and *Dose Response* journals [Belchior *et al.*, 2013].

Chapter 6: Does the number of irradiated cells influence the spatial distribution of bystander effects? In this chapter the study on the spatial distribution of *bystander signals* through the cellular culture and its dependence with the number of irradiated cells is presented. In this, the γ-H2AX assay is described as the methodology used to perform the

quantification of cellular damage. Additionally, a discussion of the results obtained within this work is presented.
The work presented in this chapter was submitted to the *Dose Response* journal.

Chapter 7: Gene expression in directly and bystander A549 cells after low doses of α-radiation. This chapter presents a study of gene expression levels of GADD45A and BCL2A1 genes in both directly irradiated and bystander cells after 4h of exposure to several doses of α-radiation.

Chapter 8: Conclusions and future work. This chapter presents a set of conclusions extracted from the results obtained in this thesis, points the way to future research, and lists the set of publications produced during the PhD.

CHAPTER 2

BIOMARKERS OF RADIATION EXPOSURE AND EFFECTS

2.1 Introduction

The term **biomarker** has been defined as any measurement reflecting an interaction between a biological system and an environmental agent, which may be chemical, physical or biological [WHO, 1993]. There are three classes of biomarkers defined by the WHO [1993]:

- **Biomarker of exposure**: an exogenous substance or its metabolite or the product of an interaction between a xenobiotic agent and some target molecule or cell that is measured in a compartment within an organism;
- **Biomarker of effect**: a measurable biochemical, physiological, behavioral or other alteration within an organism that, depending upon the magnitude, can be recognized as associated with an established or possible health impairment or disease;
- **Biomarker of susceptibility**: an indicator of an inherent or acquired ability of an organism to respond to the challenge of exposure to a specific xenobiotic substance.

Selecting the most reliable biomarker is a complex process, mainly, due to the dependence on biological samples [Schulte *et al.*, 1991 and Bonassi and Au, 2002]. Ideally, a biological marker should be consistent over a range of exposure, including low dose exposures, and should be specific for the purpose of a specific study.

Within the nucleus of a cell, the DNA molecule consists of two strands of nucleotides twisted into a double-helix and joined by hydrogen bonds between the complementary bases. Any modification on this structure may induce deleterious effects in cells. Genotoxic agents, chemical and/or physical, have the capacity to interact with the DNA molecule and damage it. Thus a specific damage on the structure of DNA that is found after the exposure to a genotoxic agent can be defined as a **biomarker of exposure**. Additionally, the detection of any subsequent effect related to the genotoxic exposure is classified as a **biomarker of effect** [Shugart, 2000].

2.2 Biomarker of radiation exposure

The molecule of DNA consists of two long strands of nucleotides twisted into a double helix of sugar (deoxyribose)-and phosphate backbones (see **Figure 5**). DNA contains two purines (adenine and guanine) and two pyrimidines (cytosine and thymine). The two strands are connected by pairs of complementary bases (adenine and thymine or cytosine and guanine) with hydrogen bonds between them.

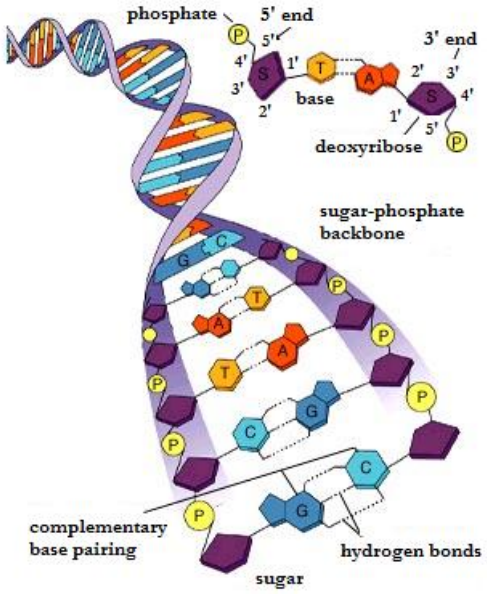

Figure 5: The DNA molecule. *Adapted from* McGrawHill education website (**https://catalogs.mhhe.com/mhhe/home.do**)

A cellular exposure to a genotoxic agent usually disrupts the normal cellular functions as a consequence of DNA structural modifications. Some of the more common DNA structural modifications are presented in **Table 1**.

Table 1: DNA structural modifications caused by a genotoxic agent (physical or chemical).

Genotoxic agent	*Type of modification*	*Mechanism*
Physical	Thymine-thymine dimer	Dimerization of Pyrimidine bases
	Strand breaks	Formation of free radicals
Chemical	Adduct	Covalent attachment of genotoxic agent
	Altered bases	Chemical modification of existing bases
	Abasic sites	Loss of chemically unstable adduct or damaged base
	Strand breaks	Breakage of phosphodiester linkages due to the formation of free radicals and abasic sites
	Hypomethylated DNA	Interference with post-replication
	Mutation	Interfrence with DNA repair

According to the literature, the main multiple lesions affecting the DNA with respect to radiation, as a genotoxic agent, include, among others [Tubiana *et al.*, 2006]:

- single strand breaks (SSBs);
- double strand breaks (DSBs);
- alterations of bases;
- destruction of sugars;

In this thesis, the DNA damage induced by α-radiation was quantified in directly irradiated cells and in bystander cells. In the next sub-sections the effects that can be induced by radiation at the DNA scale in both types of cells, will be described.

2.2.1 The cell cycle

As illustrated in **Figure 6**, the cell cycle is divided, mainly, in two parts: mitosis and interphase. Mitosis corresponds to nuclear division, corresponding to the separation of daughter chromosomes, ending, usually, with cell division- cytokinesis. During interphase, the chromosomes are concentrated and distributed throughout the nucleus. There are three stages of interphase; G1-phase, G2-phase and S-phase. Each, of these phases, ends when a

cellular checkpoint tests out the accuracy of the stage's completion before proceeding to the next.

Briefly, after Mitosis, M phase, cells are metabolically active, i.e. continue to grow, however, DNA does not replicate. This interval between mitosis and DNA replication corresponds to G1-phase. This phase is followed by S-phase in which the replication of DNA takes place. After completion of DNA replication, the cell initiates the G2-phase, during which cell growth continues and proteins are synthesized in preparation of mitosis.

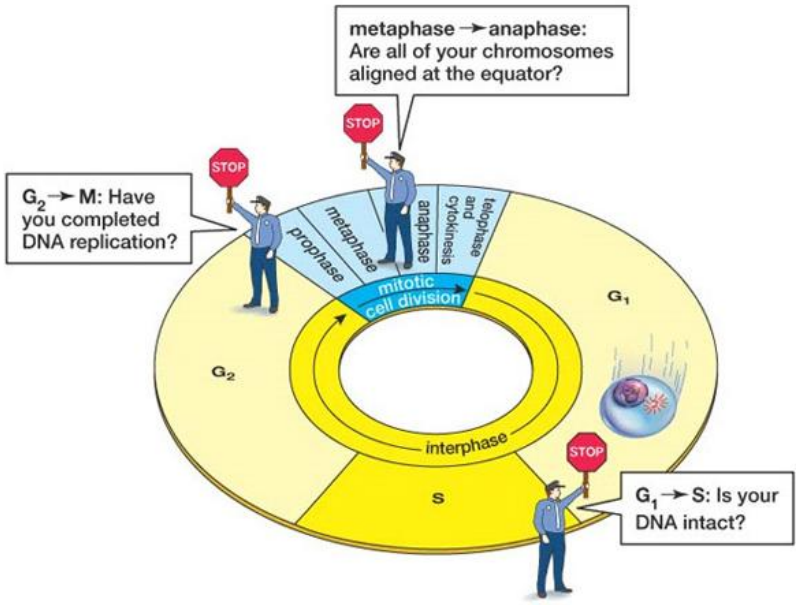

Figure 6: Phases of the cell cycle

As previously mentioned, several checkpoints function to ensure that complete genomes are transmitted to daughter cells. DNA damage not only arrests the cell cycle in G2-phase, but also in G1-phase by repair damage before cell enter the S-phase, and finally in S-phase in which the replication of DNA is monitored to ensure that damaged DNA is repaired before its own replication.

Cell cycle arrest at the G1, S and G2-checkpoints is initiated by a protein-complex, sensor proteins, which bind to damaged or unreplicated DNA. These sensor proteins activate a signaling pathway that leads not only to cell cycle arrest, but also to the activation of DNA repair and programmed cell death, as described in the following section.

2.2.2 DNA damage response

To maintain genomic integrity, DNA must be protected from damage induced by environmental agents (physical or chemical) or generated spontaneously during DNA metabolism. Therefore, cells developed a sophisticated machinery to detect DNA damage and protect themselves against injures caused by DNA structural modifications. The DNA damage response (DDR) is a complex signal transduction pathway that has the ability of

detects the damage and transduces this information to the cell in order to influence its response [Ciccia and Elledge, 2010]. **Figure 7** shows a general outline of the DNA damage response. At first, sensor proteins, Meiotic recombination 11 (Mre11), Rad50 and Nijmegen breakage syndrome 1 (Nbs1), detect DNA damage and/or chromatin alterations which occur after the induced damage. This protein complex, named MRN complex, consisting of Mre11, Rad50 and Nbs1, is fundamental for DNA repair, being assumed as a downstream effector of Ataxia Telangiectasia Mutated (ATM) or Ataxia Telangiectasia and Rad3-related protein (ATR) [Tauchi, 2002 and Bressan, 1999].

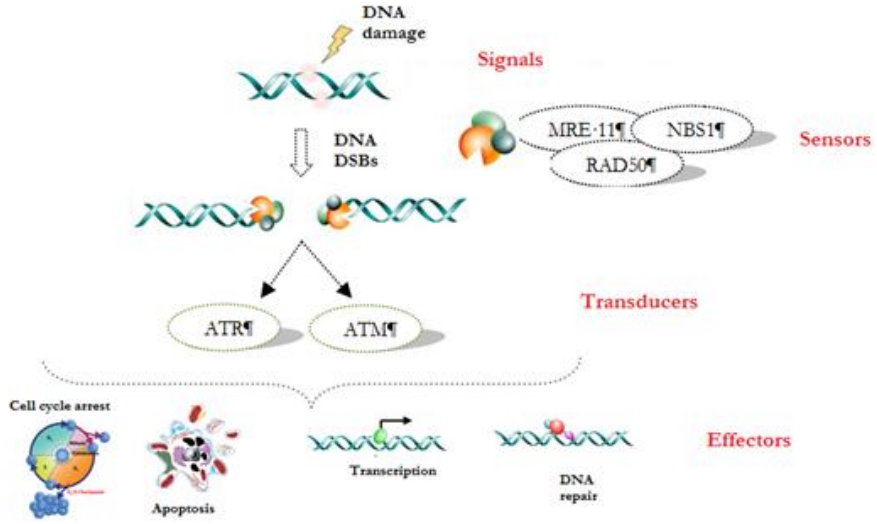

Figure 7: A view of the general outline of the DNA damage response pathway. DSBs are recognized by the MRN complex [Petrini and Stracker, 2003]. MRN recruits proteins of the phosphatidylinositol 3-kinase like preotein kinase (PIKKs) family – ATM, ATR that encode DSB-inducible protein kinases. The consequent cellular responses include cell cycle arrest, apoptosis and DSB repair. [Nagaria *et al.*, 2013].

In human and murine cells, ATM is required for early response to DNA DSBs induced by IR, while ATR responds to single-stranded breaks. McGowan and Russel [McGowan and Russel, 2004] stated that ATM plays a unique and fundamental role on cell survival fraction after IR, since cells that lack ATM process are extremely sensitive to IR.

Current evidence suggests that ATM and ATR control downstream DNA damage response by two families of checkpoint kinases (CHK), the CHK1 and CHK2 kinases, which are essential for cell-cycle arrest before mitosis in response to DNA damage [Walmorth *et al.*, 1993] or DNA replication-monitoring S/G2 checkpoint [Murakami and Okayama., 1995], respectively.

At the end of the chain, involved in specific pathways, are the effectors. The DDR can result in a variety of cellular responses: cell cycle arrest, induction of stress response genes, DNA repair and cell death.

Figure 8 describes the proposed model for an ionizing radiation-induced signaling pathway. Following IR, the intermolecular phosphorylation of ATM dimmers occurs, resulting in ATM monomers. IF DNADSB are present, several proteins, including histone H2AX, BRCA1, 53BP1, and NSB1, are recruited to the sites of breaks. These phosphorylation events contribute to the initiation of cell cycle checkpoints and DNA-repair; as example, p53 and CHK2 initiate the G1-phase arrest, NSB1 the S-phase arrest and BRCA1 the G2-phase arrest [Kastan, 2007]. The phosphorylation of SMC1 reduces chromosomal breakage and enhances cell survival [Kastan, 2007].

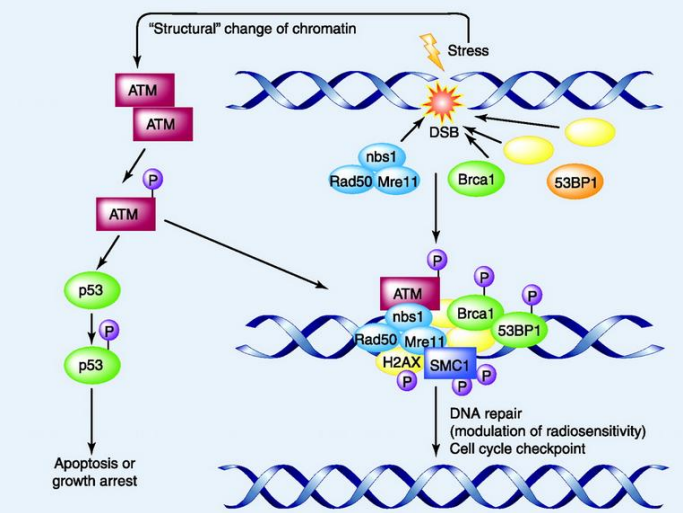

Figure 8: Proposed model for an IR – induced signaling pathway.

2.2.2.1 DNA damage signaling

2.2.2.1.1 DNA single- strand breaks (SSBs)

A SSB corresponds to a single break in the DNA molecule. There are two main ways through which this breaks could occur; i) at the level of the phosphate diester bond (between the phosphate and the deoxyribose) and, ii) at the level of the bond between the base and the deoxyribose.

This type of injury, often referred endogenous DNA lesion, can be induced by; i) the hydroxyl free radical, **OH·** or, ii) the repair of abasic sites. In intact DNA, SSB are of little biological consequence because they can be easily repaired using the opposite strand as a template.

2.2.2.1.2 DNA double- strand breaks (DSBs)

For being the most complex to remove from the genome, DSBs are the most widely investigated DNA lesions. In the simplest way, a DSB is induced by two SSBs taking place in close proximity on opposite DNA strands. Or, a SSB can arise indirectly, as described in section 2.2.1.1..1, during base-excision repair (BER) or by the disruption of the sugar-phosphate backbone [Singh *et al.*, 2011]. Vilenchik [Vilenchik *et al.*, 2003] studied that, in normal cells, approximately 1% of SSBs are converted to approximately 50 DSBs, per cell per cell cycle. **Figure 9** shows the three pathways by a DSB can be induced.

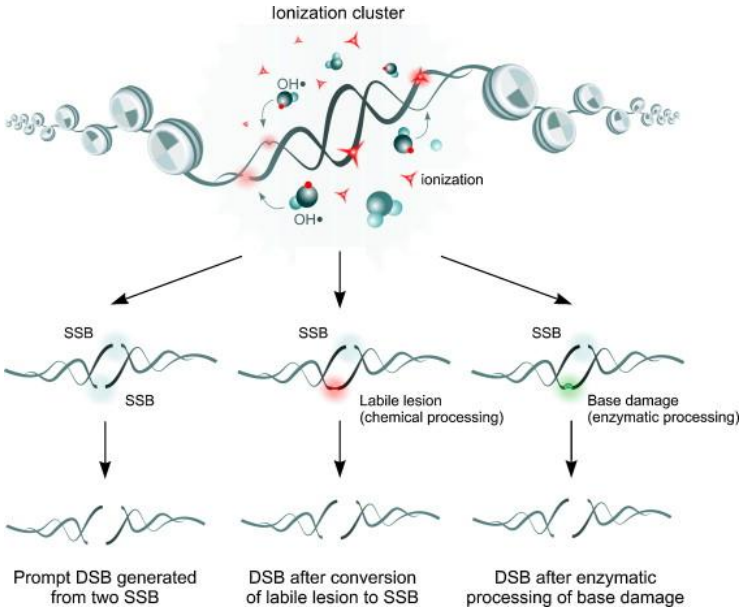

Figure 9: Induction of DSBs by IR. At the end of radiation tracks, the energetic electrons deposit their energy raising multiple ionizations (clustering), which in turn induce complex DNA damage. The principal concern of ionization cluster is that IR interacts with the molecule of DNA at several locations, within the cell area. This interaction leads to i) promptly DSBs when two SSB occur in DNA, ii) SSB after sugar lesions within clustered-damaged sites after chemical processing and iii) SSB after BER by leading breaks in DNA after replication. *Figure extracted* from Mladenov *et al.*, 2011.

2.2.2.1.3 DNA alteration of bases

Additionally to SSBs and/or DSBs, another deleterious effect of DNA damage induced by IR, is the disruption or chemical modification of the pyrimidine and purine bases. The effects observed on the bases are, mainly, induced by indirect effects of radiation, in other words, by free radicals. Most frequently, they suffer hydroxylation, by the hydroxyl radical, with the formation of hydrogen peroxide, which in known for its high toxicity. The radiosensitivity of the bases is different, being the pyrimidine more radiosensitive than the purine base.

2.2.2.1.4 DNA disruption of the sugar-phosphate backbone

As shown in **Figure 9**, the disruption of sugar-phosphate backbone can induce a SSB, assuming, as a consequence, an important effect provoked by radiation exposure. However, an alteration of the deoxyribose is not so common. The most important reaction is the oxidation of the sugar molecule, followed by the liberation of a base, causing or not a breakage in the phosphodiester bond.

2.3 Biomarkers of DNA damage

In this thesis, the cytogenetic assays, described below, were applied to assess the radiation effects to DNA-damaging agents. The applied cytogenetic protocols include micronuclei, γ-H2AX and clonogenic assay.

The **micronucleus assay** is one of the preferred methods to quantify the DNA damage at the chromosome level, allowing the reliable measurement of both chromosome loss and chromosome breakage. This assay is applied in a wide range of applications, such as, various cell types for population monitoring of genetic damage, screening of chemicals for genotoxic potential, prediction of the radiosensitivity of tumours and the inter-individual variation in radiosensitivity Micronuclei can only be expressed in cells that have completed a nuclear division, so a special method was developed making use of cytochalasin-B, a microfilament-assembly inhibitor [Fenech, 2000]. The cytokinesis-block micronucleus (CBMN) assay allows better precision because the data obtained are not confounded by altered cell division kinetics caused by cytotoxicity of agents tested or sub-optimal cell culture conditions [Fenech, 2000]. The CBMN assay allows quantifying, using morphological criteria, chromosome breakage, chromosome loss, chromosome rearrangement (nucleoplasmic bridges), cell division inhibition, necrosis and apoptosis.

The **γ-H2AX assay** is a sensitive method to the early detection of double strand breaks (DSB) *in vitro* and *in vivo* [Rogakou *et al.*, 2000]. If an exogenous damage occurs in cells, after exposure to physical or chemical agents, the H2AX becomes phosphorylated on serine 139, being recruited to damage sites. For this, recent studies points out the ability of the γ- H2AX assay as a potential assessment method to detect tumors. After the phosphorylation of H2AX, preceded by DNA damage, specific antibodies recognize immunofluorescent foci in nuclei. One of the main advantages of this technique, compared with micronuclei assay or chromosomal aberrations, is that it can detect DSB in intact cells, which allows fluorescent visualization and the physical location of the DSBs.

The **clonogenic assay** (CA) is an *in vitro* technique used to analyze the ability of a single cell to grow into a colony. The CA is the method of choice to determine cell reproductive death after treatment with ionizing radiation, but can also be used to determine the effectiveness of other cytotoxic agents [Franken *et al.*, 2006].

2.3.1 The cytokinesis blocked micronuclei assay

Micronuclei are fragments of genetic material that contain either acentric fragments (resulting from DNA breaks), whole chromosomes, or complex rearrangements that are unable to properly attach and be pulled to the poles by the mitotic spindle. This generates chromosomal material that is not included in any final nuclei, and remains in the cytoplasm of the cell, involved by its own nuclear envelope, as can be seen in **Figure 10**. Instead of detecting the chromosomal aberration in the cell metaphase, we detect the loss of portions of genetic material from the nucleus after the cell completes nuclear division.

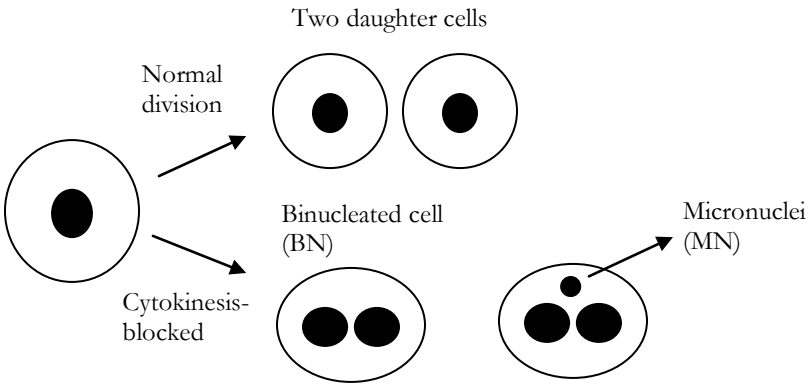

Figure 10: Schematic view of the micronucleus formation process. The upper process describes the normal cellular division, in which a cell divides into two separate daughter cells, each containing one nucleus. By adding cytochalasin B, an inhibitor of actins, the cell is blocked from the cell division after the completion of nuclear division. The resulting cell called a binucleated (BN) cell contains two nucleus. When a fragment of DNA is broken due to damage, one or more micronuclei (MN) appear within the binucleated cell.

Cytochalasin B arrests cells in binucleated (BN) state by permanently blocking them at the G2/M cell cycle phase. Cells are generally incubated with cytochalasin B for approximately 1 – 2 cell cycle times in order to gather the majority of the cells at the binucleated state. The concentration of cytochalasin – B must be taken into account due to the toxicity to cells.
The advantage of this assay is that it simplifies the scoring, and is able to detect clastogenic (loss of portions of chromosomes) and aneuploidic (whole chromosome loss) effects. Inclusively, the origin of the fragment visualized as a MN can be determined by the use of anti-kinetochore marked antibodies or fluorescent probe for centrometric DNA sequences: both identify MN that is likely to be the result of a whole chromosome loss. A disadvantage of the MN assay is that it may have lower sensitivity that the chromossomal aberrations (CA) method, because it requires the completion of the cell cycle; severely damaged cells may not be able to do so and are not scored. In compensation, a larger number of cells can be scored in this assay in comparison to CA. **Figure 11** shows two images, of BN cells, obtained in this work during the quantification of cellular damage using the MN assay.

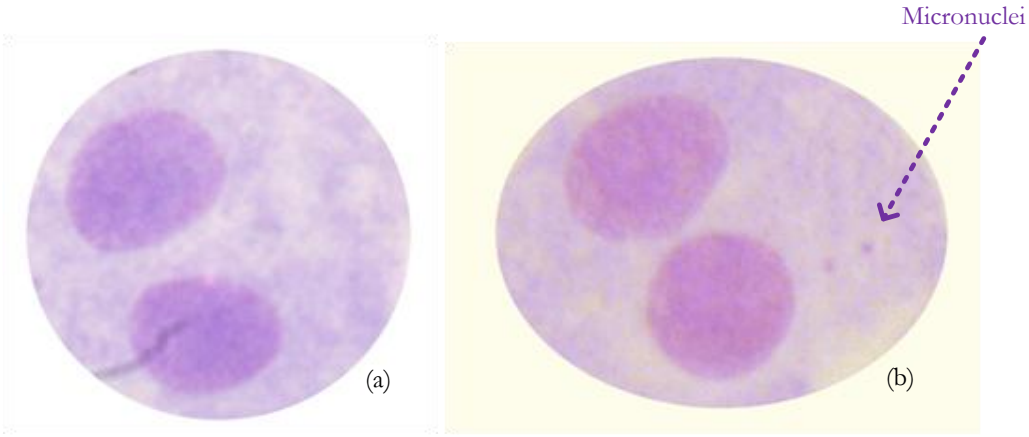

Figure 11: Images obtained during the MN quantification performed in this work. (a) binucleated cell and (b) a binucleated cell with 2 micronuclei.

2.3.2 The γ-H2AX assay

Upon the induction of DNA DSBs by IR, hundreds of molecules of multiple DNA damage response protein species accumulate at DSB sites large nuclear aggregates, known as IR induced foci (IRIF) [Nakamura *et al.*, 2010], which co-localize with γ-H2AX foci [Fernandez-Capetillo *et al.*, 2004].

H2AX is a member of the histone H2A family, one of the five families of histones presented into the DNA chromatin (see **Figure 12**). One hundred and forty-seven base pairs of DNA (red) are wrapped around a nucleosome (yellow) consisting of eight histone proteins (two H2A/H2B dimers and two H3/H4 dimers), thus forming the DNA in chromatin (see **Figure 12 A**). The histones dimerize via the histone fold motif and four histone dimers form the nucleosome core. Nucleosomes are separated by linker DNA sections of 20–80 bp in length. The DNA wraps in 1.7 turns around the nucleosome forming 142 hydrogen bonds at the DNA histone interface. **Figure 12 B** shows the schematic representation of the core histones. All histone proteins share the highly conserved histone fold motif (displayed in color) containing the three alpha helices involved in nucleosome core organization. A model of the nucleosome core particle showing DNA interactions with core histones is shown in **Figure 12 C**. The H2AX C-terminus, which is 14 amino acids longer than that of H2A, is drawn in black with a red arrow marking the phosphorylation site (see **Figure 12 C**) only for demonstration purposes, because there are no structural data available [Kinner *et al.*, 2008].

H2AX phosphorylation is a key DDR component being required; i) for checkpoint-mediated arrest of cell cycle and, ii) for efficient repair of DNA DSBs. It becomes rapidly phosphorylated, what makes H2AX unique, at its carboxyl terminus to form the so-called γ-H2AX at DNA sites [Bonner *et al.*, 2008] being a key component of numerous signaling

response pathways to DNA DSBs [Bonner *et al.*, 2008, Paull *et al.*, 2000 and Rogakou *et al.*, 1999].

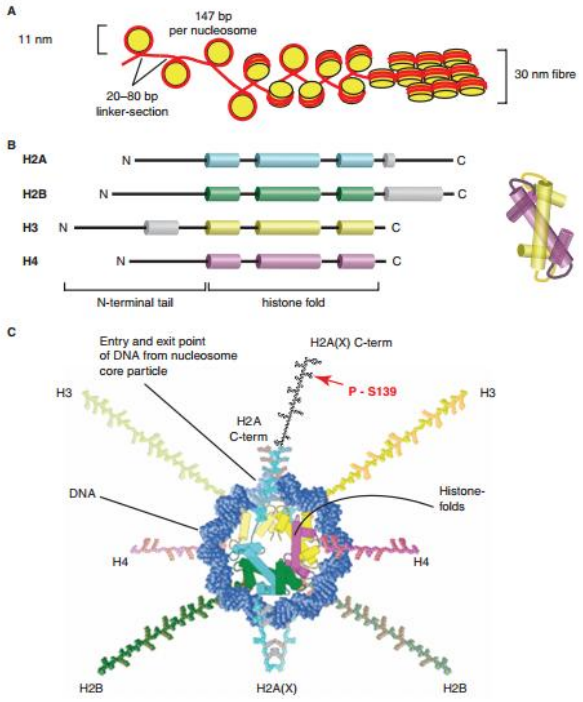

Figure 12: H2AX in the context of chromatin. (**A**) Organization of DNA in chromatin. (**B**) Schematic representation of the core histones (**C**) A model of the nucleosome core particle showing DNA interactions with core histones. The DNA entry and exit points are localized at the H2A/H2B dimer. [Extracted from Kinner *et al.*, 2008]

H2AX is rapidly phosphorylated by ATM on serine 139; as a result it raises γ-H2AX. The formation of γ H2AX foci is an early event, occurring seconds after DNA damage, which corroborates the evidence that ATM is one of the first kinases to be activated in response to DSBs. The phosphorylation of H2AX is apparent within a minute and reaches the maximum in 10 minutes [Redon *et al.*, 2002].

ATM seems to be the more related to γ-H2AX formation under normal conditions, however the other two, ATR and DNA-PK, can also phosphorylate H2AX [Stiff *et al.*, 2004, Shrivastav *et al.*, 2008].

The γ-H2AX is required for further DDR signal amplification, which in turns allow the accumulation of numerous DDR proteins at DSBs sites to form nuclear foci known as IR induced foci (IRIF) [Paull *et al.*, 2000, Celeste *et al.*, 2002, and Huen *et al.*, 2010]. H2AX phosphorylation can extend up to several thousand nucleossomes from the DSB *site* labeling the surrounding chromatin for requiring DNA damage signaling and repair.

Figure 13 illustrates the γ-H2AX foci formation. If repair mechanisms fail to repair the cellular damage induced by radiation, foci will arise in a proportion directly related with the

number of DSB induced. In this work, we used two antibodies (primary antibody (mouse anti γ-H2AX) and FITC-conjugated anti-mouse second antibody) against γ-H2AX to be capable to quantify the γ-H2AX foci using fluorescence microscopy.

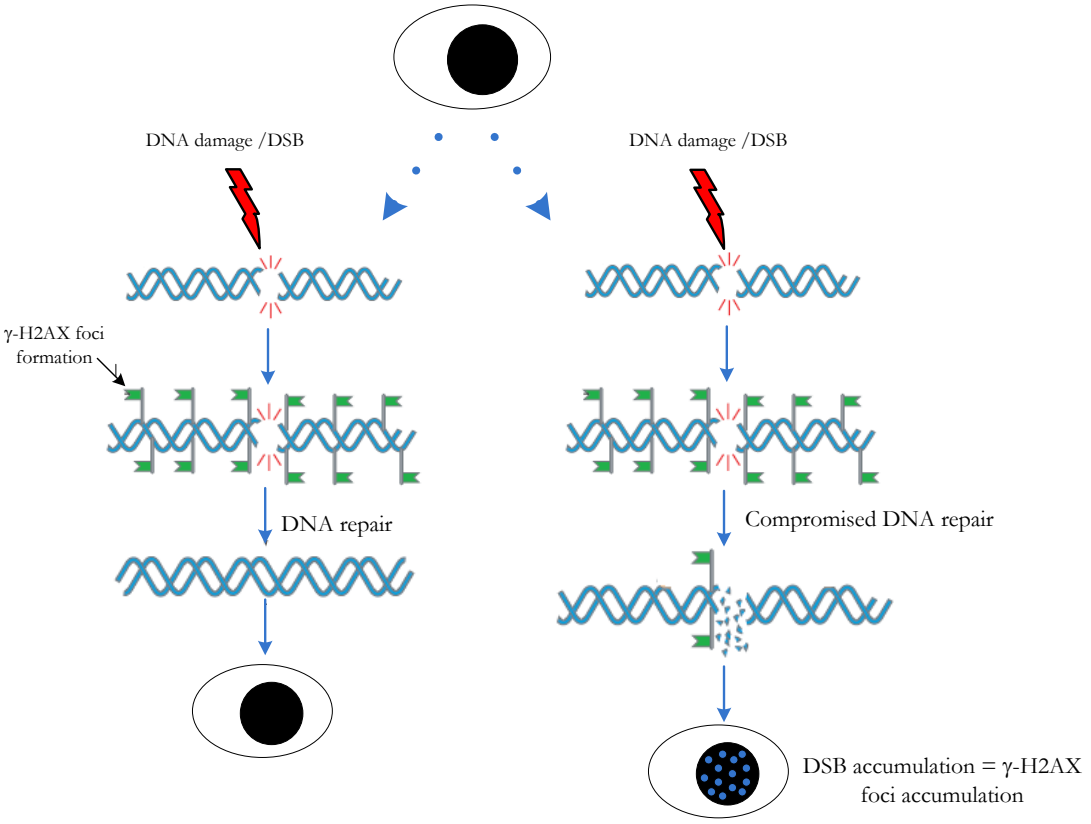

Figure 13: γ-H2AX foci formation. Immediately after a DSB, the phosphorylated form of H2AX is formed γ-H2AX, being accumulated at sites of DNA DSB. If the DNA repair machinery is no efficient, the DNA does not repair and an accumulation of foci is observed in the nuclei. Figure adapted from: *Efficient DNA Repair: A Cell's Fountain of Youth?*

Figure 14 shows two images obtained in this work during the quantification of cellular damage using the γ-H2Ax assay.

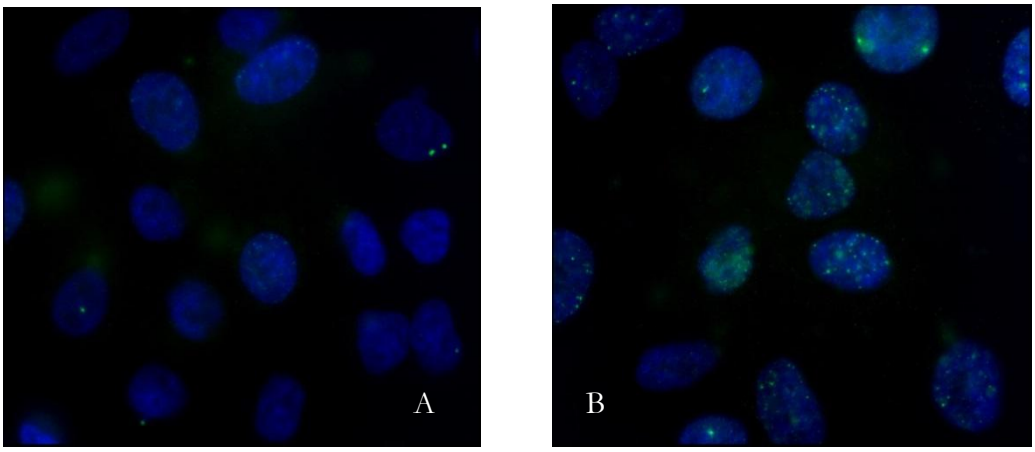

Figure 14: Representative image of DSBs positive cells obtained in this work; non-irradiated (A) and irradiated cells with 100 mGy (B).

2.3.3 The clonogenic assay

The clonogenic assay is an *in vitro* technique based on the ability of a single cell to grow into a colony. This method allows testing all cells in the overall population for its ability of dividing. This technique reveals to be the method of choice to measure the cell viability/death after exposure to ionizing radiation of a population of cells.

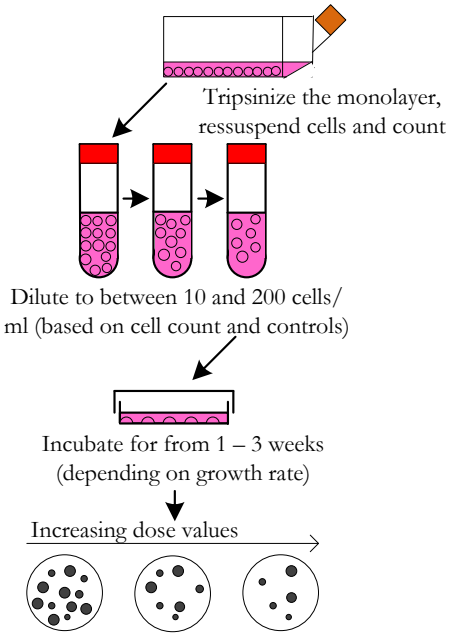

Figure 15: Clonogenic assay for cells growing in monolayer. Cells are trypsinized, counted, and diluted. The colonies are fixed and stained when they reach at least 50 cells each.

Figure 16 shows three cultures of colonies, obtained during the clonogenic assay study in this work, for doses of 0, 5, and 100 mGy, respectively.

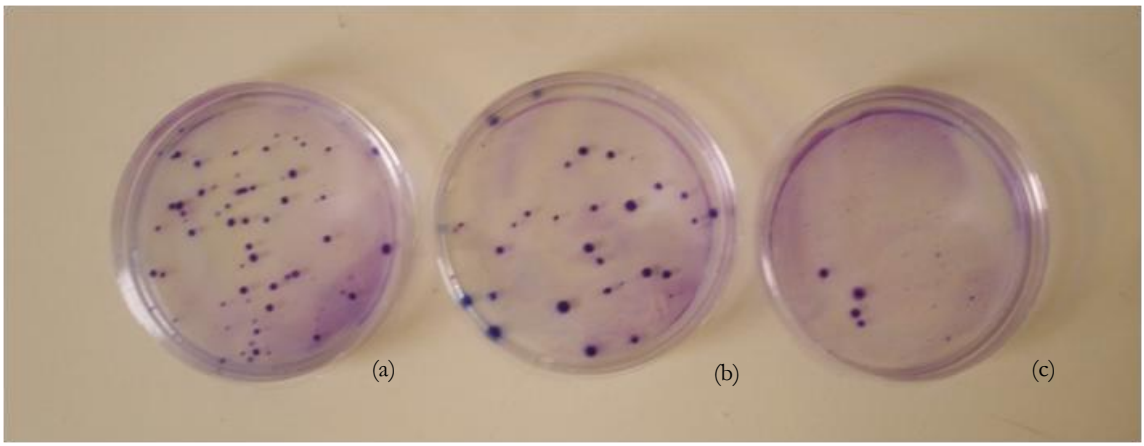

Figure 16: Cultures of colonies obtained during this work with clonogenic assay; (a) 0 mGy, (b) 5 mGy and (c) 100 mGy.

2.3.4 Laboratory and experimental procedures

2.3.4.1 The cytokinesis blocked micronuclei assay

A population of approximately $1x10^5$ cells was cultured in 3 mL of DMEM medium supplemented with 10 % of fetal bovine serum and 1% of Penicillin-Streptomycin solution. After 24h of incubation, the cell cultures were exposed to several doses, afterwards shown, of α-radiation. Control cultures were submitted to the same experimental conditions but not irradiated. At 44h of incubation, cytochalasin B with a concentration of 2 mg/ml was added to the culture medium to inhibit cytokinesis, and allow identification of binucleated cells At the end of incubation cells were harvested by centrifugation and submitted to a mild hypotonic shock to enlarge the cytoplasm of the cell. The cells were then smeared onto clean glass slides, allowed to dry, fixed with methanol: acid acetic and finally stained with Giemsa 4% (see complete protocol in annexes-Protocol I). MNs were identified according to the criteria previously published by Fenech [Fenech, 2000]. The frequency of binucleated cells containing one or more MN was also determined.

2.3.4.2 The γ-H2AX assay

A population of approximately $1x10^5$ cells was cultured in 3 mL of DMEM medium supplemented with 10 % of fetal bovine serum and 1% of Penicillin-Streptomycin solution. After 24h of incubation, the cell cultures were exposed to several doses, afterwards shown, of α-radiation. Control cultures were submitted to the same experimental conditions but not irradiated. Immediately after irradiation the cells were washed with phosphate-buffered saline

solution (PBS) and fixed with 4% formaldehyde in PBS for 15 minutes. After being washed with PBS, cells were permeabilized with Triton X-100 (0.5%) at room temperature for 5 minutes, washed twice with 1% Bovine Serum Albumin (BSA) (Sigma-Aldrich, St. Louis, USA) and blocked during 1 hour with BSA 4%. Then, cells were incubated with the γ-H2AX primary antibody (mouse anti-γ-H2AX (ser139), Stressgen, bioreagents Corp., Canada) at 2 μg/ml for 2 hours, washed twice with BSA 1%, incubated with FITC-conjugated anti-mouse second antibody (Santa Cruz Biotechnology, USA) at 1mg/ml for 1 hour, washed three times more and incubated with Hoechst (Sigma-Aldrich, St. Louis, USA) at 1ug/ml for 5 minutes and finally mounted with anti-fade (Vectashield mounting medium H-100, Vector Laboratories, Burlingame, Canada) (see complete protocol in the annexes-Protocol II). Cells were analyzed at 64x amplification by a fluorescence microscope. Images were randomly obtained in each slide. Image analysis of γ-H2AX foci was performed by the freeware Cellprofiler [Carpenter *et al.*, 2006]. At least 100 nuclei were analyzed per experiment per dose.

2.3.4.3 The clonogenic assay

A population of approximately $1x10^5$ cells was cultured in 3 mL of DMEM medium supplemented with 10 % of fetal bovine serum and 1% of Penicillin-Streptomycin solution. After 24h of incubation, the cell cultures were exposed to several doses, afterwards shown, to α-radiation. Control cultures were submitted to the same experimental conditions but not irradiated. After exposure to ionizing radiation, cells are seeded out in appropriate dilution (**Figure 15**) to form colonies in 1 -3 weeks, depending on growth rate. When each colony reaches at least 50 cells, the culture medium is removed and afterwards washed with a saline solution; colonies are fixed with methanol: acid acetic (3:1) and stained with crystal violet (1%) (see complete protocol in the annexes-Protocol III). Colonies of cells formed were subsequently counted. The Platting Efficiency (PE) ratio is defined as:

$$PE(\%) = \frac{\text{no. of colonies formed}}{\text{no. of cells cultured}} x100 \quad (1)$$

PE values were determined using the non-irradiated cells. The cell surviving fraction (SF) is the number of cell colonies that arise after irradiation of cells, expressed in terms of PE:

$$SF = \frac{\text{no.of colonies formed after irradiation}}{\text{no.of cells cultured x PE}} \quad (2)$$

CHAPTER 3

INTERACTION OF HEAVY CHARGED PARTICLES WITH MATTER

3.1 Introduction

The biological effects resulting from the exposure to any form of radiation – x-or γ-rays, charged particles or neutrons - represent the end product of several processes triggered by a series of physical, chemical and biochemical cellular responses. The absorbed energy, in biological material, could induce molecular damage in critical targets, such as DNA, through **direct** and **indirect actions** (see **Figure 17**). In **direct action**, the atoms of the target itself are ionized or excited initiating the chain of events that leads to biological damage. This represents the dominant process for high linear energy transfer (LET) radiation, such as neutrons or α-particles. On the other hand, the radiation may interact with other atoms or molecules in the cell, namely water, producing free radicals, with high reactivity and, therefore with short lifetimes (10^{-10}–10^{-9}s), that are able to diffuse far enough to reach and damage critical targets. This represents the **indirect action** of radiation. In this, water radiolysis, which originates high reactivity species such as, a hydrated electron, a hydrogen atom, and a hydroxyl radical, assumes the major role in radiation effects on biological tissues and organisms.

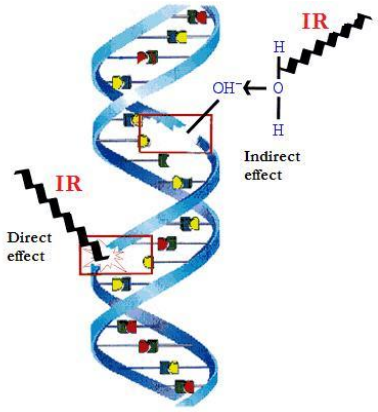

Figure 17: Direct and Indirect effects of IR in DNA. The creation of a OH^- ion is depicted, as an example of indirect effects.

Figure 18 shows the chain of events triggered after interaction of radiation with biological material, as well as the time scale for each of these events.

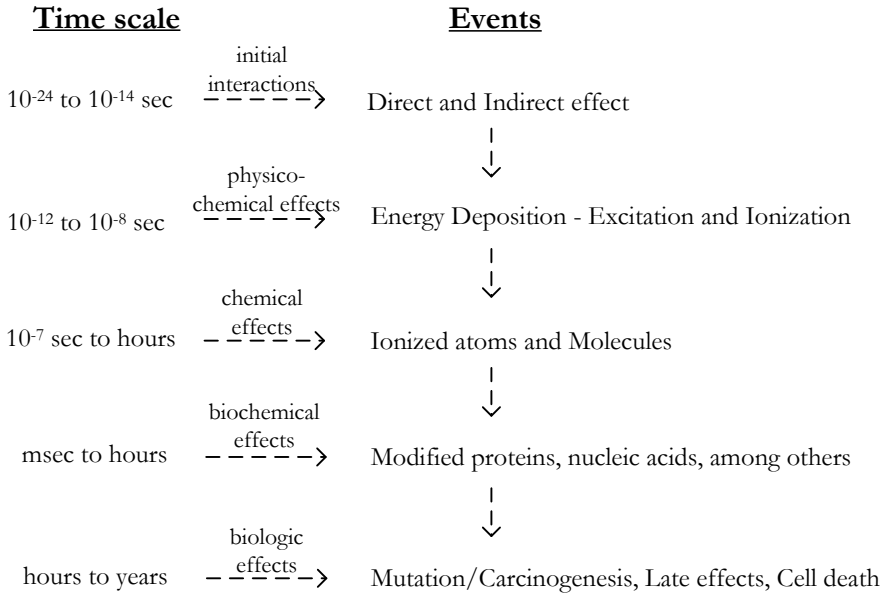

Figure 18: Sequence of events after radiation energy absorption.

As can be seen in **Figure 18**, there are large differences in the time scale for each type of event. The initial interactions, leaving to direct or indirect actions, occur very quickly. The primary radicals, produced by the ejection of an orbital electron, generally have a lifetime of 10^{-10} seconds due to its high reactivity. A free radical is an atom or molecule carrying an unpaired orbital electron in the outer shell, which can be either repaired by thiols or nitroxides or fixed by oxygen. This last, increases the biological effectiveness of radiation,

being the lifetime of the free radical approximately 10^{-5} instead of 10^{-9} seconds. Following the chain events, the ionized atoms or molecules, not promptly repaired, triggers biochemical effects, namely in proteins and nucleic acids. At this point in time, if DNA is reached, strand breaks, double or single, may occur. Two main mechanisms may occur in the cell after the DNA molecule has been reached. As a mechanism of defense, the cell could undergo cell death (apoptosis and/or necrosis) or not proliferate. Alternatively, mutated DNA may proliferate, resulting in long-term genetic effects including cancer. Other late effects such as fibrosis and vascular damage result from the permanent damage over the course of months to years.

3.2 Energy loss of charged particles

While traversing a material, a charged particle experiences a large number of interactions transferring and imparting part of its kinetic energy to the medium. The particle's path changes through elastic and inelastic scattering with the charged particles (orbital electrons and protons) in the atoms of the medium, it loses energy to the by collisional or radiative loss. The rate of energy loss per unit path length by a charged particle in a medium is called the stopping power (described in section 3.2.1). According to the type of process through which the particle loses its energy, there are two types of stopping power; the radiative and the collisional stopping power.

The radiative stopping power is related to emission of photons due to *bremssthahlung* when the incoming particle changes direction along its trajectory. The energy loss due to this process is significant only for light charged particles in materials of high atomic number.

The collisional stopping power results from charged particles Coulomb interactions with orbital electrons. Both light and heavy particles suffer these types of interactions that result to energy transfer to orbital electrons, i.e., excitation and ionization of absorber atoms.

As illustrated in **Figure 18**, the initial events taking place when radiation interacts with a biological material are ionization and excitation.

The **ionization** event occurs when the incident particle has enough energy to overcome the binding energy of the orbital electron and consequently detach it (the orbital electron) from the atom (see

Figure 19).

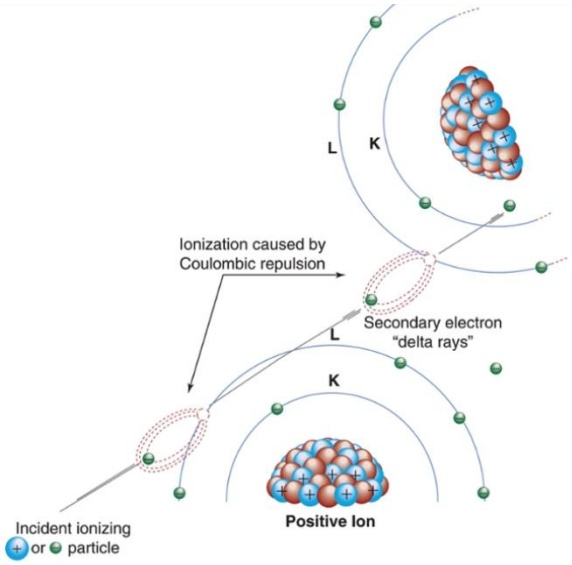

Figure 19: Ionization event. If the energy transferred to an atom, due to coulomb forces exerted when a charged particle passes near the electric field generated by the atom's electrons and protons, exceeds the electron's energy binding, the result is an ion-pair (i.e. an ejected electron and a positively charged atom). If the energy of the ejected electron is sufficient enough, a secondary electron, named delta ray, could be produced. Thus, further ionizations are produced by secondary ionizations events. Figure extracted from [Bushberg *et al.*, 2012]

For heavy charged particles, the number of primary and secondary ion pairs formed per unit length, denominated specific ionization (SI), depends on the mass and velocity (kinetic energy) and charge of the incident particle. It increases with the square of the electrical charge and decreases with the square of the incident particle velocity; $SI \propto Q^2/v^2$. As a consequence, a larger mass and charge of the incident particle implies a highest specific ionization.

Alternatively, the charged particle could leave the atom in excited, non ionized state; if the energy is not sufficient to knock an electron out of an atom (see **Figure 20**). An **excitation** event implies that an electron is transferred to a more external orbital. In an excitation event, the energy transferred to the electron is never higher than its binding energy. Following excitation, the electron returns to a lower energy level in the form of electromagnetic radiation or Auger electrons.

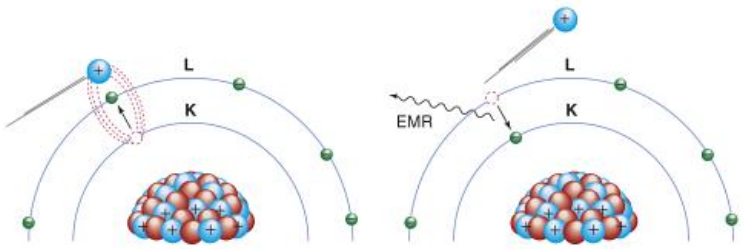

Figure 20: Excitation event (left), an electron (represented in green) is transferred to a higher energy level. De-excitation event (right), occurs when the electron returns to a lower energy level emitting either electromagnetic radiation or an Auger electron. Figure extracted from [Bushberg *et al.*, 2012].

3.2.1 Interaction between charged particles and the electrons of the medium

The required energy, to the occurrence of an excitation event, is on the range of 10-100 eV and consequently the energy loss of the impinging heavy charged particle is small, being this kind of collisions, called **soft collisions**. These types of collisions, takes place when the classical impact parameter *b* is much larger than the atom radius *a* (see **Figure 21**). When the impact parameter *b* is of the order of the atomic radius *a*, the charged particle most likely interacts with a single atomic electron which receives most of the incident particle's kinetic energy. This type of collisions is called **hard collisions**, and can result in the ionization of the atom, if the incident particle transfers to the orbital electron enough energy to overcome the binding its energy.

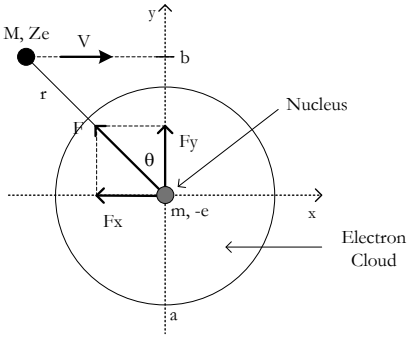

Figure 21: Parameters for a charged particle (mass M, charge ze and velocity V) collision with an electron (mass m and charge –e) where *a* is the classical radius of the atom and *b* is the classical impact parameter. *Adapted from* Turner, 2007

The incident charged particle continuously slows down, mostly due to the interaction with electrons. The Coulomb force (F) between heavy charged particle and the electron is calculated by **equation 3**:

$$F = \frac{ze^2}{4\pi\varepsilon_0}\ \frac{1}{r^2} \tag{3}$$

where,
ze is the charge of the incident particle,
e is the charge of the electron,
ε_0 is the permittivity of free space, and
r is the distance between the two particles.

As a consequence of the Coulomb force between the two charges, the kinetic energy (E_k) of the heavy charged particle is transferred to the electron, putting it in motion. The amount of energy transferred (Q) to the electrons depends primarily on the distance between the incident particle and the electron, i.e. on the impact parameter *b*.

3.2.2 Momentum Transfer from the incident charged particle to orbital electrons

The calculation of the collisional stopping power (S_{col}) of a heavy charged particle is based on the variation of the momentum (Δp). **Figure 21** shows the components, *x* and *y*, of the Coulomb force (**equation 4**) that the heavy charged particle exerts to the electron. Based on this, the momentum imparted to an electron by a charged particle can be determined by the following equation:

$$\Delta p = \int_{-\infty}^{\infty} F_y\, dt = \int_{-\infty}^{\infty} F \cos\theta\, dt = \frac{ze^2}{4\pi\varepsilon_0}\int_{-\infty}^{\infty} \frac{\cos\theta}{r^2}\, dt \tag{4}$$

Assuming, that (**Figure 21**):

- t=0 is the exact time at which the heavy particle crosses the y-axis, and
- $\cos\theta = \frac{b}{r}$

The momentum, in **equation 5**, could be expressed as:

$$\Delta p = \frac{ze^2}{4\pi\varepsilon_0}\int_0^{\infty} \frac{b}{r^3}\, dt = \frac{ze^2}{4\pi\varepsilon_0}\frac{2}{Vb} \tag{5}$$

where
V is the velocity of the incident particle, and
b is the impact parameter

Equation 5 demonstrates that a higher distance between the incident particle and the orbital electron translates into a lower momentum transferred to the orbital electron. This implies that, depending on the impact parameter *b*, the energy transfer to the orbital electron could be minimal or maximum, as described in sections 3.2.4 and 3.2.5.

3.2.2.1 Collisional Stopping Power

As described above, a heavy charged particle transfers its kinetic energy mainly to orbital electrons. Thus, in this section, due to its higher relevance, it will be described only the collision stopping power.
The total energy loss of the charged particle is obtained by integrating the overall values of energy loss with respect to the impact parameter *b*.

$$-\frac{dE}{dx} = \int_{b_{min}}^{b_{max}} \Delta E(b) \frac{\Delta n}{\Delta x} \tag{6}$$

where
$\Delta E(b)$ is the energy transferred to the orbital electron from the heavy charged particle for a single interaction with an impact parameter b, obtained by **equation7,** and $\Delta n/\Delta x$ is the number of electrons per unit path length.

$$\Delta E(b) = \frac{(\Delta p)^2}{2m_e} = 2\left(\frac{e^2}{4\pi\varepsilon_0}\right)^2 \frac{z^2}{m_e v^2 b^2} \tag{7}$$

Figure 22 shows an annular cylinder with length *dx* centered in the heavy charged particle trajectory.

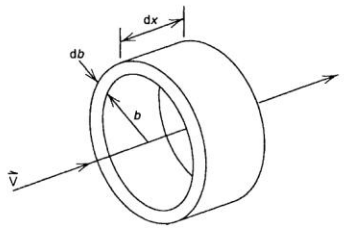

Figure 22: Annular cylinder of length dx. The cylinder's axis is aligned with the trajectory of the heavy charged particle. Extracted from [Turner *et al.*, 2007].

The number of electrons Δn contained between *b* and *b*+*db* is:

$$\Delta n = N_e dm = \left(\frac{ZN_A}{A}\right) dm \tag{8}$$

where
N_e is the number of electrons per unit mass of the material
dm is the mass contained in the annular cylinder between *b* and *b*+*db*

The term, *dm*, is approximately equal to:

$$dm=\varrho dV=\varrho\pi(b+db)^2\Delta x-\varrho\pi b^2\Delta x\approx 2\pi\varrho b\ db\ \Delta x \tag{9}$$

Thus,

$$\frac{\Delta n}{\Delta x}=2\pi\varrho\left(\frac{ZN_A}{A}\right)b\ db \tag{10}$$

The mass collisional stopping power S_{col} is then equal to:

$$S_{col}=-\frac{1}{\varrho}\frac{dE}{dx}=4\pi N_e\left(\frac{e^2}{4\pi\varepsilon_0}\right)^2\frac{z^2}{m_e v^2}\int_{b_{min}}^{b_{max}}\frac{db}{b}=4\pi\frac{Z}{A}N_A\left(\frac{e^2}{4\pi\varepsilon_0}\right)^2\frac{z^2}{m_e v^2}\ln\frac{b_{max}}{b_{min}} \tag{11}$$

The collisional stopping power, **equation 11**, is linear proportional to z^2 and exhibits an inverse proportionality to v^2.

3.2.3 The Bethe-Bloch formula for stopping power

The following equation was derived by Bethe-Bloch to calculate the stopping power for heavy charged particles [Berger and Seltzer, 1964].

$$\left(\frac{S}{\varrho}\right)_{col}=\frac{2\pi r_e^2 m_0 c^2}{\beta^2}\left(\frac{N_A Z}{A}\right)\left[\ln\frac{\tau^2(T+2)}{2\left(I/m_0c^2\right)}+F(\tau)-\delta-2\frac{C}{Z}\right] \tag{12}$$

whit,

$$F(\tau)=1-\beta^2+\left[\frac{\tau^2}{8}-(2\tau-1\ln 2)\right]\Big/(\tau+1)^2 \tag{13}$$

where:

m_0c^2 is the electron rest energy = 0.510976 MeV
τ is the kinetic energy in units of mc^2
$\beta=v/c$ is the speed of the particle in relation to c
N_AZ/A is the number of electrons per grams in the medium
I is the mean excitation energy of the medium
δ is the density correction factor
C/Z is the shell correction

The values for I are given in ICRU report 37 [ICRU 37, 1984]. The value of I for an absorber is influenced by the atomic number Z, being equal to, 19 eV when Z=1, 11.2 + 11.7 Z eV when $2 \leq Z \leq 13$ and 58.2 + 8.71 Z eV for Z > 13.

The density correction factor, δ, is used due to the fact that charged particles can polarize the medium along its path. This correction factor becomes more important for higher energies and for more dense materials.

By **equation 12**, one can inferred that higher the Z and the density of the absorber, the greater the stopping power.

3.2.4 Maximum energy transfer in a single collision

Higher values of energy transfer occur for small values of the impact parameter *b*. Assuming that a heavy-charged particle moves rapidly compared with the electron and that the energy transferred is large compared with the binding energy of the electron in the atom, the maximum energy transfer in a single collision can be expressed as:

$$\Delta E_{max} = \frac{4 m_e M}{(M+m_e)^2} E_k \qquad (14)$$

where
M is the mass of the incident particle,
V is the velocity of the incident particle,
E_k is the kinetic energy of the incident particle, and
m is the mass of the electron considered free and at rest.

Assuming that m << M, the maximum energy transfer to the orbital electron is:

$$\Delta E_{max} = 4 \frac{m_e}{M} E_k = 4 \frac{m_e}{M} \frac{M v^2}{2} = 2 m_e v^2 \qquad (15)$$

From this expression it can be inferred that a heavy charged particle can transfer only a small fraction of energy in a single electronic collision. Thus, the deflection in the collision is negligible. As a consequence, a heavy charged particle travels an almost straight path through matter, losing small amounts of energy at each collision.

3.2.5 Minimum energy transfer in a single collision

Smaller values of energy transfer occur for large value of the impact parameter *b*. The energy transfer is smaller than the binding energy of the orbital electron or excitation potential. Thus, negligible energy is transferred to the orbital electron if $b>b_{max}$, where b_{max} corresponds to the minimal energy imparted, referred as **mean ionization-excitation potential (I)**. This value is obtained by **equation 5** assuming the maximum value of the impact parameter *b*.

$$\Delta E_{min} = \frac{(\Delta p)^2}{2m_e} = 2\left(\frac{e^2}{4\pi\varepsilon_0}\right)^2 \frac{z^2}{m_e v^2 b_{max}{}^2} \tag{16}$$

3.3 Slowing down of charged particles

As described above, the passage of a heavy charged particle through a material consists of a large number of Coulomb interactions (ineslastic collisions) with electrons, leading to different values of energy transfer, Q. Radiation of bremssthrahlung photons also contribute to the reduction of the incident particle´s kinetic energy. The total amount of energy transfer to the material corresponds to the sum of each value of energy lost by the incident particle, dE, over a distance dx. The ratio between the total energy lost, dE, and the distance traveled, dx, is denominated stopping power (S) of the medium for the particle (expressed in $MeV.cm^{-1}$). This could be also referred to as linear energy transfer (LET) of the particle, expressed in $keV.\mu m^{-1}$. These quantities are of fundamental importance in radiation physics and dosimetry, being closely related to the absorbed dose in the medium from the incident heavy charged particles. The absorbed dose is a measure of the total energy deposited per unit mass of the constituent material of the medium (tissue, when studying the biological effects of ionizing radiation); however, equal doses of different types of radiation do not produce an equal biological effect. This is due to the pattern of energy deposition at microscopic scale. The effectiveness of different types of radiation for inducing a biological effect is commonly referred to as relative biological effectiveness (RBE). The RBE is defined as the ratio of the dose of the reference radiation (usually, X-rays) to the dose of a particular radiation that produces the same biological effect (the same survival fraction of irradiate cells, for instance). Consequently, the LET value is associated to the RBE of different kinds of radiation. In terms of biological effectiveness it is known that a high-LET radiation involves a more severe damage in living organisms that low-LET radiation, namely due to the higher density of ionizations along the track, which increases the probability of a direct effect on the target molecule.

3.3.1 Linear-energy transfer (LET)

The linear-energy transfer (LET) is the energy transferred per unit length of the track. This quantity is normally expressed in keV.μm^{-1}, and can be calculated according to the following equation:

$$LET = \left(\frac{dE_L}{dl}\right) \quad (17)$$

where
dE_L is the energy locally imparted to the absorbing material, and
dl is the distance of path length.

The LET value is dependent on the type of radiation. Neutrons or α-particles are denominated high-LET radiation, whereas γ-radiation or X-rays are considered to be low-LET radiation. As said before, the LET value is directly related with the biological effectiveness of the radiation, as shown in **Figure 23**.

The LET at which the RBE reaches a peak is much the same (about 100 keV/μm) for a wide range of mammalian cells, being considered optimal in terms of biologic effect. The main reason is that, the separation between events at this ionization density coincide with the diameter of DNA helix (about 2 nm), then the probability to cause a double-strand break is much higher. γ or X-rays have a low RBE because the ionization patterns is more sparsely, so, to cause a double-strand break it is necessary more than a single track. After the optimum value of LET the RBE starts decreasing. This is mainly due to the proximity of the events which makes this type of radiation inefficient in terms of biological effect.

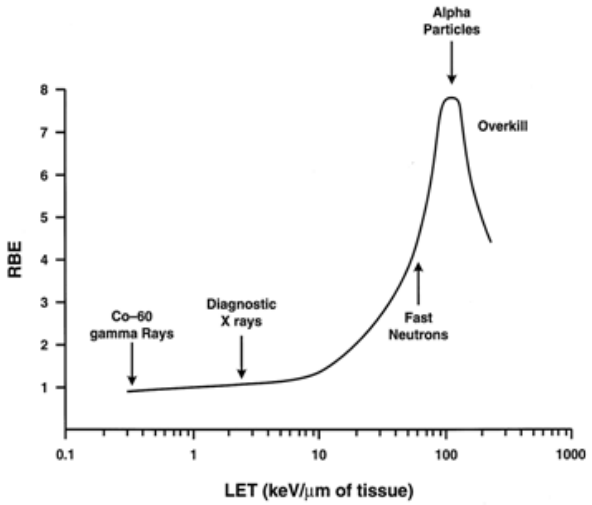

Figure 23: Variation of relative biologic effectiveness (RBE) with linear energy transfer (LET) in tissue. It can be inferred that high-LET particles, such as α-particles, protons and neutrons, cause a higher damage to the crossing tissues.

When low-LET radiation hits cells, it produces sparse ionization and individual DNA lesions, such as single and double-strand breaks, chemical modification of DNA-bases, and DNA-protein crosslinks, which could be easily repaired (see **Figure 24.a**). High-LET radiation produces clusters of DNA damage that are difficult to repair (see **Figure 24.c**). The high cytotoxicity of high-LET radiation is independent of dose rate since DNA double-strand breaks can be produced by a single hit. Contrary to what happen with low-LET, high LET-radiation is independent of oxygenation, as, due to high ionization density pattern the biological effects would be the result of direct effect of target molecules. An intermediate LET radiation is considered to be Auger – electrons (see **Figure 24.b**). Auger electrons emitters can be used for labeleling of DNA base analogs and emit cascades of electrons that produce densely localized ionizations and excitations within DNA, inducing poorly repairable damage.

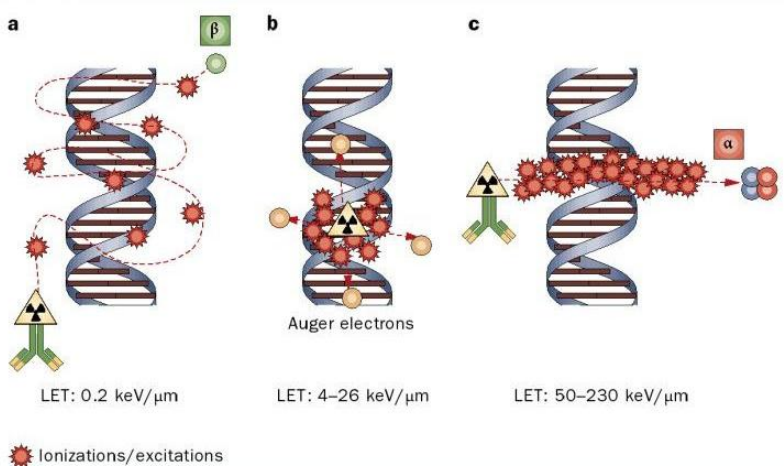

Figure 24: Patterns of DNA damage caused by different types of radiation. a) Low-LET radiation produces sparse ionizations and excitations within DNA along a track, resulting in individual DNA lesions that are easily repairable. b) Cascades of Auger electrons (with intermediate LET). c) α-particles with high LET produce densely localized ionizations and excitations along a linear track, resulting in locally, and multiple damaged sites that are poorly repairable. Extracted from [Pouget *et al.*, 2011]

3.3.2 Range

As a result of the interaction with matter, charged particles lose their energy through inelastic Coulomb collisions (mainly ionizations) and radiative collisions. For light charged particles (electrons and positrons) these interactions may translate in large deflections, whereas for heavy charged particles (α- particles) their deflection in each collision is negligible. Other main difference is that, for heavy charged particles the energy loss from radiative processes is negligible and the energy transfer in a single electronic collision is small. At a certain penetration distance, over the material, the energy losses reach a maximum, which corresponds to the peak in the stopping power curve for lower energies. This peak corresponds to the Bragg peak, and it is represented in the **Figure 25**.

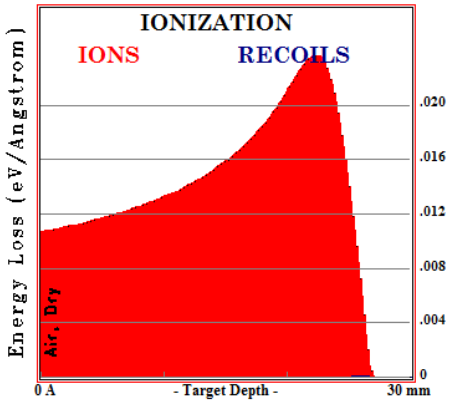

Figure 25: Energy loss of an α-particle with 4 MeV of energy reaching a layer of air. Results obtained with SRIM, 2008.

The range of a charged particle in matter can be calculated, using the continuous slowing down approximation (csda), by the following equation [Berger and Seltzer, 1983]:

$$R_{csda} = \int_0^{E_{ki}} \frac{dE}{S_{tot}(E)} \tag{18}$$

where; R_{csda} is the csda range (mean path-length) of the charge particle in the medium, E_{ki} is the initial kinetic energy of the charged particle, and $S_{tot}(E)$ is the total Stopping power of the charged particle as a function of the particle´s kinetic energy.

For heavy charged particles, as it essentially moves in a rectilinear path, R_{csda} is a good approximation to estimate the average range over an absorbing medium. **Figure 26** shows the pattern of an α-particle in air, as well as, the dependence on the energy of the incident particle. The results are obtained using the state-of-the-art computer program SRIM.

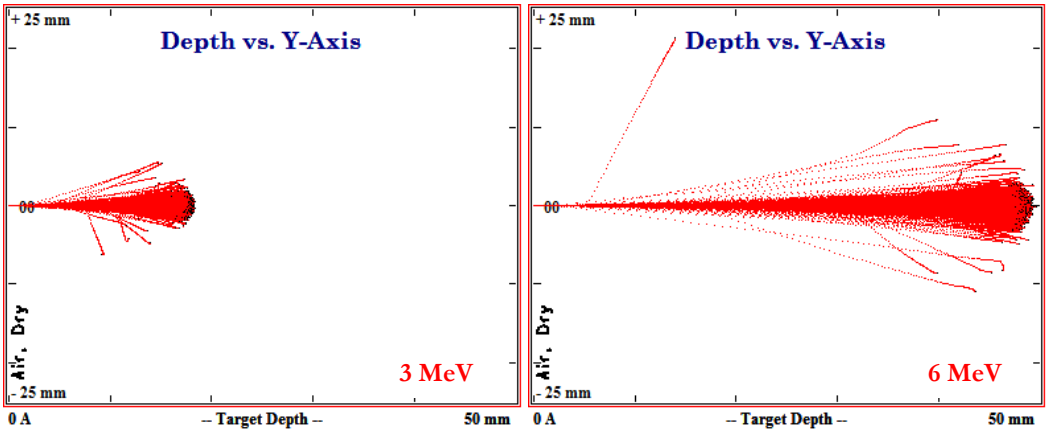

Figure 26: The range of 3 and 6 MeV α-particles in air. Doubling the energy of the incident particles allow the particles to travel a higher distance in air. In this simulation, the range differs by a factor of 3. Results obtained using the state-of-the-art computer program SRIM.

CHAPTER 4

DOSIMETRY OF AN α-PARTICLE DEVICE FOR IN VITRO CELLS IRRADIATION

4.1 Introduction

Cell irradiation studies with α-particles play an important role for understanding the biological effects produced by low doses of high LET radiation. Exposure devices for similar experiments were constructed using isotopes of Am-241 [Neti *et. al.*, 2004 and Ishigure *et. al.*, 1991], Pu-238 [Inkret *et al.*, 1990 and Metting *et al.*, 1995] and Po-210 [Soyland and Hassfjell, 2000 and Szabó *et al.*, 2002]. The α-particle irradiator designed by Noele Meeting [Metting *et al.*, 1995] includes a Plexiglas beam delimiter and a stainless steel honeycomb delimiter to constrain the direction of the beam. Special features of this irradiator also include a helium environment, a reciprocal collimator that allows the utilization of collimator setups with different transmission factors to achieve different dose–rate values and a precision photographic shutter that allows the accurate delivery of doses as low as 0.01 mGy to the monolayer of cells. Based on the design described, Prasad Neti [Neti *et al.*, 2004] built an advanced multi-port alpha-particle irradiator. The major changes are an electronic shutter system, multiple exit windows to facilitate simultaneous irradiation of replicate samples and/or different fluences, and the use of inexpensive and readily available Am-241 sources as opposed to a Pu-238 source.

A new experimental design for α-particle irradiation of cells *in vitro* based on ^{210}Po radioactive source was built by Soyland and Hassfjell [Soyland and Hassfjell, 2000]. This irradiator includes a collimator of polyethylene with 8 mm long and is open to surrounding air. A custom-made cell dish, in which cells grow directly on a 12 μm thick α-particle detector, is irradiated from below on top of collimator. Based on the design described above, Szabo [Szabó *et al.*, 2002] designed an *in vitro* cell irradiation system using a Po-210 source that will be described in detailed in section 4.2.1, since in this work we used this irradiator.
The aim of our work was to investigate the effect of α-particle irradiation, emitted by a ^{210}Po source, on human lung cancer cells *in vitro*, with the purpose of exploring the possibility of increasing cellular damage due to direct and bystander effects at the low α-particle dose region. In order to successful undertake this investigation; a well-characterized irradiation device is mandatory. The energy spectrum at the cell monolayer was obtained using a passivated implanted planar silicon (PIPS) detector. The energy spectrum was then converted in LET spectrum by using published energy-LET tables for α-particles available in the NIST database [Berger *et al.*, 2005]. Simulations were performed in order to understand the influence of different incident angles at the cell monolayer as well as to study the behavior of the different LET values in the cell monolayer. Finally, the average dose rate to the monolayer of cells was calculated from the average α-particle flux and LET values.

4.2 Materials & Methods

4.2.1 The α-particle irradiator setup

As mentioned before, the ^{210}Po irradiator used in this work is the device developed by Szabó [Szabó *et al.*, 2002] (see **Figure 27**). The ^{210}Po isotope was chosen in this work, because it is a monoenergetic (5.297 MeV) and practically pure α-particle emitter. The activity of the source was 200 kBq (26.June.2006). It was electroless deposited on the surface of silver discs of 130 mm diameter and 0.2 mm thickness, with a useful diameter of 90 mm. The source was fixed in aluminum holders. A brass collimator can be used to produce a parallel α-particle beam and to provide a perpendicular angle of incidence in the cell monolayer. The collimator, fixed to the holder with a removable nut, has 46 cylindrical channels of 2 mm diameter and height of 6.2 mm, thus it covers 18% of the useful surface. Both the source and collimator are covered with Mylar foils of 2.2 μm thickness to avoid the accumulation of dust and other agents on the source. During the execution of this work, the collimator was not used due to the low activity of the source.
Petri dishes with 35 mm diameter and 10 mm height type NUNC (Denmark) were used as holders for cell cultures. The petri dishes are placed in an aluminum support allowing exposure windows with the same diameter as the petri dishes (see **Figure 27** down). At the bottom of the dishes a hole, 15 mm in diameter, was cut out and covered by a Mylar foil of 6.3 μm in thickness. This was the base where the cells were grown. During irradiation this base is positioned at a distance of 2 mm above the exit window, so the α-particles traverse

2.2 μm Mylar foil, 2 mm of air and 6.3 μm Mylar foil before arriving to the cellular monolayer medium.

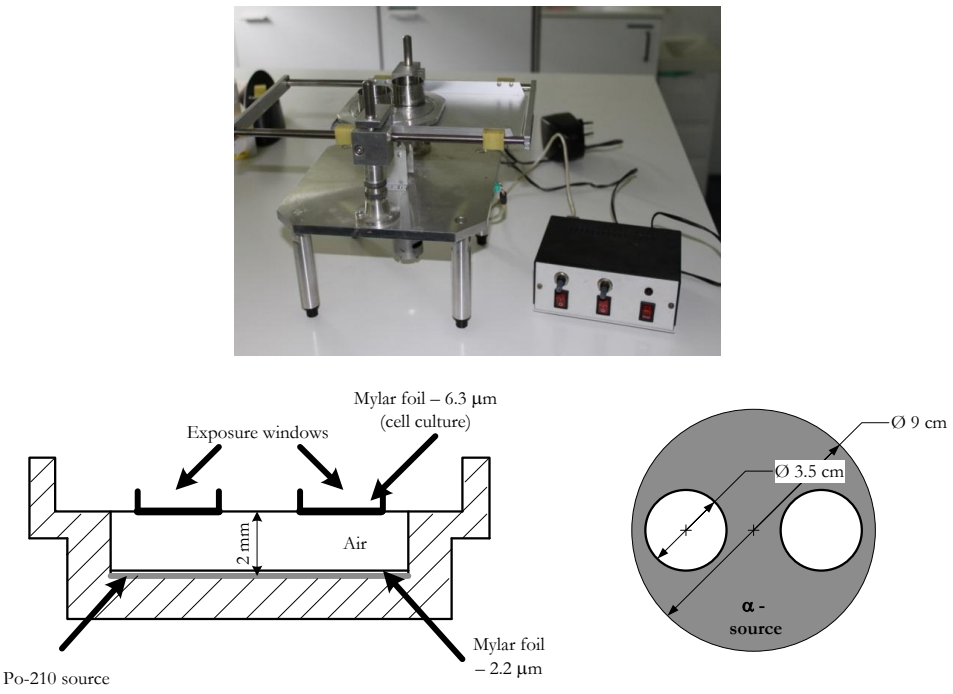

Figure 27: Irradiation device (up), cross – section of the exposure device (down).

4.2.2 Monte Carlo modeling and simulation of the experimental setup

Due to the absence of the collimator, the α-particles hit cells from different incident angles, leading to different path lengths through the cells medium and hence to different absorbed doses. As previously mentioned, the irradiator allows the utilization of a collimator, however due to the lower activity of the source; the irradiation of cells was performed without the collimator. As a consequence a set of computational were performed to extract the energy and LET spectra at the cell monolayer.

Two Monte Carlo (MC) simulation programs were used;

- SRIM (Stopping and Range of Ions in Matter) [Ziegler et al., 2008] and
- MCNPX (Monte Carlo N-Particle eXtended), version 2.5.0. [Pelowitz, 2005]

Both programs use MC methods to perform particle transport simulation of individual particles and record the key particle parameters at each position, namely direction (direction cosines can be obtained from the three components of the linear momentum vector), mass and energy of each track. However, the output produced by both codes is different. SRIM allows a microscopic evaluation of the damage in materials imparted by radiation, briefly; it

lists the 3D dimensional distribution of the ions in the material, the concentration of vacancies, sputtering rate, ionization, and phonon production in the target material and the energy deposition rate. Differently, MCNPX allows a macroscopic evaluation of the damage induced by radiation due to its high accuracy for defining complex geometries, in which dosimetric quantities such as flux and dose over a volume could be computed with different tallying methods.
SRIM was used in the first stage of the dosimetric study, in order to optimize the experimental apparatus, namely choosing different distances between the source and the cellular monolayer to determine the optimum distance for obtaining a higher LET value at the cell monolayer. On the other hand, MCNPX was used to study the behavior of α-particles through matter, including the cellular monolayer and also to determine the dose rate value at the cellular monolayer. MCNPX was also used to evaluate how the LET value varies with depth in the cell monolayer.

4.2.2.1 SRIM

SRIM is part of a package used worldwide to calculate the stopping and range of ions (up to 2 GeV/amu) in matter using a quantum mechanical treatment of ion-atom collisions. TRIM (the Transport of Ions in Matter), another component of the package, accepts complex targets made of compound materials with up to eight layers, each of a different material and calculates both the final 3D distribution of the ions and also all kinetic processes and phenomena associated with the ion's energy loss: target damage, sputtering, ionization, and photon production, amongst others. All atom cascades in the target are followed in detail. The version used in this work was SRIM 2008.

4.2.2.1.1 Structure of the program

In order to run the simulation, two types of information were needed: the Ion Data and the Target Data. The Ion Data included the name of the ion, the initial energy of the ion and the angle of incidence. The target consisted of multiple layers. The Target Data included the material and thickness of the all compounds that alpha radiation will pass through before hitting the monolayer of cells in the medium. The program includes some common target compounds, included Mylar film ($C_{10}H_8O_4$), air dry and water liquid used in this work. Once a material was chosen, the program calculates the overall density and the components of the material automatically. The program tracks the path of each individual ion and produces a record for it. The movement of all the ions could be visualized in four different views: XY Longitudinal, XZ Longitudinal, XY Ions Only, YZ Lateral. All the input information and results were output to the SRIM sub-directory "SRIM Output" in txt files.
By choosing different inputs, the SRIM simulations were used to examine the optimum LET value at the cellular monolayer. This previous study allowed us to establish a certain distance between the α-source and the cell monolayer. Additionally, by choosing different angles of incidence of the α-particles, we quantified the most common angle of incidence into the monolayer, and consequently the variability of LET values.

4.2.2.2 MCNPX

Over the years, different Monte Carlo simulation programs used to performed particle transport simulation using Monte Carlo (MC) methods have been gradually improved. These computer programs codes become an important and crucial tool for understanding all phenomena involving the interaction of ionizing radiation with matter. Some of the most used simulation programs for Monte Carlo methods are EGS4 [Nelson and Rogers, 1998], MCNPX [Pelowitz, 2005], PENELOPE [Baró *et al.*, 1995], FLUKA [Ferrari *et al.*, 2011], GEANT [Agostinelli *et al.*, 2003]. The accuracy of these methods depends on the type of particles and on the energy ranges of physical interactions considered, on the accuracy of the materials and their geometric description, on the accuracy of the source term definition, among others.

MCNPX is a general-purpose Monte Carlo code for particle transport, with applications in several fields such as dosimetry, detector designs, shielding calculations, medical physics, and nuclear safeguards, among others. MCNPX 2.5.0, the version used in this thesis, is a superset of MCNP4C [Briesmeister, 2000] and MCNPX 2.4.0 [Waters, 2002]. The improvement involved a formal extension of MCNP to all particles and all energies; improvement of physics simulation models; extension of neutron, proton, and photonuclear libraries to 150 MeV; and the formulation of new variance-reduction and data-analysis techniques [Pelowitz, 2005]. MCNPX is written in Fortran 90, with some C++ routines, mainly involving graphics capabilities.

4.2.2.2.1 Transport and interaction physics

4.2.2.2.1.1 Charged Particle Transport

In MCNPX, for heavy charged particles transport, the formalism used by Bethe-Bloch was improved by using the values of I, recommended in ICRU report 37 [ICRU 37, 1984] (see **section 3.2.3**). Moreover, the density-effect factor correction, δ (see **section 3.2.3**), was also improved using for this the parameterization of Sternheimer [Sternheimer *et al.*,1982]. The shell correction, (C/Z), for stopping power have been tailored from Janni [Janni, 1982], which tabulates values for 92 elements and 63 compounds. MCNPX does not track transverse displacements in charged-particles subsets, being the theory of angular defections addressed [Waters *et al.*, 2007]. For energy straggling, MCNPX uses the Vavilov logic [Prael, 2000].

4.2.2.2.1.2 Data Libraries

In MCNPX, several data libraries are available, such as; continuous-energy neutron, photonuclear, proton, neutron thermal data, photoatomic (up tp 100 GeV), and electron interaction data (up to 1 GeV). With the exception of, photoatomic and electron data which depends only on Z, all the other libraries contain isotopic data. The aforementioned data libraries are valid to use for energies below ~150 MeV, otherwise some other models such as; Bertini [Bertini, 1963], ISABEL [Yariv and Fraenkel, 1979 and Yariv and Fraenkel, 1981], CEM03 [Mashnik *et al.*, 2006], and INCL [Cugnon *et al.*, 1997], should be used.

Data libraries for photon interactions include cross sections for Thompson, Compton, photoelectric and pair-production effects. For electron interactions the available cross sections are for ionization and bremsstrahlung effects. Finally, for nuclear and photonuclear interactions, the data libraries contain total, elastic, (n, xn), fission, and (n, γ) cross sections. MCNPX does not access directly the aforesaid data libraries. These data must be, first, processed into ACE format, by codes such as NJOY [MacFarlane et al., 1982a and MacFarlane et al., 1982b].

4.2.2.2.2 Structure of the *input file*

In MCNPX, all the information for the simulation to be developed is inserted into one file; a *.txt* file, containing a deck of control cards for running the simulations.

The format of this file should be divided in four main cards; **title**, **cell**, **surface** and **data** cards (see **Figure 28**). Cell, surface, and data cards must all begin within the first five columns, and, the entries should be separated by one or more blanks.

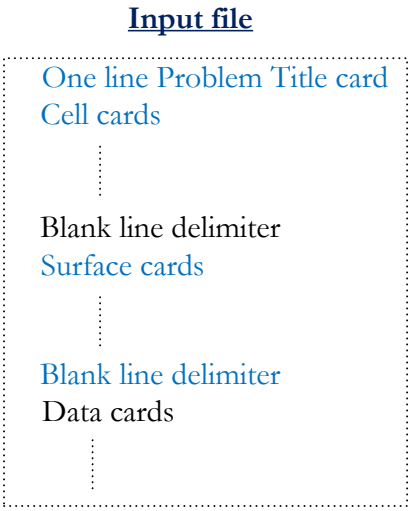

Figure 28: Input file structure

On the **title card**, the user only has to specify a title for the simulation problem.

On the **cell card**, the user must describe the volumes, cells, which define geometrically the physical system. In this definition, the following information, ordering like it is described, is required for each cell:

- The cell number
- The material number which fills the volume represented by the cell. The material is described on a material card (Mn), within the data card, with *n* representing the material number specified for each cell.
- The density of the referred material. A positive entry means that the density in units of 10^{24} atoms/cm3, while a negative entry represents the density in g/cm^3.
- The surfaces (described on the surface card) that bound the cell. In this, side pointers must be defined before the number of the surface. This side pointer will indicate the direction, on the xx, yy, and zz axis, of each surface, according to the desired volume.

In a void cell, both the material and density should be zero (0).

The **surface card** must include all the surfaces necessary to implement the desired geometry. The first entry represents the number of the surface, followed by a mnemonic indicating the surface type. Then, according to the surface, the numerical coefficients of the surface equation must be indicated in the proper order. A complete list of the available surface equations are described in [Pelowitz, 2005].

The **data card** must be fulfilled with the following information. A more detailed description is depicted in the subsequent sub-sections.

- Mode. The mode card indicates to MCNPX the type of the particle to be tracked. In this, a mnemonic, for each type of particles, should be used. For example, N for neutrons, P for photons, E for electrons and A for alpha-particles.
- Cell and surface parameters. In this, an importance, for particle tracking or not, should be indicated for each cell. If 1, the particle is transported within the cell, otherwise if 0, the program does not take into account its contribution.
- Source specification, SDEF. The SDEF card defines the parameters of the source. Some of which are:
    - POS – allows specifying the position of the source.
    - CEL – defines the starting cell number of the cell
    - ERG – defines the starting energy of the source
    - WGT - defines the starting weight of the source particles
    - PAR – defines the source particle type.
- Tally specification, Fn and En. The tally cards allow the user to specify the desired output from the Monte Carlo calculation.

- Material specification, Mn. This card is used to specify the isotopic composition of a material and the necessary cross sections.
- Problem cutoffs, NPS. It is used to specify the parameters to terminate the execution of MCNPX. NPS means number of particles to be simulated.

4.2.2.2.2.1 The definition of the geometry

The geometry description in a Monte Carlo treated problem is crucial. The particles interact differently depending on the type of crossed material and for that reason, the accuracy of the geometry description is important.

MCNPX allows the description of complex geometries, from smaller (micrometers) up to larger (meters) dimensions. The MCNPX geometry is described by an arbitrary, user-defined, three-dimensional configuration. It allows defining volumes – denominated, *cells* – from the intersection, unions, and complements of the regions bounded by surfaces. Surfaces are defined by supplying coefficients to the analytic surface equations or, for certain types of surfaces, through geometric shapes such as cubes, cylinders and spheres, among others. Voxel geometries are also available in MCNPX. For this, a specific tool, integrated on the Image J program, was implemented. The available tool to plot and debug the geometry, X-Deep, is available for free.

4.2.2.2.2.2 The definition of the materials

The materials used on MCNPX should be specified by the following card:

Mm ZAID1 fraction 1 ZAID2 fraction2 …

The m corresponds to the material number on the cell card and ZAID is the nuclide identification number, where Z is the atomic number of the element or nuclide and A the mass number of the nuclide. The atomic fraction of each element into the material should be placed after the ZAID. A negative entry, on the atomic fraction, represents the weight fraction.

4.2.2.2.2.3 The Source definition card: *SDEF* card

MCNPX code allows the user to specify a wide variety of source conditions. Probability distributions may be specified for source variables, such as energy, time, position, and direction. Not only a point source could be used, geometrical extent of the source can also be given. Additionally, source variables may depend on other source variables (for example, energy as a function of angle). In addition to probability distributions for source variables, certain built-in functions are available, including; analytic functions for fission and fusion

energy spectra such as Watt, Maxwell, and Gaussian spectra; Gaussian distribution for time; and power law or exponential for direction, radius and extension.

4.2.2.2.2.4 The *tallies*

The term *tally* is a concept used in the MCNPX program that is associated with the type of format and contents of the simulated results (flux of particles through surfaces, energy deposited or absorbed dose within a volume, charge deposition from a detector, etc.) and the way they are displayed. The code allows eight different types of *tallies* described in the following table.

Table 2 – Type of *tallies* that can be used in MCNPX.

Mnemonic	Tally description	Units
F1	Current integrated over a surface	Particles
F2	Flux averaged over a surface	Particles / cm^2
F4	Flux averaged over a cell	Particles / cm^2
F5	Flux at a point or ring detector	Particles / cm^2
F6	Energy deposition averaged over a cell	MeV/g
F7	Fission energy deposition averaged over a cell	MeV/g
F8	Energy distribution of pulses created in a detector	Pulses or MeV
+F8	Charge deposition	charge

The MCNPX code, also, allows plotting *mesh tallies*. This are fluxes, heating, doses, fluencies, and other tally quantities plotted on a 3-D mesh, which could be rectangular, cylindrical, or spherical.

In this work, the F8 *tally* was used in order to determine the energy distribution in the detector.

4.2.2.2.2.4.1 The *tally* F8

The *tally* F8 is different from the other *tallies*, described in **Table 2**, for being a pulse height tally, and not a track length estimator, as some of the remaining. It provides the energy distribution of pulses created in a *cell* that describes a physical detector. The reason why F8 *tally* is unique is because it requires the entire set of tracks for a history to be completed, on the other hand the track length estimator *tallies* are calculated as soon as the particle exists or collides in a cell.

The way as the events are accounted is illustrated in **Figure 29**.

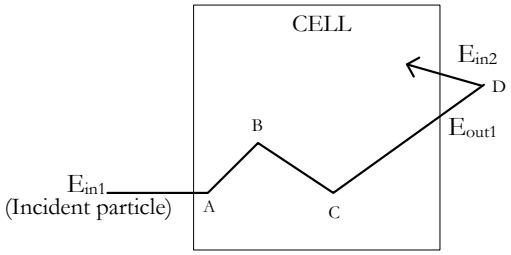

Figure 29: Example of a particle´s trajectory in a cell. In this, the particle experiences a set of interactions, resulting in several tracks, before leaving the cell. The track length estimator tally scores a different value of energy for each track. The resulting energy, using the pulse height tally, is the accounting of all energies (entering and leaving the cells) involved, i.e., in this example, the resulting energy is equal to $E_{in1} + E_{in2} - E_{out1}$.At the end of history, the account in each cell is dividing by the source weight determining in which energy bin the score is put in. *Adapted from* [RSICC, 2006].

4.2.3 Dosimetry experiments

4.2.3.1 Alpha-particle energy spectra

A Si(Li) surface barrier detector for charged particle spectroscopy (Canberra, model LEC 100-1000) was used to measure both the flux and the energy spectra of the ^{210}Po α-particles under different conditions. The active area of the detector is 100 mm^2 and its energy resolution (FWHM) is 30 keV for the ^{210}Po energy. A multichannel analyzer Canberra ASA-100 with the software package Genie- was used to obtain the alpha particle energy spectrum. The detector was calibrated by using a custom-made ^{232}U source in vacuum. The energies of the peaks used in the calibration were the following: 8.785 MeV (Po-212), 6.777 MeV (Po-216), 6.287 MeV (Rn-220) and 5.684 MeV (Ra-224). The ^{210}Po α-particles energy spectrum were measured after crossing the 2.2 μm Mylar® cover and and extra 6.3 μm Mylar foil in which the cells are cultured.

4.2.3.1.1 Energy to LET conversion

The energy spectrum of the alpha particles at the cell position was converted to an LET spectrum by a point by point interpolation using published Stopping Power and Range tables from the National Institute of Standards and Technology database.
Using the simulation methods described above, the LET spectrum at cell position was also obtained and compared to the obtained by the experimental methodology.

4.2.3.1.2 Dose calculation

Using the methodology of Charlton and Sephton [Charlton and Sephton, 1991], the absorbed dose received (D_{cell}) by a single track through the cell nucleus can be calculated according to the following equation:

$$D_{cell}\ (Gy) = \frac{0.16 * LET\left(keV/\mu m\right)}{A(\mu m^2)} \quad (19)$$

where A is the cross-sectional area of the cell nucleus. The factor 0.16 is a unit conversion factor. This formula is valid where the ranges of α-rays are small compared with the nucleus diameter. The average absorbed dose rate at the cells monolayer was determined using **equation 20**.

$$\dot{D}(Gy) = F \times A \times D_{cell} \quad (20)$$

where F is the fluence of particles hitting the cell monolayer per μm^2. The dose rate values were obtained by using **equation 20**.

4.3 Results

4.3.1 The simulation results

4.3.1.1 Results from SRIM

In the absence of the collimator, the α-particles hit the cell monolayer from different incident angles, leading to different path-lengths through the monolayer and hence to different energy deposition and absorbed doses. The energy and LET values at the cell monolayer were investigated using the simulation program SRIM. In order to run the simulation, two types of information are needed: The Ion Data and the Target Data. The Ion Data included the ion type, the initial energy of the ion and the angle of incidence. In this work, the ion was He; the initial energy was equal to 5.297 MeV and the angles of incidence range from 0° to 70°. The target consisted of multiple layers, such as, 2.2 μm of Mylar, 2 mm of air, 6.3 μm of Mylar and finally, 10 μm of water liquid. The Target Data included the material and thickness of the all compounds the alpha particles will cross before hitting the cell monolayer. The program includes some common target compounds, incorporating the used in the simulations and described above.

After a set of experiments, we came to conclusion that the optimum distance between the source and the cell monolayer was to be 2 mm, since under this conditions the dose rate value is close to the higher possible value.

By varying the angles of incidence, i.e. defining different angles for incident particles on the cellular monolayer, it is visible from Figure 30 that the maximum values of LET are achieved in the range of 50° to 60°.

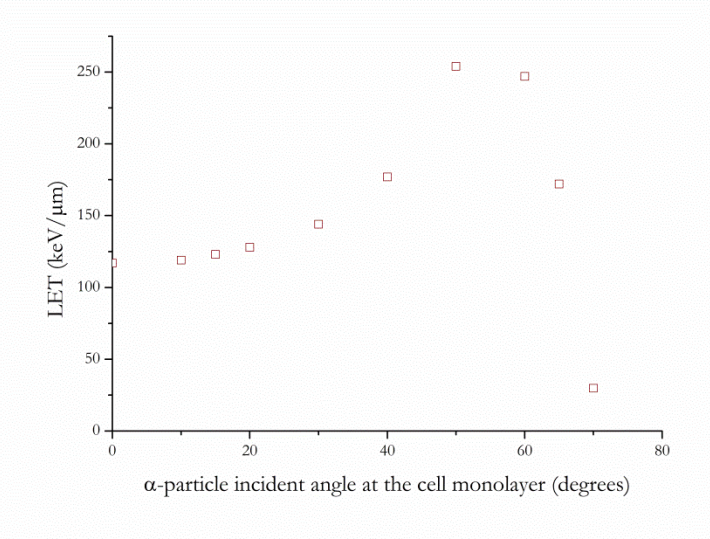

Figure 30: Study of the LET as a function of incidence angles of the alpha particles in the cell monolayer. Note that, 0° of incidence means the beam is perpendicular to the target.

With higher incident angles, α-particles have to travel a higher distance to reach the cellular monolayer. Consequently, its entry energy is lower causing them to lose much of their energy within the monolayer of cells.

4.3.1.2 Results from MCNPX

4.3.1.2.1 Modeling and simulation of the response of the Sil(Li) detector

As described in the previous section, a Si(Li) detector was used to obtain the energy spectrum of the particles leaving the cell monolayer. This spectrum was used to verify the MCNPX simulation of the entire setup. MCNPX is suitable for modeling the detector response, since it contains a special tool for energy scoring and averaging each energy bin (the *Tally F8* previously described). A standard Gaussian energy broadening of the energy deposited in the Si(Li) detector was used to define the full width at half maximum (FWHM) and to obtain a realistic spectrum:

$$\text{FWHM} = \left(0.1088 - 0.0159\sqrt{E}\right) \quad (\text{MeV}) \tag{21}$$

The parameterized function, **equation 21** represents a linear fit of the observed energy resolution values using the U-232 calibration source. A schema of the Si(Li) detector structure is presented in **Figure 31**.

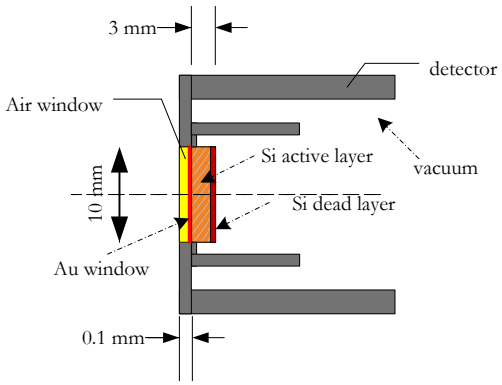

Figure 31: Schematic representation of the configuration used to model the response of the Si(Li) detector with MCNPX. All the components are cylindrical in shape. Dimensions are not to scale.

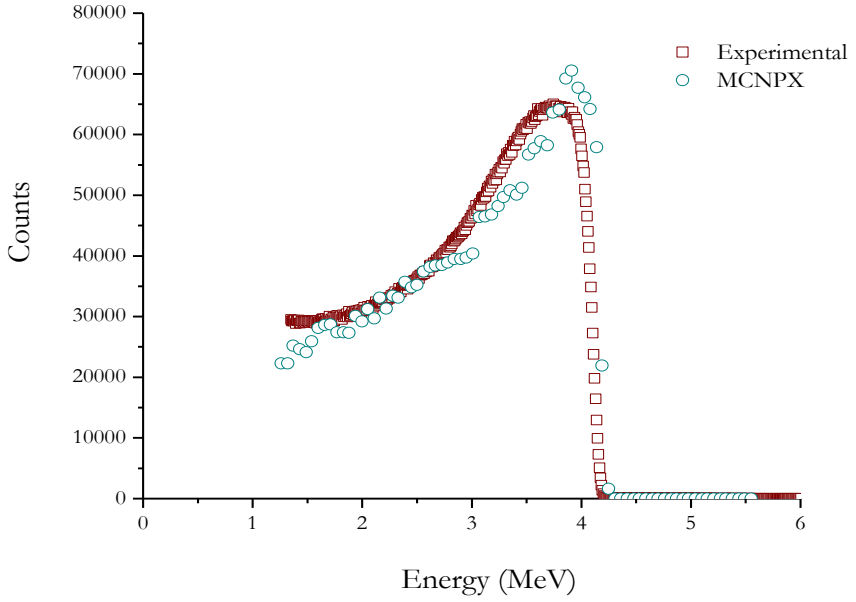

Figure 32: Comparison between the measured alpha-particles energy and the MCNPX simulation.

A key factor in quantitative analysis using a Si(Li) detector is the detector intrinsic efficiency. It depends on the crystal material and dimensions, the thickness of the gold simulated energy spectra in **Figure 32** could be explained by these factors.

4.3.1.2.2 Modeling and simulation of the experimental setup

The MCNPX code was used to simulate the experimental setup and further to obtain the LET values as a function of deep penetration at the cell monolayer. The geometry and materials of the experimental setup were accurately modeled and implemented in MCNPX and all the experimental conditions were maintained, i.e., same distance between the source and the Mylar® layer were the cells are cultured as well as the thickness of both Mylar® foils.

In order to study the dependence of the LET value with the cellular monolayer depth, a MCNPX simulation dividing the cell monolayer in 10 water sub-layers of 1 mm height each and 3.5 cm in diameter was performed. This model is closer to the experimental cell irradiation condition for the reason that, the cell culture is irradiated, when the cells reach about 85-90% of confluence. Dividing the monolayer into 10 equal parts of 1 μm height, we analyzed the influence of the energy deposition per μm of depth. **Figure 33** presents the LET value obtained in these conditions.

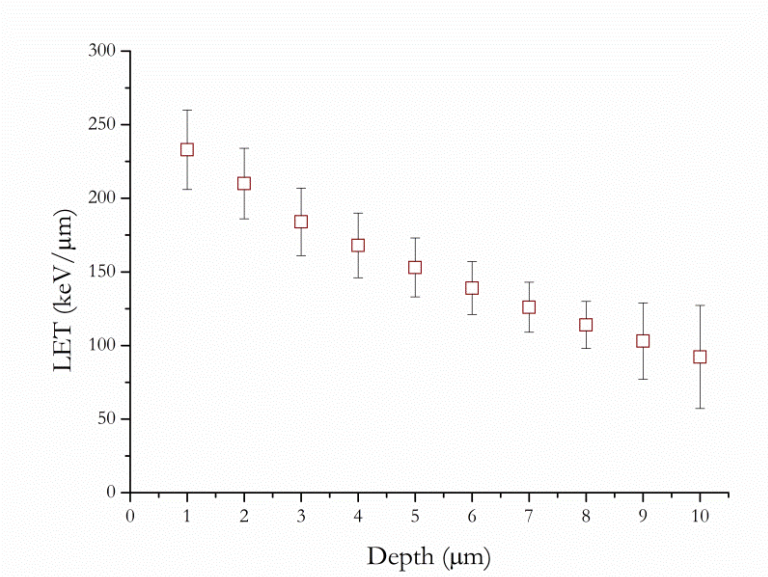

Figure 33: Results obtained by MCNPX for the dependence of LET values with the water monolayer depth.

The result in **Figure 33** seems to indicate that α-particles with long paths in the Mylar layer exist and hit the monolayer with a lower energy, and consequently depositing a higher energy value. The main contribution of these α-particles will thus be in the first μm of the cellular monolayer. The average value of LET obtained by MCNPX simulations was (151 ± 27) keV/μm, which is in good agreement with the experimental value. Using the equations (19) and (20) the averaged value of the dose rate obtained by MCNPX is

$$\dot{D}_{MCNPX}=29.629 \pm 0.004 \text{ mGy/min}$$

in good agreement with the obtained experimental value of 32.1 ± 1.9 mGy/min (the uncertainty is purely statistical, from the Monte Carlo simulations).

4.3.2 The dosimetry measurements

4.3.2.1 Energy and flux measurements of the ^{210}Po source

As previously stated, a Si(Li) surface barrier detector for charged particle spectroscopy (Camberra, model LEC 100-1000) was used to measure both the flux and the energy spectra of the Po-210 α-particles under different conditions. The detector active area is 100 mm^2; the energy resolution is 30 keV. A multichannel analyzer software package (Genie) was used to obtain the alpha particle energy spectra. The detector was calibrated by measuring a standard U-232 source in vacuum.

Figure 34 illustrates both the spectra for U-232 and Po-210 in vacuum. The **Figure 34**, also, shows the peaks at the U-232 spectrum used for the calibration.

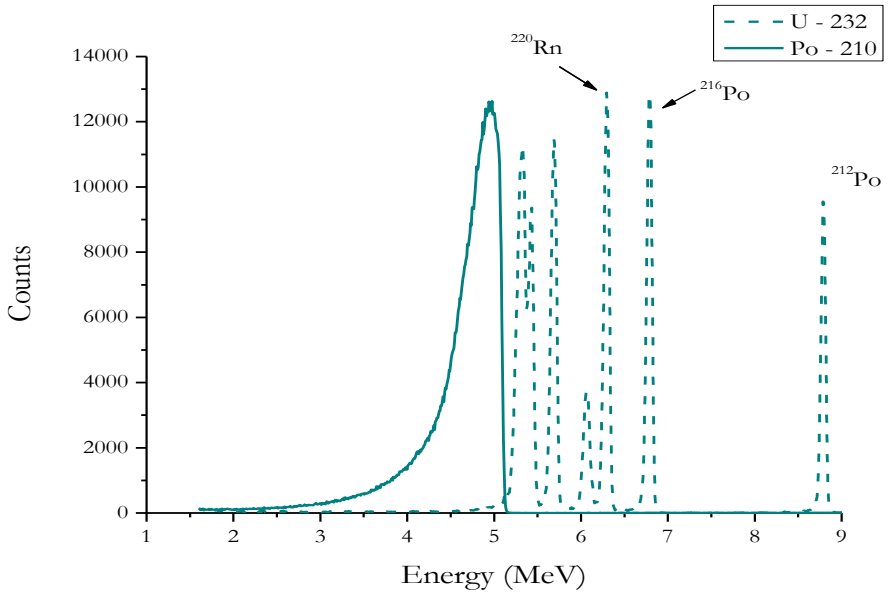

Figure 34: Energy spectra of ^{232}U and ^{210}Po. The dash curve corresponds to the energy peaks used to perform the calibration. The peak energies used in the calibration are the following: ^{212}Po– 8.785 MeV, ^{216}Po - 6.777 MeV, ^{220}Rn - 6.287 MeV and ^{224}Ra – 5.684 MeV

From the calibration procedure, the following relationship was derived:

$$\text{Energy}=0.3028\ (\pm\ 0.0025)+\ 8.79\ \text{x}\ 10^{-3}\ \left(\pm\ 3.35\ \text{x}\ 10^{-8}\right)\ \text{*channel number (MeV)} \qquad (22)$$

Both the energy spectra and the flux of the α-particles emitted from the ^{210}Po sources were measured directly above the 6.3 μm– thick Mylar membrane, i.e. in the cell irradiation position. The E_{max} is progressively attenuated and the peak is broadened due to the energy straggling of the alpha particles trough the 2.2 μm of Mylar, 2 mm of air and 6.3 μm of Mylar. Due to the un-collimated nature of this planar source, the energy spectrum is skewed with a tail of lower energies. The surface barrier detector was also used to measure the alpha particle flux, dividing the total number of recorded particles by the measurement time and the effective detector area.

4.3.2.2 Alpha-particle energy and LET spectra at the cell irradiation position

The measured energy spectrum of the ^{210}Po was also taken under the same experimental conditions when compared with the cells irradiation in laboratory. In this case, the detector was positioned above the Mylar® where the cells are cultured with an existing distance of 2

mm between the source and the referred Mylar®. **Figure 35** displays the energy spectra at the cell monolayer position, i.e., at the same position as in laboratorial irradiations.

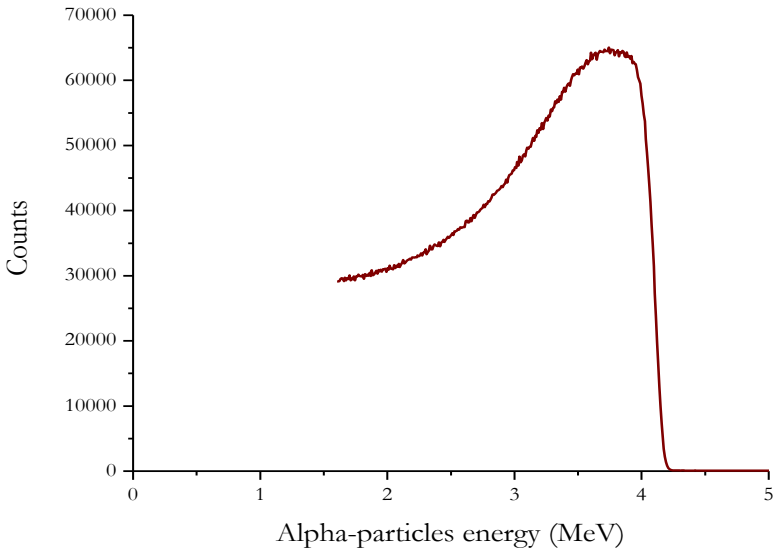

Figure 35 – Energy spectrum at cell position

From **Figure 35**, it can be spotted a low energy tail, due to the absence of collimator during this calibration. The collimator was removed because it covers 18% of the useful surface and due to the lower activity of the source, the dose rate value will be low and consequently the time of cell irradiation will be high. In order to characterize the influence of the absence of the collimator at the cell monolayer, i.e., to study how the angles of incidence of the alpha particles at the cell monolayer contribute to the overall LET value, some simulations using SRIM were performed.
Detailed information about the source is known, including the nominal activity, however the measurement of the alpha-particle flux was also obtained by using the Si(Li) detector. The obtained count rate was 360 α-particles/cm^2.s. Three independent spectra were obtained in order to address the reproducibility of the system. The reproducibility error of the system was 2.5%. So the count rate was 360 ± 9 α-particles/cm^2.s.

The geometric efficiency of the system is 2.73 $x10^{-3}$, so the emitted number of the particles was calculated taking into account this value. The geometry efficiency was obtained by using a Monte Carlo code developed by Professor Luis Peralta. In this, it is necessary to fulfill an input file with the following information:

- Number of events
- Radius of the detector, R.
- Distance between the source and the detector, d.
- Deviation of the source according to the axis, h.

- Radius of the source, r.
- Length of the source, L.

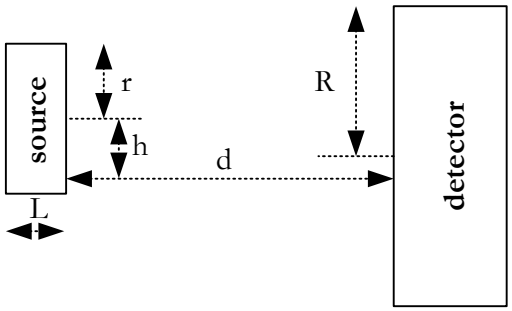

Figure 36: Schematic view of the parameters included on the input file.

The energy spectrum of the alpha particles at the cell position was converted to an LET spectrum by a point by point interpolation using published Stopping Power and Range tables from the National Institute of Standards and Technology database. As an alpha particle travels through matter, it loses energy continuously and a peak occurs because interaction cross section increases as the charged particle's energy decreases. This is the called Bragg peak.

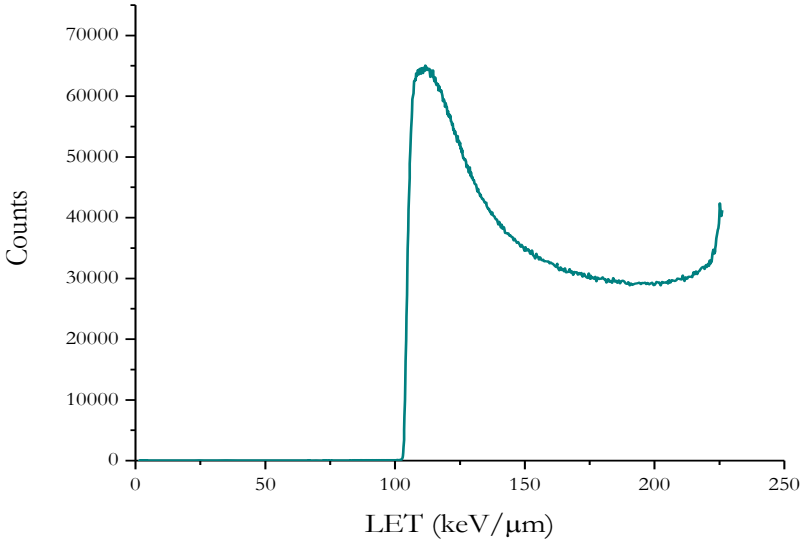

Figure 37: LET spectrum at cell position

From the LET spectra represented in **Figure 37**, an average LET value was obtained by using the alpha particle counts per channel as the weighting factor. The average LET of the alpha particles at the cell position was 154 keV/μm. The uncertainty in stopping power

values is expected to be 5% [ICRU, 93] depending on the energy value of the particles and the materials composition. So, the average LET value was (154 ± 8) keV/μm.

4.3.2.3 Dose calculation

As described in section 4.2.3.1.2 the average dose in the cell monolayer was obtained by **equation 20**. At the beginning of the study, the number of α-particles emitted by the source was 1697 $\alpha/cm^2.s$. The initial dose rate used in this work was equal to 25 mGy/min. According to the literature, the ^{210}Po has a half-time of 138 days, for that reason, whenever a new irradiation is performed, the value of the dose rate should be verified.

4.4 Discussion

As mentioned above, in order to deliver an accurate value of dose into the cellular monolayer a robust dosimetric study of the experimental setup is mandatory and the validation of the Monte Carlo modeling and simulations. The main goal of this thesis is to apply different cytogenetic techniques to quantify the response of cells when exposed to different doses of Po-210. As so, this chapter described the dosimetric characterization of the irradiation device, suitable for studies *in vitro*, used in this work.

In the absence of a collimator, if α-particles may have to travel through different materials (e.g. Mylar and/or air used in this work) before reach the target, the trajectory of each particle became singular. As a consequence, the angle of incidence of each particle in the target is variable, leading to a large range of absorbed dose values delivered by the α-particles. This behavior is corroborated in **Figure 35** which display the measured energy spectrum using a PIPS detector.

Measurements also revealed, in the absence of a collimator, a low energy tail with energies down to 1.5 MeV. By using a point-by-point interpolation, the energy spectrum, measured by the PIPS detector, was converted into a LET spectrum using the NIST database. As a step further, the mean dose in the cellular monolayer was calculated using the aforementioned LET values.

From **Figure 30** it can be spotted that particle reaching the target with higher angles of incidence, i.e. having a higher path before reaching the target, impart a higher amount of energy per μm in the medium. This conclusion came out by using the SRIM code. Also, it can be concluded that the higher LET value is obtained for an incidence range of 50 – 60º.

The MCNPX results showed that the mean dose value at cellular position was in accordance with those obtained by the interpolation method. Moreover, they showed that the α-particles reaching the monolayer with higher angles of incidence deposit a great amount of energy in the entrance of cells, meaning that, the main contribution to the overall dose belongs to the first micrometers of cells. This can be seen in **Figure 33**, where the cell was divided into 10 slices of 1 μm each being the LET value obtained in each layer.

From this study, regarding not only the dose deliver but also the behavior of the α-particles before reach and throughout the cellular monolayer, the following can be summarized;

i) α-particles reaching the monolayer feature a wide range of incident angles. Higher values of LET were obtained for an incidence, at the cell monolayer, in the range of 50 up to 60º. These results show that a higher energy is delivered in the entrance of the cell, i.e. in the first μm of cellular thickness, having these particles a higher contribution to the overall dose delivered.

ii) The applied interpolation methodology, using the NIST database, to calculate the mean dose value, seems to be appropriate for this kind of studies. This conclusion arises from the agreement between the obtained dose values with those achieved by the Monte Carlo simulation codes MCNPX and SRIM.

CHAPTER 5

DOSE AND TIME DEPENDENCE OF TARGETED AND UNTARGETED EFFECTS AFTER α-PARTICLE IRRADIATION OF HUMAN LUNG CANCER CELLS

5.1 Introduction

The work presented in this chapter includes two distinct studies. At the beginning of this thesis, a first study was performed in order to evaluate the cellular response, using the A549 cell line, to α-radiation. As was mentioned in a previous Chapter of this thesis, the cells show a different behavior according to the radiation type, so, the aim of this first study was to assess the cellular lesion induced by the α-radiation in A549 cells. For that, the clonogenic and micronuclei assays were used to evaluate the cell survival and the cellular lesion, respectively. It must be mentioned that for this first study only direct radiation was considered.

Afterwards, a second study, also described in this chapter was undertaken. Having in mind, the lack of information about low dose exposures, and by observing an effect below 100 mGy in directly irradiated cells, we focused our study in the range under 100 mGy. Using the same methodology of Bowler *et al.* (2006), we investigated the time and dose dependence of targeted and untargeted effects in the region of very low doses (<100 mGy).

The study presented in this chapter includes three distinct cell culture conditions:

i) a culture of irradiated cells,

ii) a medium transfer culture with non-irradiated cells and

iii) a culture with irradiated cells after centrifugation.

Through the cytokinesis blocked micronuclei assay, we provide evidence that human A549 cells display a dependence of bystander effects with dose values, in the region of very low doses. Moreover, in this region, the induced cellular damage could not be negligible because it is similar to that obtained in cells directly irradiated. This trend persists in time, since after 6-7 population doublings the bystander effect remains in the culture leading to a cellular damage similar to that of directly irradiated cells. It has been reported that post-irradiation instability is not universally expressed in mammalian cells *in vitro* or *in vivo* [Kadhim *et al.*, 1995, Dugan and Bedford 2003 and Whitehouse and Tawn 2001]. Our study reveals that A549 cells express radiation-induced genomic instability after exposure to low doses of α-radiation, both in direct and bystander cells.

A set of *in vitro* studies have corroborated the existence of hyper-radiosensitivity (HRS) to doses below 0.3 Gy in several mammalian normal and tumour cell lines. Indeed, Mothersill *et al* (2002) studied the relationship between the bystander effect and the low-dose HRS, concluding that a considerable variation in the expression of both phenomena suggests that cell lines with a large bystander effect do not show HRS. On the other hand, Nuta and Darroudi (2008) concluded that the HRS might be causally related to bystander factors in the low-dose region. The results obtained and presented in this thesis seem to indicate a low-dose HRS effect at 10 mGy for bystander cells. Although our results suggest that the *bystander signal* has a prominent effect in the overall cellular damage induced, we cannot conclude about the influence of this in the HRS phenomenon. Analyzing the trend of the dose-response curves obtained, our results provide some evidence, albeit with no statistical relevance, for a higher sensitive effect of cellular response at doses lower than 10 mGy, both in irradiated and bystander cells.

Summarizing, the results presented in this thesis emphasize that the risks attributable to very low dose radiations encompass a complex cellular response and cannot simply be extrapolated from higher doses. Hu *et al.* (2006) showed that the bystander-signal derived from irradiated cells could be transferred to anywhere in the culture dish, so, the observed bystander effects described in our work show that a cellular lesion could be induced in the progeny of irradiated cells. These results raise important questions about potentially detrimental effects associated with low dose exposures, which are not included in a simply linear extrapolation.

5.2 Materials & Methods

5.2.1 Cells directly irradiated

A549 cells were cultured at 37°C with 5% CO_2 in DMEM medium containing 10% FBS and 1% penicillin-streptomycin solution. Log-phase cells were seeded onto 3.5 cm culture dishes with 6.3 μm of Mylar base 24 hours before irradiation. Cells at exponential growth were exposed to 2000, 1500, 1000, 500, 100, 50 mGy using the monoenergetic ^{210}Po source described in the chapter IV. Control cultures were submitted to the same experimental conditions but not irradiated. At 44h of incubation, cytochalasin B with a concentration of 2 mg/ml was added to the culture medium and 24h later the cytokinesis blocked micronuclei technique was performed as described in section 2.3.4.1.
To quantify the cell survival fraction, immediately after the irradiation, cells were pooled from the Mylar®, counted and seeded in Petri dishes with a concentration of, approximately, 200 cells.

5.2.2 Medium transfer study

A549 cells were cultured at 37°C with 5% CO_2 in DMEM medium containing 10% FBS and 1% penicillin-streptomycin solution. Log-phase cells were seeded onto 3.5 cm culture dishes with 6.3 μm of Mylar base 24 hours before irradiation. Cells at exponential growth were exposed to 1000, 500, 100, 50, 10 and 5 mGy using the monoenergetic ^{210}Po source described in the chapter IV. Control cultures were submitted to the same experimental conditions but not irradiated. Immediately after the irradiation, cells were recovered from the Mylar dish using 3 ml of total fresh DMEM medium. The pooled cells were counted and divided into separate groups each containing approximately the same number of cells; 1x 10^5 cells/flask in 5 ml of supplemented DMEM medium. The different groups used in this study are illustrated in **Figure 38** and can be described as follows;

Group I – Irradiated cells, collected in supplemented fresh medium, are re-cultured with an appropriate cell concentration for cytogenetic studies at 2 and 6 days post-irradiation. The re-culture implies that a small portion of irradiated medium, in contact with irradiated cells, coming from the Mylar dish remains in the culture.

Group II – On replicate Mylar dishes, cells were irradiated and collected in fresh medium as in Group I. These cells were collected by centrifugation at 1200 rpm for 5 minutes; the medium was filtered through a 2. 2 μm membrane filter (Millipore). The filtered medium was transferred to non-irradiated cells and cytogenetic studies were performed 2 and 6 days after irradiation. This medium will be denominated as irradiated medium, in the sequence.

Group III – The irradiated cells collected from Group II were cultured in an appropriate concentration for cytogenetic studies 2 and 6 days post-irradiation. The main difference between this and the group I is that in this case the radiation induced bystander effect is minimized due to the re-suspension in supplemented fresh medium after centrifugation.

In all groups, in order to maintain a non-confluent monolayer the referred appropriate concentration of cells denotes to approximately 1000 cells/culture for studies after 2 days of irradiation, and approximately 200 for delayed studies. To analyze the cellular survival, after the time of incubation (2 or 6 days), cells were seeded in an appropriate dilution (± 200 cells per culture) within Petri dishes and incubate for more 10 days. In **Figure 38**, the label control refers to non-irradiated cells maintained in the same conditions as the irradiated ones.

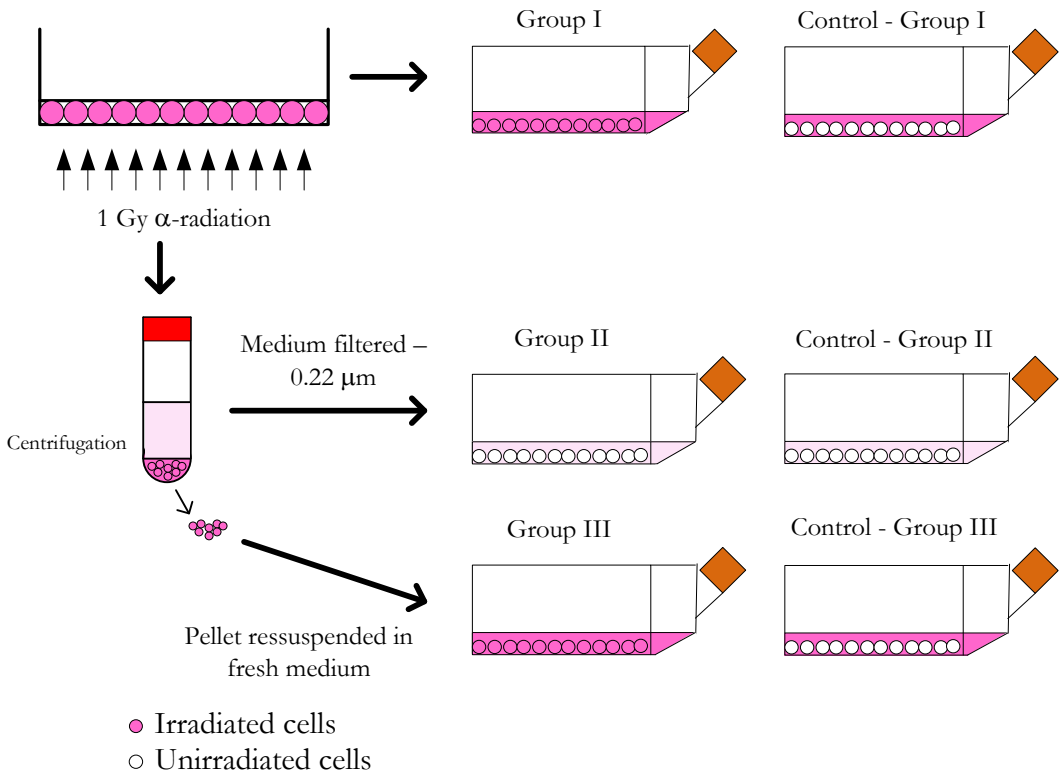

Figure 38: Medium transfer study for 1 Gy of exposure; the same methodology was used for the others values of dose. In group I irradiated cells were cultured with fresh medium after exposure to the aforementioned radiation doses. In group II, non-irradiated cells received irradiated medium. Finally, group III corresponds to irradiated cells cultured after centrifugation with supplemented fresh medium.

For all groups (I to III), cultures were assessed for survival and cytogenetic endpoints 2 and 6 days after irradiation. Survival was assessed by the clonogenic assay as described in section 2.3.4.3. The cytogenetic evaluation was performed by micronucleus assay as described in section 2.3.4.1.

5.2.3 Statistical analysis

Analysis of variance was performed using the ANOVA method (Origin 7.5 statistical package, for MS Windows). To analyze the significance of the results at 2 and 6 days post irradiation the t-student test was applied. The MN distributions were analyzed by Papworth's *u* test [Edwards *et al.*, 1979]. The test used the relative variance (σ^2/y) and the dispersion index (u) of the mean number of observed MN per BN cell (y) in order to judge whether they are significantly different. The variance was calculated by **equation 23** and dispersion index by **equation 24**.

$$u = \frac{\left[\left(\sigma^2/_y\right)-1\right](N-1)}{\sqrt{2(N-1)\left[1-\left(1/_{Ny}\right)\right]}} \tag{23}$$

$$\sigma^2 = \frac{(0-y)^2N_0+(1-y)^2N_1+(2-y)^2N_2+\cdots+(i-y)^2N_i}{(N_0+N_1+N_2+\cdots+N_i)-1} \tag{24}$$

where, N is the total number of cells scored, N_0, N_1, N_2…N_i is the number of cells carrying 0, 1, 2 … i micronuclei, respectively. Positive or negative values of *u* refer an over or under-dispersion, respectively. If the value of u is greater than ± 1.96, the dispersion is significant at 95% confidence level [Edwards *et al.*, 1979].

5.3 Results & Discussion

5.3.1 Radiation-induced cellular effects immediately after irradiation

Figure 39 depicts the number of MN present in 1000 BN cells scored and **Figure 40** the MN distribution in BN cells.

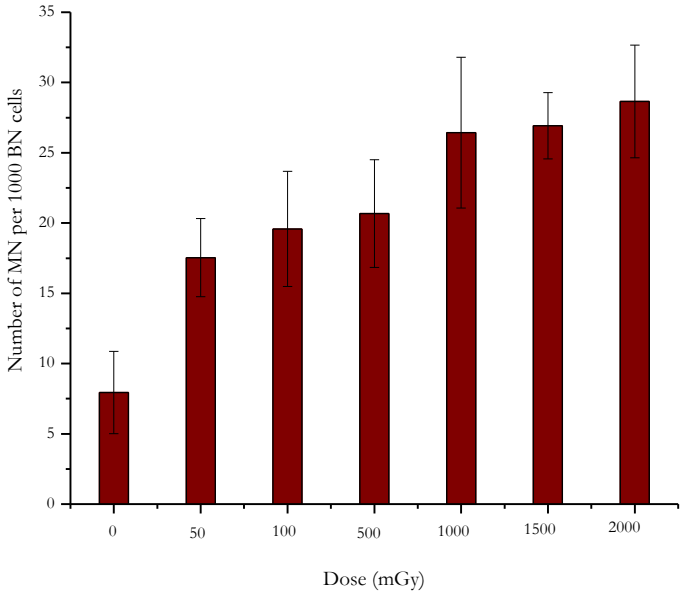

Figure 39: Dose response curve. Number of MN in 1000 BN cells (mean ± SEM) of 3 independent experiments. By analyzing the results, it can be summed up that there is a significant increase of MN per 1000 BN cells when the result of each dose is compared with the control (non-irradiated cells). This indicates that the cellular damage increase with dose values, as each MN represents a specific lesion.

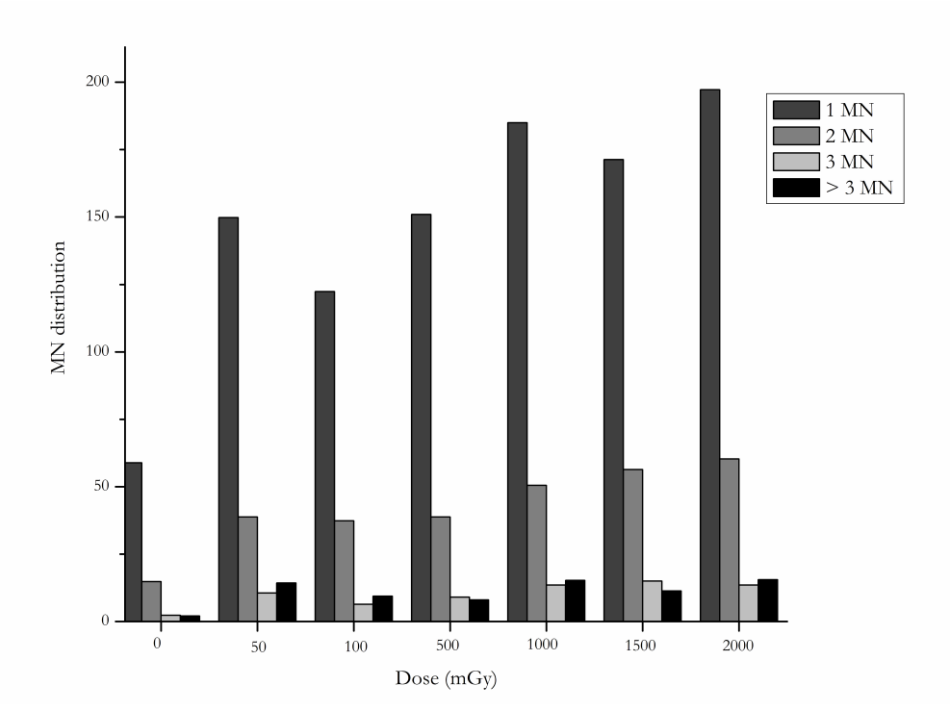

Figure 40: MN distribution in BN cells. 1 MN, 2 MN, 3 MN and >3 MN means that BN cells contain one, two, three and more than three MN. The obtained results show that genetic lesion results essentially in BN cells with only one MN. As dose values increase, the frequency of 2 MN becomes more evident. By the appearance of more than one MN, one can predict that higher doses are more damaged to the cell.

It can be inferred that the genetic lesion induced by ^{210}Po α-particles in A549 cells increase with increasing dose values, which is clear from the increase in the number of MN in BN cells. **Figure 40** shows that genetic lesion results essentially in BN cells with only one MN. As dose increases, the frequency of 2 MN or more also increases in the BN cells scored, which could indicate that higher dose values result in a different genetic lesion when compared to lower dose value ones.

5.3.2 Radiation and bystander-induced cellular damage (2 and 6 days after irradiation)

Early cellular damage was quantified 2 days post-irradiation and genomic instability was evaluated by cytogenetic analysis 6 days after irradiation (referred to as "early cellular damage" and "delayed cellular damage" in the sequence, respectively). All groups were compared to their own controls.

5.3.2.1 Survival Fraction

The assessment of the survival fraction (SF) was performed using the clonogenic assay and the results are presented in **Tables 3 and 4**. At both time points analyzed, early and delayed cellular damage (2 and 6 days after irradiation, respectively), the survival fraction was reduced in irradiated and bystander cells at all irradiation doses compared with its own controls (i.e. non-irradiated cells). With the exception of group III, irradiated cells expanded with fresh media, at day 2 the survival fraction is very similar to the matched control ($p=0.84$) at 10 mGy. For each Group, when both time points were compared by dose values, the difference of SF was not significant, however a higher survival fraction is observed at day 2 post-irradiation (see **Figure 41**).

Table 3: Values of SF, obtained by clonogenic assay, at day 2 after irradiation. The results represent the mean of three independent experiments ± standard error of the mean (SEM).

Dose (mGy)	**GROUP I** Survival Fraction (SF) ± s.e.m.	**GROUP II** Survival Fraction (SF) ± s.e.m.	**GROUP III** Survival Fraction (SF) ± s.e.m.
0	1	1	1
5	0.690 ± 0.093	0.870 ± 0.066	0.910 ± 0.060
10	0.670 ± 0.082	0.510 ± 0.120	0.920 ± 0.030
50	0.560 ± 0.027	0.750 ± 0.140	0.700 ± 0.130
100	0.540 ± 0.113	0.620 ± 0.260	0.580 ± 0.030

Table 4: Values of SF, obtained by clonogenic assay, at day 6 after irradiation. The results represent the mean of three independent experiments ± standard error of the mean (SEM).

Dose (mGy)	**GROUP I** Survival Fraction (SF) ± s.e.m.	**GROUP II** Survival Fraction (SF) ± s.e.m.	**GROUP III** Survival Fraction (SF) ± s.e.m.
0	1	1	1
5	0.604 ± 0.100	0.860 ± 0.089	0.730 ± 0.010
10	0.568 ± 0.042	0.650 ± 0.030	0.640 ± 0.060
50	0.410 ± 0.080	0.700 ± 0.008	0.560 ± 0.020
100	0.380 ± 0.100	0.530 ± 0.020	0.600 ± 0.200

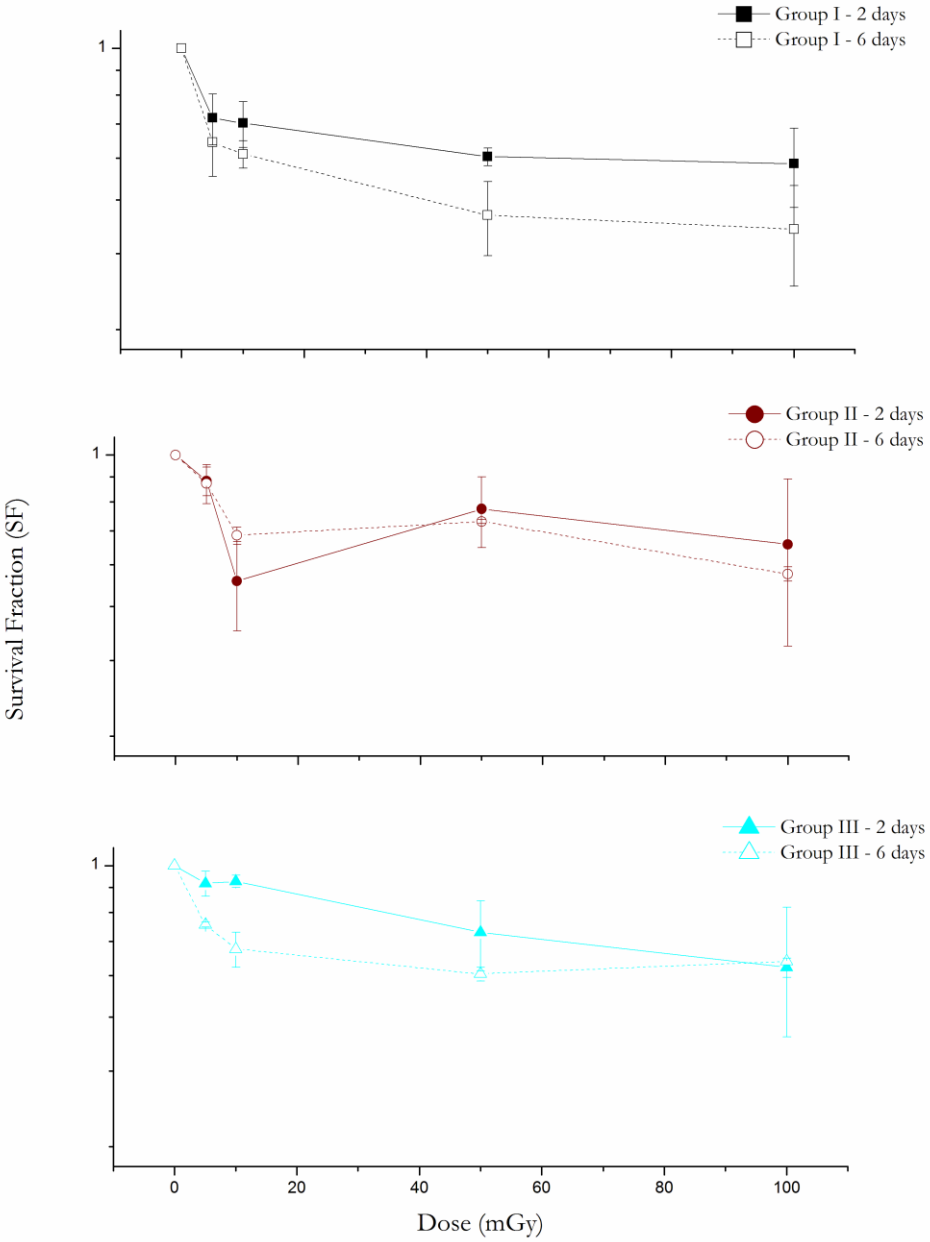

Figure 41: Survival fraction (SF), obtained by clonogenic assay, for each group, i.e. I, II and III. The results represent the mean of three independent experiments ± standard error of the mean (SEM). Note: The lines are purely eye guided.

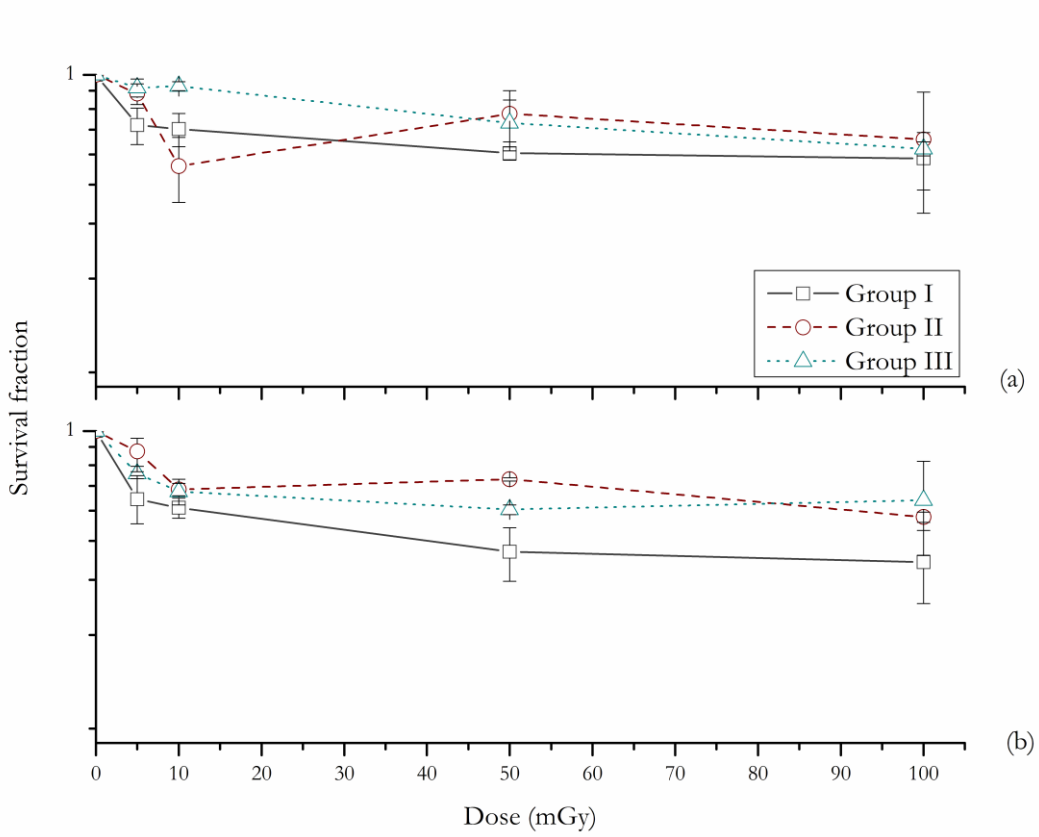

Figure 42: Survival fraction (SF), obtained by clonogenic assay, at day 2 (a) and at day 6 (b). The results represent the mean of three independent experiments ± standard error of the mean (SEM). At both time points and for all groups, survival is significantly reduced compared to its own controls. The only exception is observed for Group III at day 2, at 10 mGy, being the survival fraction similar to unirradiated control ($p=0.84$). In the media transfer experiment, group II a lower survival fraction is observed at 10 mGy, which corroborates with the HRS observed, by means of MN assay, at this dose value. Note: The lines are purely eye guided.

At day 2, when irradiated and bystander cells were compared for each dose value, survival was lower in irradiated cells, group I, but was significant only at 5 mGy ($p<0.2$) (**Figure 42**a). At 10 mGy the survival fraction for group II is significantly lower than group III ($p<0.05$) and similar to group I ($p=0.34$). This result is in agreement with the HRS, described below, at this dose value, by means of MN assay.

At day 6, comparing the irradiated cells with bystander ones, it is also noticeable that cell survival is lower at group I, with a higher significance between groups for each dose value. For 100 mGy, a moderate difference was observed ($p=0.28$), but for 5, 10 and 50 mGy the difference was statistically relevant ($p<0.2$ for 5 and 10 mGy and $p<0.05$ at 50 mGy). The comparison of the result obtained for 50 mGy with 10 mGy ($p=0.27$) and 100 mGy ($p<0.05$) provides some evidence for a HRS phenomena. However, the cellular damage, quantified by the MN assay, doesn´t corroborates this finding.

5.3.2.2 Micronuclei frequency – Early cellular damage

Figure 43 shows the results obtained, at day 2, for the aforementioned three experimental groups (Group I to III) and different dose values.

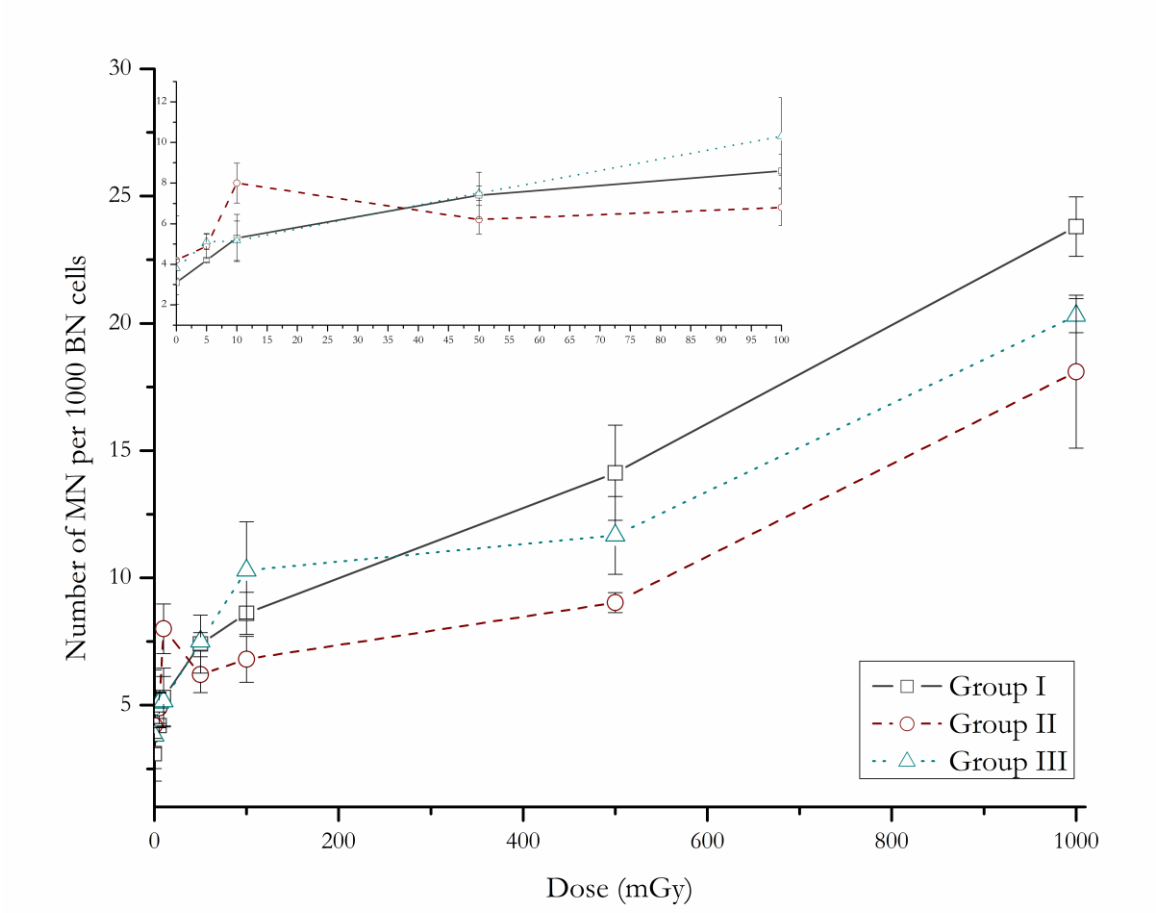

Figure 43: Number of MN per 1000 BN cells for each value of dose; 5, 10 50, 100, 500 and 1000 mGy at day 2 after irradiation for groups I to III. The non-irradiated cell cultures are marked as 0 mGy. Data represent means of 3 independent experiments, ± SEM. Note: the lines are purely eye guided.

Analyzing **Figure 43**, one can observe an increase, with dose values, in the number of MN per 1000 BN cells for all groups, comparing with its own control ($p<0.05$). However, in the range of 5 up to 100 mGy, none of the pair wise dose comparisons between groups I to III were significant ($p=0.24$, $p=0.5$, $p=0.87$, $p=0.35$, for 100, 50, 10 and 5 mGy, respectively).
The trend of the dose response curve corresponds toan increase of the cellular damage with dose values, but, for group II this dose dependence is more moderate, namely for 50 mGy and 100 mGy. Our results provide some evidence for a plateau of bystander effects after 50 mGy. Also, in group II a HRS is observed at 10 mGy, since at this dose value the number of MN significantly increase when compared with 5 ($p<0.1$) and 50 mGy ($p=0.21$). This phenomenon was also observed by clonogenic assay with the evidence for a lower survival fraction at this dose value.

5.3.2.3 Micronuclei frequency – Delayed cellular damage

Radiation significantly increased the number of MN, at day 6, in all groups compared to their non-irradiated controls (see **Figure 44**), with the exception in group III for 5 mGy were the increasing of MN was almost similar (p=0.68).

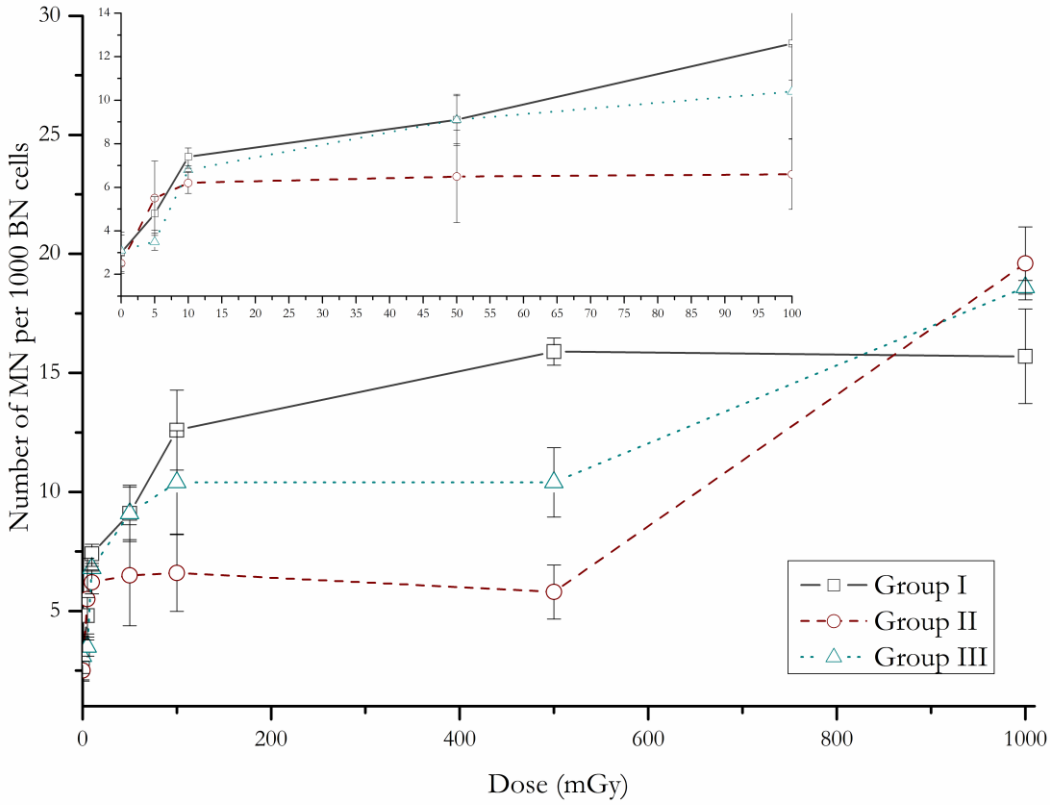

Figure 44: Number of MN, 6 days after irradiation for groups I to III, per 1000 BN cells_for each value of dose, i.e., 5, 10, 50, 100, 500 and 1000 mGy (a). (b) refers to a detailed view for lower doses. The non-irradiated cell cultures are marked as 0 mGy. Data represent means of 3 independent experiments, ± SEM. In all groups, radiation significantly increased the number of MN when compared with its own controls ($p<0.05$), with exception in group III for 5 mGy where the increasing of MN was almost the same ($p=0.68$). Similarly to earlier effects, the trend to reach a plateau after 10 mGy for group II is observed. Note: the lines are purely eye guided.

At this time point, we also observe an increase in the number of MN compared to the matched controls ($p<0.05$). Also, comparing the results obtained for each group, by dose value, a non-significant difference was found. However, at a delayed time, the trend of the dose response curve is different, for each group, when comparing with the cellular damage induced after 2 days. Between 10 and 50 mGy, our results give some evidence for a plateau, more evident for bystander, but also notable for irradiated cells. After this dose value, the

trend of the cellular damage for irradiated cells is to slightly increase, but for bystander the plateau remains.

5.3.2.4 Micronuclei distribution

Tables 5 and **6** show the MN yield and their distribution, 2 and 6 days after irradiation, respectively, in all groups. There is clear evidence that BN cells with only one MN are the most frequent. For a higher radiation exposure, in both day 2 and 6 post irradiation, the occurrence of 2, 3 or more than 3 MN per BN cell are more relevant than for lower dose values.

Table 5: The distribution and yield of MN in the aforementioned groups and dose values, 2 days after irradiation

	Dose (mGy)	Cells scored	Total MN	MN distribution					MN yield (y) ± SEM	σ^2/y	u
				0MN	1MN	2MN	3MN	4MN			
Group I	0	8000	296	7751	210	35	0	4	0.037±0.004	1.362	22.88
	5	3000	128	2875	122	3	0	0	0.044±0.001	0.974	-1.00
	10	3000	167	2840	153	7	0	0	0.056±0.016	1.029	1.10
	50	3000	255	2777	196	23	3	1	0.085±0.020	1.213	8.26
	100	3000	295	2743	226	26	3	2	0.098±0.011	1.221	8.59
Group II	0	7000	247	6783	189	27	0	1	0.035±0.006	1.232	13.73
	5	3000	202	2819	160	21	0	0	0.067±0.014	1.141	5.46
	10	3000	276	2760	204	36	0	0	0.092±0.012	1.169	6.55
	50	3000	214	2814	162	22	3	1	0.071±0.009	1.246	9.56
	100	3000	239	2796	176	23	3	2	0.079±0.016	1.289	11.18
Group III	0	6000	255	5775	187	38	0	0	0.043±0.005	1.284	15.58
	5	3000	171	2847	137	14	2	0	0.057±0.003	1.177	6.86
	10	3000	170	2845	140	15	0	0	0.057±0.007	1.120	4.65
	50	3000	255	2775	198	25	1	1	0.085±0.006	1.182	7.05
	100	3000	382	2691	258	38	4	9	0.127±0.023	1.418	16.17

Table 6: The distribution and yield of MN in the aforementioned groups and dose values, 6 days after irradiation.

	Dose (mGy)	Cells scored	Total MN	MN distribution					MN yield (y) ± SEM	σ^2/y	u
				0MN	1MN	2MN	3MN	4MN			
Group I	0	7000	233	6791	191	15	0	3	0.033±0.006	1.250	14.79
	5	3000	148	2860	132	8	0	0	0.049±0.005	1.059	2.29
	10	3000	231	2779	213	7	0	1	0.077±0.003	1.036	1.39
	50	3000	279	2739	247	12	0	2	0.093±0.013	1.079	3.07
	100	3000	487	2622	311	41	10	16	0.162±0.026	1.524	20.29
Group II	0	7000	166	6810	138	14	0	0	0.029±0.003	0.919	-4.73
	5	3000	175	2839	149	11	0	1	0.058±0.012	1.136	5.28
	10	3000	199	2816	169	15	0	0	0.066±0.005	1.085	3.28
	50	3000	226	2800	174	25	1	0	0.076±0.016	1.171	6.64
	100	3000	189	2826	164	7	1	2	0.063±0.011	1.170	6.59
Group III	0	6000	184	5816	166	18	0	0	0.031±0.004	1.257	14.08
	5	3000	116	2891	102	7	0	0	0.039±0.002	1.082	3.19
	10	3000	208	2797	198	1	0	0	0.069±0.002	0.979	-0.81
	50	3000	296	2735	241	20	1	3	0.098±0.013	1.178	6.92
	100	3000	375	2688	266	33	9	4	0.125±0.028	1.323	12.52

The yield of MN, MN yield (y), was calculated as the ratio of the total number of MN to the scored BN cells. As a result of cellular damage, MN was produced in irradiated cells and its yield increased in a dose-dependent manner in almost all doses values and groups.

At 10 mGy a HRS effect is observed in group II (see **Table 5**), i.e., there is a low dose sensitive effect of MN induction. However, this trend is inverted after 50 mGy, being the MN yield for group II lower than for group I and III. Also, at low doses, unexpectedly group I showed a lower MN yield when compared to group III ($p<0.05$). This could indicate that the bystander contribution to the overall cellular lesion, at doses lower than 10 mGy, could be due to intercellular gap-junction contact. Since due to centrifugation released in group III any bystander signal presented in the culture medium is removed from the culture.

The results obtained 6 days after irradiation show a similar trend of response when compared to the earlier effects of radiation. At group II, the low dose sensitive effect is no more observed at 10 mGy although slightly occurs at 50 mGy. This result is not in agreement with the higher survival fraction observed at this dose value by clonogenic assay.

5.4 Conclusions

The appraisal of how the risks associated to a low-dose exposure could be exactly determined remains unclear. Some authors claim that a *revision* of the implemented models, such as those based on the LNT hypothesis is needed, namely in the dose range up to 100 mGy. However, in this dose range, there are no epidemiologic data and *in vitro* studies include mechanisms such as, apoptosis, bystander effects, genomic instability, among others, which sometimes reveal a different outcome according to cell lines. As of today, it is not clear how the assessment of health risks associated to low- dose radiation exposure could be correctly estimated and evaluated.

In this study, we investigated if bystander effects are induced in A549 cells after irradiation to very low doses of α-particle, and its dependence with dose and time. Also, the trend of cellular response of A549 cells exposed directly to α-particles irradiation was studied. Previous studies using medium transferred have shown that medium from irradiated cells can induce bystander effects in non-irradiated cells at low doses and in a time-dependent manner [Mothersill and Seymour 1998b; Mothersill *et al.*, 2001]. However, these studies included only dose dependent effects few minutes after irradiation and with doses higher than 100 mGy. We have extended our assessment to a time interval up to six days, in order to understand the earlier and delayed induced cellular damage, not only in bystander but also for direct effects, and for doses lower than 100 mGy.

We assessed the cellular damage induced and survival in lung epithelial cell line (A549) at very low doses of α-particles, in order to understand the trend of the dose-response curve not only for irradiated but also for bystander cells.

The obtained dose-response curves for both early and delayed times pinpoint, for each value of the dose and for all groups, an increase of cellular damage, compared with the matched controls. Regarding the trend of the curves it should be highlighted the non-linear pattern of the curves at all groups. It seems that up to 10 mGy the cells are more sensitive to radiation being the increase of the MN more evident.

The studies of Shao *et al.* (2006) suggested that the bystander effect is not dose dependent, but our study provides evidence for a dose-dependent behavior at the region of very low doses, up to 10 mGy. Moreover, the results obtained for all groups suggest that at very low doses the bystander effects are not be negligible since they result in a cellular damage similar to those obtain by direct irradiation. Ojima *et al.* (2008) concluded that DNA double strand breaks induced by very low X-ray doses (1.2 to 200 mGy) are largely due to bystander effects. The study included the inhibition of cell-to-cell contact in order to test the supralinear dose-response relationship obtained without treatment. In our study, comparing group I and III, **Figure 43** and **Figure 44**, it is noticeable that irradiated cells at group I show a higher induced lesion than cells in group III. This corroborates the assumption that bystander effects have an important contribution to the overall lesion induced by radiation.

Data obtained in other cell lines show that the induction of cellular damage in bystander cells persists with time, probably as a consequence of the formation of bystander factors that themselves generate ROS, leading to a self sustaining system responsible for delayed effects [Yang *et al.*, 2005]. Our results are in agreement with these evidences showing a persistent bystander signal at a delayed time. As in earlier induced cellular damage, one important remark of this study is the similar evidence for bystander effects when compared to directly irradiated cells. As a consequence of an environmental exposure to α-radiation, from radon for example, the deposition of such particles onto bronchial epithelial cells will unavoidably induce a cellular damage. This study suggests that the quantification of the possible cellular damage induced should be quantified considering its time dependence.

Some studies showed that, for doses below 0.5 Gy, the determinant factor for the observed HRS in bystander effects is not the DNA damage [Mothersill and Seymour 2000 and Seymour and Mothersill 2000]. Moreover, Wykes *et al.* (2006) found that the prevalence of low-dose hypersensitivity is not related to DNA DSBs. Our results endorse these outcomes since the difference in the magnitude of cell survival between groups (see Figure 3), suggests that the cell irradiation itself cannot be the unique mechanism to induce cell damage/killing. Comparing group I and III (**Figure 43**) it is noticeable that group I shows a lower cell survival fraction which could indicate that the clastogenic factors, including free radicals, release immediately after and a few minutes after irradiation could be involved in the magnitude of cellular response. Moreover, in group II, the survival fraction at each dose value decreased when compared to the matched controls. At day 2, it is observed an HRS effect at 10 mGy for group II, which is in accordance with the induced cellular damage. These results put in evidence the importance of well quantifying the low dose exposure. It is notable, **Figure 43a**), that the survival fraction at 10 mGy is lower than the one observed for irradiated cells. This pattern could suggest that also the irradiated cells are more sensitive at this dose value producing more detrimental "bystander signals" that would impart deleterious effects in non-irradiated cells. In fact, the magnitude of survival fraction reveal that group III (without any bystander signal produced a few minutes post-irradiation) discloses a slightly decrease of cell survival when groups I and III are compared. Lorimore *et al.* (1998) found no increase in cell killing that could be attributed to bystander cells. While this pattern is similar to our results, mainly after 50 mGy, where exists a plateau, we observed a prominent decrease of cell survival namely up to 10 mGy, which suggested that cell killing is affected by bystander signals.

It can be stated that the response of lung epithelial cells exposed to low doses of α-particles exhibit dynamic effects and the interaction of different cellular processes, such as DNA damage, cell killing and HRS.

The results here reported emphasize that the risks attributable to the exposure to low dose radiations encompass a complex variable cellular response and cannot simply be extrapolated from higher doses. Moreover, they raise important questions about the potentially detrimental effects associated with very low doses exposures.

Recent data has revealed the complexity and efficacy of biological defense mechanisms against genotoxic agents (physical and chemical) at cell (DNA repair and apoptosis), tissue (role of neighboring cells), and whole body (immunosurveillance) level, in which ionizing radiation is likely to induce, at different levels depending on cells, apoptotic responses, which are the consequence of intra and inter-cellular signaling. However, ionizing radiation can also induce mutations, which interfere with apoptosis and consequently permit the survival of damaged cells. In turn, mutation constitutes one of the steps of carcinogenesis. Concerning the effects of direct radiation exposure, the obtained results reveal an increase in the number of cellular lesions as a consequence of increasing absorbed dose values, as quantified by MN number after cell irradiation. The results obtained also show that the more frequent lesion observed after cell absorbed dose ranging from 50 to 2000 mGy is the presence of 1 MN per BN cell. For higher doses it is evident an increase in the frequency of 2 or more MN per BN cell. Micronuclei are fragments of genetic material that contain either acentric fragments (resulting from DNA breaks), whole chromosomes, or complex rearrangements that are unable to properly attach and be pulled to the poles by the mitotic spindle. So, although this study is not able to identify the occurred genetic lesions, it presents clear data showing that higher absorbed doses by cells result in more DNA lesions. These lesions could, in turn, incite a biological mechanism unsuitable to be repaired and consequently the death of the cell. In fact, it is known that low dose absorption and irradiation from low dose rate radiation may be able to induce significant apoptosis. Moreover, apoptosis may be one of the mechanisms by which low dose absorption causes growth inhibition [Joniani *et al.*, 2000; Dewey *et al.*, 1995 and Hickman, 2002], which challenges the LNT model's validity. Moreover, concerning cell killing, the obtained results reveal a significant decreasing with dose increasing, due to a decrease in the surviving fraction with dose. This study and associate findings must be complemented by more accurate quantification of cell survival in order to better understand the results obtained. Previous studies on biological untargeted effects of irradiation using medium transfer have shown that medium from irradiated cells can induce bystander effects in non-irradiated cells [Azzam *et al.*, 2002; Hu *et al.*, 2006; Lyng *et al.*, 2000]. In this context, the aim of our work was to study the influence of the irradiated medium that induce cellular damage in unirradiated cells, in early and delayed effects. At day 2 after cell irradiation, a more evident increase of the number of MN per BN cell in group I was observed when compared to group III. This is due to the fact that any expected radiation induced damage/bystander factor originating from irradiated cell cultures was removed from group III by centrifugation of cells and re-culture in fresh medium. Group II shows a clear increase in the frequency of MN in BN cells when compared to the nonirradiated control. In order to study delayed cellular damage, a cytogenetic analysis was performed 6 days after irradiation. The delayed response of cells to radiation is similar to the response obtained 2 days after irradiation, in which concerns the increase in the number of MN in exposed cells when compared to controls. However, in Group II, the comparison of results obtained for delayed and earlier responses, one can notice an increase in the number

of MN in the delayed response. Data obtained in other cell lines show that the induction of cellular damage in bystander cells persist in time, probably as a consequence of the formation of bystander factors that themselves generate reactive oxygen species ROS, leading to a self-sustaining system responsible for delayed effects [Yang *et al.*, 2005; Sokolov *et al.*, 2005]. Our results are in agreement with these evidences and add additional proof to the existence of a bystander signal that may be responsible for cellular damage late after cell irradiation. The obtained results may provide clues for the biodosimetric determination of radon dose to airway cells at cumulative exposures.

CHAPTER 6

INFLUENCE OF THE NUMBER OF IRRADIATED CELLS IN THE SPATIAL DISTRIBUTION OF BYSTANDER EFFECTS

6.1 Introduction

Though several studies have been published on bystander effects, the explanation of the kinetics and mechanisms by which they occur remains unknown, especially the time and spatial effects of how the bystander factors released in the culture medium are propagated.
Hu *et al.* [2006] reported that increased DSBs in irradiated and unirradiated bystander areas could be visualized 2 min after radiation and reached its maximum 30 min after radiation. Moreover, they showed that the bystander signal could be transferred to anywhere in the dish and the percentage of DSBs in the bystander cells were not dependent on the irradiation dose. Belyakov *et al.* [2001] reported an increase in micronuclei (MN) formation in an unexposed quadrant of the dish, when scored 3 days later, even though only a single cell is targeted. Some other studies show an increase of cell killing in unirradiated areas 3 days after-irradiation with X-rays [Schettino *et al.*, 2003]. These studies suggest a time and distance dependence on the bystander response. Hu *et al.* [2006] studied how early bystander factors could induce a cellular damage and shown also that the percentage of DSBs in non-irradiated bystander cells was not dependent on the dose delivered. However, our previous studies,

described in chapter 5, seem to indicate that, using medium transfer technique, dose dependence exists, not only for targeted cells abut also for untargeted ones.

The aim of the present study was to investigate how the *bystander signals* released after low-doses of α-radiation are influenced by the number of irradiated cells. In order to investigate if bystander effects are affected by the number of irradiated cells, two irradiated areas were used, differing by a factor of 2 in radius and two distinct bystander areas were defined containing the same number of cells in each. The radiation induced extranuclear/extracellular assay, γ-H2AX, allows us to quantify cellular damage, by means of DSBs, *in situ* and immediately after irradiation. As a consequence, this assay was applied to evaluate the spatial distribution of bystander effects.

6.2 Materials & Methods

6.2.1 Cell culture and irradiation

A549 cells were cultured at 37°C with 5% CO_2 in Dulbecco's Modified Eagle's medium containing 10% fetal bovine serum and 1% penicillin-streptomycin solution (Sigma-Aldrich, St. Louis, USA). Log-phase cells were seeded onto 3.5 cm diameter culture dishes with 6.3 μm of Mylar®-foil base, 24 hours before irradiation. Cells at exponential growth were exposed to a monoenergetic ^{210}Po source described in chapter 4. During irradiation, part of the culture dish was shielded using 25 μm of aluminum, and in the unshielded area the cells were irradiated with the average cellular doses of 5, 10, 50 and 100 mGy (**Figure 45**). Control dishes were exposed to the same conditions of irradiation but 100% shielded. The Petri dishes, where the cells were cultured, have 3.5 cm of diameter, and, as previously mentioned , the unirradiated areas were achieved by covering them with aluminum. In two experiments performed, A and B, the studied areas, irradiated area A, irradiated area B, bystander I and II (referred in **Figure 45** as irradiated area A and B and bystander I, II), have an approximately area of 0.19, 0.78, 0.59 and 0.98 cm^2, respectively.

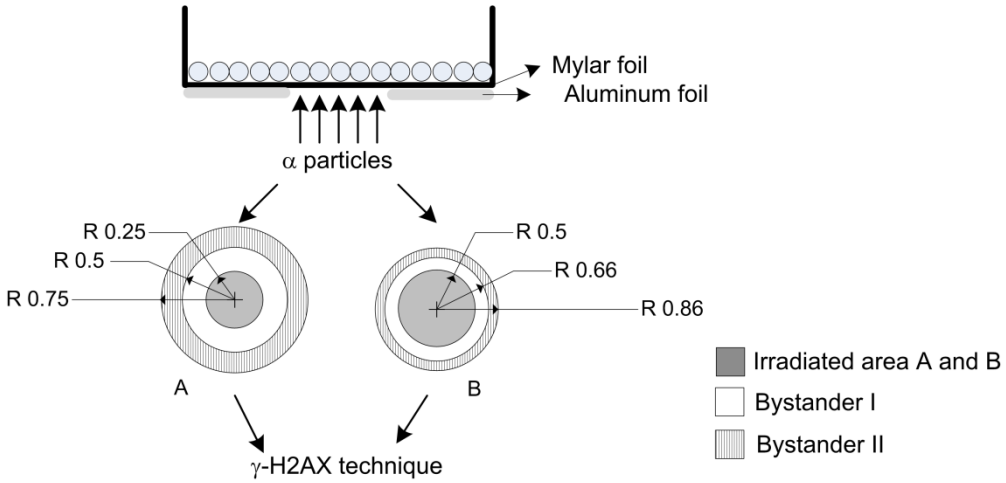

Figure 45: Schematic view of the culture dish for irradiation. The dimensions are in cm and not at scale. The cell dish has 3.5 cm of diameter and depending on the experiment (A) or (B); approximately, 98 or 92% of this area was shielded by aluminum foils, respectively. The unshielded area was exposed to 5, 10, 50 and 100 mGy of α–particles emitted by a ^{210}Po source. Immediately after-irradiation the γ-H2AX assay was performed.

6.2.2 Immunofluorescence staining

Immediately after irradiation the cells were washed with phosphate-buffered saline solution (PBS) and fixed with 4% formaldehyde in PBS for 15 minutes. After being washed with PBS, cells were permeabilized with Triton X-100 (0.5%) at room temperature for 5 minutes, washed twice with 1% Bovine Serum Albumin (BSA) (Sigma-Aldrich, St. Louis, USA) and blocked during 1 hour with BSA 4%. Then, cells were incubated with the γ-H2AX primary antibody (mouse anti-γ-H2AX (ser139), Stressgen, bioreagents Corp., Canada) at 2 μg/ml for 2 hours, washed twice with BSA 1%, incubated with FITC-conjugated anti-mouse second antibody (Santa Cruz Biotechnology, USA) at 1mg/ml for 1 hour, washed three times more and incubated with Hoechst (Sigma-Aldrich, St. Louis, USA) at 1μg/ml for 5 minutes and finally mounted with anti-fade (Vectashield mounting medium H-100, Vector Laboratories, Burlingame, Canada). Cells were analyzed at 64x magnification in a fluorescence microscope. Images were randomly obtained in each slide. Image analysis of γ-H2AX foci was performed by the freeware Cellprofiler [Carpenter *et al.*, 2006].

6.2.3 Treatment with Lindane or dimethyl sulfoxide

Prior to irradiation, cells were pretreated for 2h with lindane (Sigma-Aldrich, St. Louis, USA) to inhibit gap junctional intercellular communication (GJIC). Control cells were treated with 0.25% dimethyl sulfoxide (DMSO), an effective scavenger of reactive oxygen species, and 2% PBS as the solvent for lindane. Immediately after irradiation, the γ-H2AX assay was performed. The concentration of the two chemicals used has previously been shown to be non-toxic and non-genotoxic to the cells under the condition used in the presented studies [Harada *et al.*, 2009].

6.2.4 Statistical analysis

Data are presented as average value ± SEM (standard error of the mean). Significance levels are assessed using the *t-student* test. The statistical analysis between three independent groups was perfomed by ANOVA.

6.3 Results

6.3.1 Induction of DSB in irradiated cells

Figure 46 shows the average number of foci per cell in irradiated areas A (lower number of irradiated cells) and B (higher number of irradiated cells), represented in **Figure 45** as irradiated areas, for different doses.

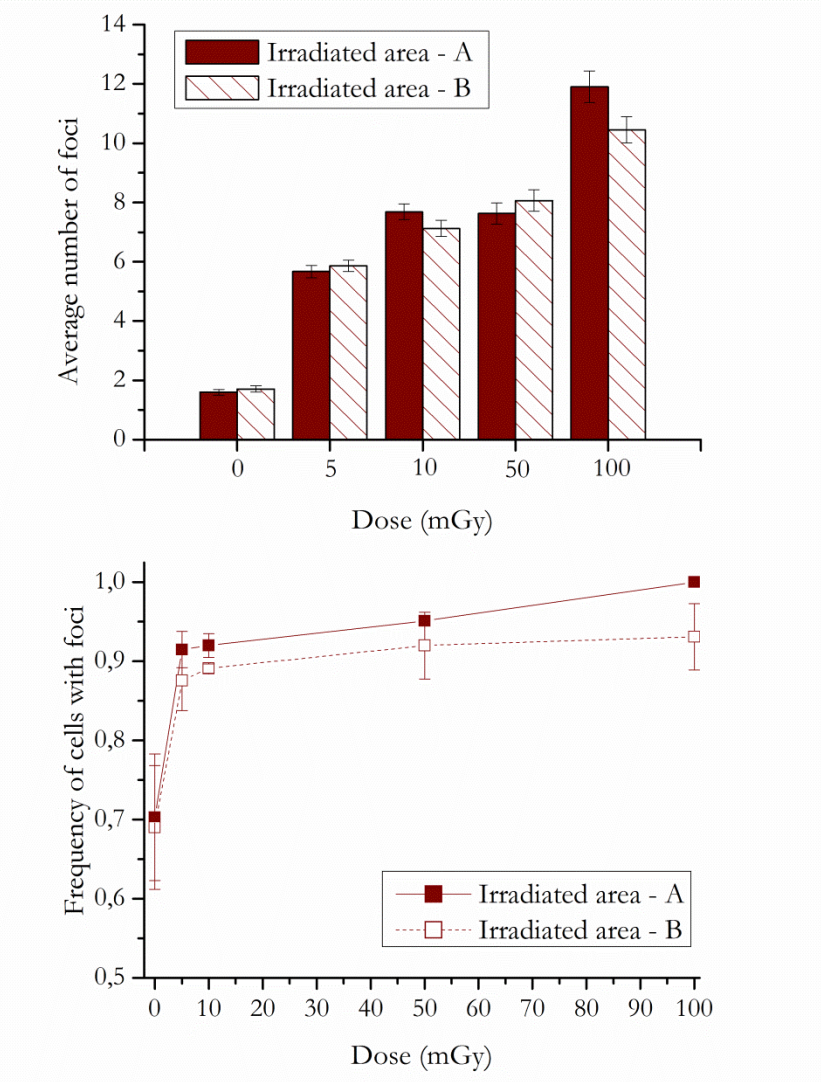

Figure 46: Induction of DSBs in irradiated cells, by means of foci number, after 5, 10, 50 and 100 mGy of α-radiation. Data were collected from three independent experiments. Error bars represents the SEM. The statistical significance between each dose value, for both irradiated area A and B, and matched controls, i.e. 0 mGy, is $p<0.005$.

At both irradiated areas, A and B, the number of foci increased with increasing irradiation dose values compared to the matched controls, as shown in **Figure 46**. As expected, the difference on foci number is not statistical different for each dose value when irradiated areas A and B are compared.

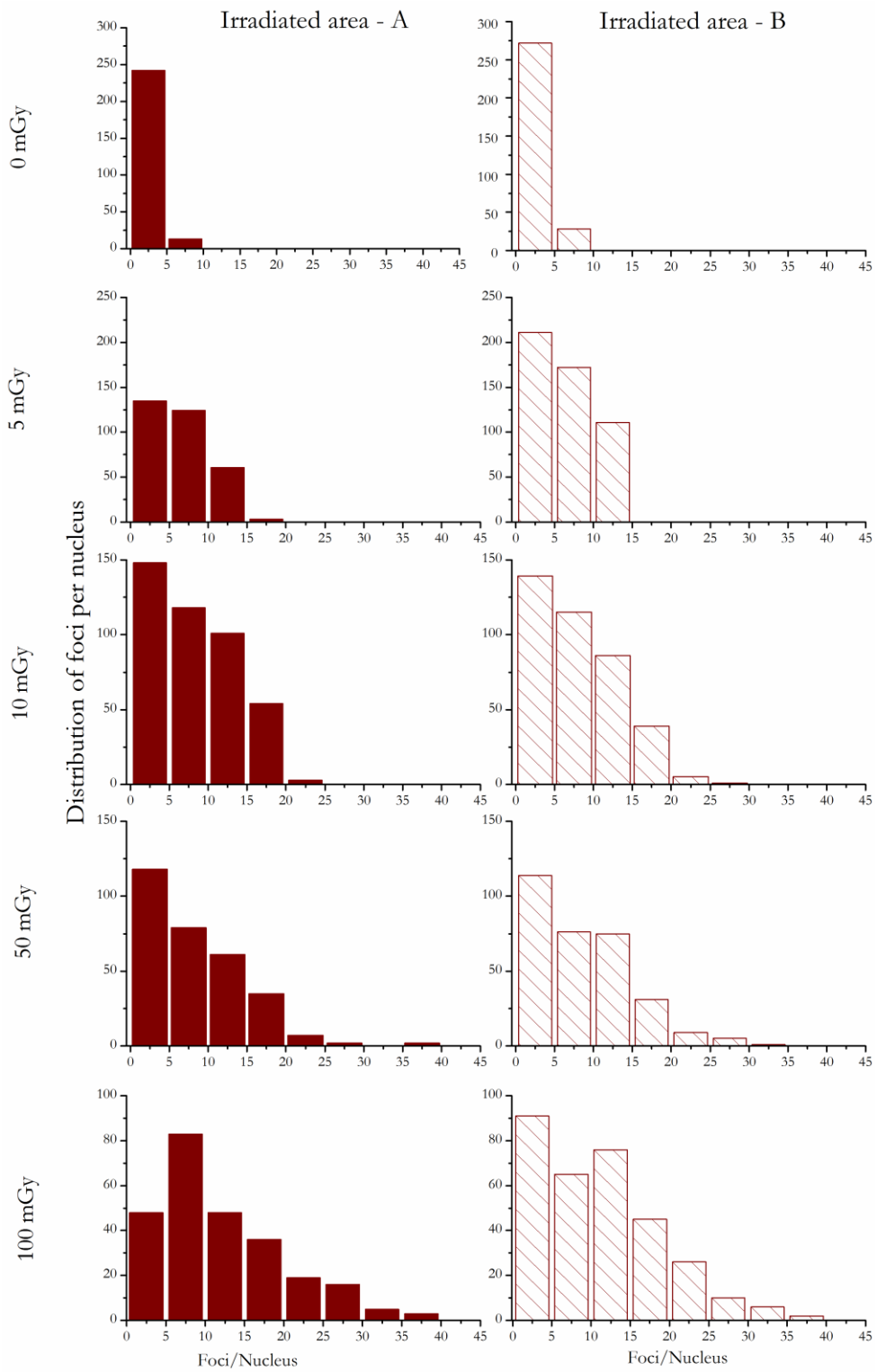

Figure 47: Distribution of foci number per cell for all dose values; left and right panels show the distribution of foci number in the irradiated areas – A and B, respectively. The histograms show cells presenting 0 to 45 γ-H2AX foci per nucleus. Data were collected from three independent experiments. Different scales were used for a better visualization.

6.3.2 Induction of DSB in bystander cells

To understand the role of the number of irradiated cells in the damage induced in untargeted cells, the non-irradiated area was divided in two contiguous areas, referred in the sequence as "bystander I" and "bystander II" (**Figure 45**). In order to have the same number of cells in each unirradiated area, bystander I and II don't have the same area, when comparing A and B experiments. That is, in experiment B, the higher irradiated area has a higher number of irradiated cells, allowing a higher cell-to-cell contact and the bystander factors released in the culture medium move a shorter distance to travel through bystander I and II, when compared with experiment A with a smaller irradiated area.

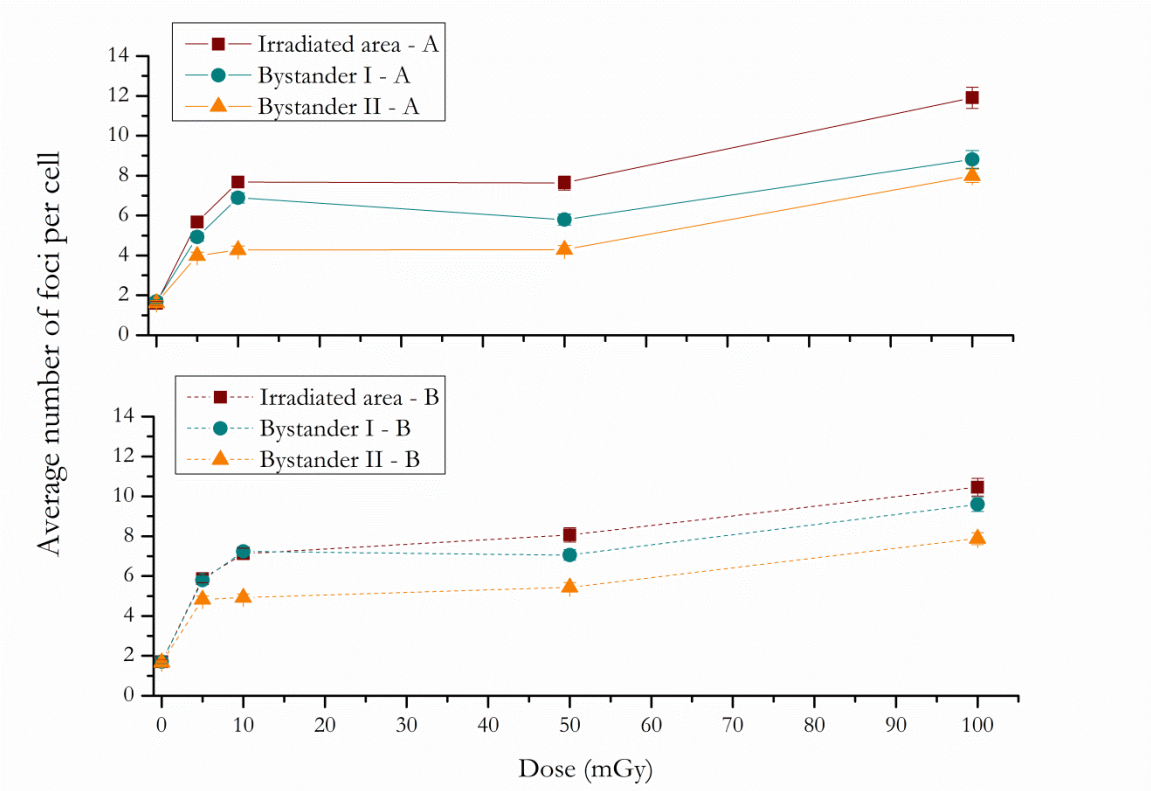

Figure 48: Average number of foci per cell in the experiment A (up) and B (down) with a lower and a higher number of irradiated cells, respectively. Irradiated area – A and irradiated area B refers to the irradiated areas, Bystander I – A and Bystander I - B, the closest to the irradiated cells, refers to the first non-irradiated area and bystander II – A and Bystander II - B to the second non-irradiated area. Data were collected from three independent experiments. Error bars represents the SEM. Note: The lines are purely to guide the eye.

As can be observed in **Figure 48**, for experiments A and B:

- As one moves away from the irradiated area, the induced cellular damage in bystander cells decreases.
- When a higher number of cells are irradiated, the trend of the cellular damage, as a dependence of dose, is the same as the one observed for a lower number of irradiated cells.
- When irradiated and bystander I – A and II - A areas were compared for each irradiation dose value, the number of foci was significantly lower, $p < 0.005$, in both bystander areas at all dose values.
- Comparing bystander I – A and II – A areas, the number of foci decreased in bystander II area at 5 up to 50 mGy ($p<0.005$, $p<0.005$ and $p<0.005$, respectively) and was similar at 100 mGy ($p=0.15$).
- When irradiated and bystander I – B were compared for each irradiation dose value, the number of foci was similar at 5, 10 and 100 mGy, $p=0.96$, $p=0.96$ and $p=0.16$, respectively, and significantly lower, $p < 0.005$, for 50 mGy.
- When irradiated and bystander II - B areas were compared for each irradiation dose value, the number of foci was significantly lower, $p < 0.005$, at all dose values
- Comparing bystander I – B and II – B areas, the number of foci decreased in bystander II area at 5 up to 100 mGy ($p<0.05$, $p<0.005$, $p<0.005$, and $p<0.005$ respectively).
- Following the same trend as irradiated cells, bystander cells at I - A and I – B areas also suggest a radio-hypersensitivity effect.
- Besides this, the plateau observed, also in bystander areas, between 10 and 50 mGy highlights the non-linear response to radiation.

6.3.2.1 Bystander I

Figure 49 displays the average number of foci per cell in "Bystander I-A" and "Bystander I-B" areas, i.e. considering a lower and a higher number of irradiated cells, respectively.

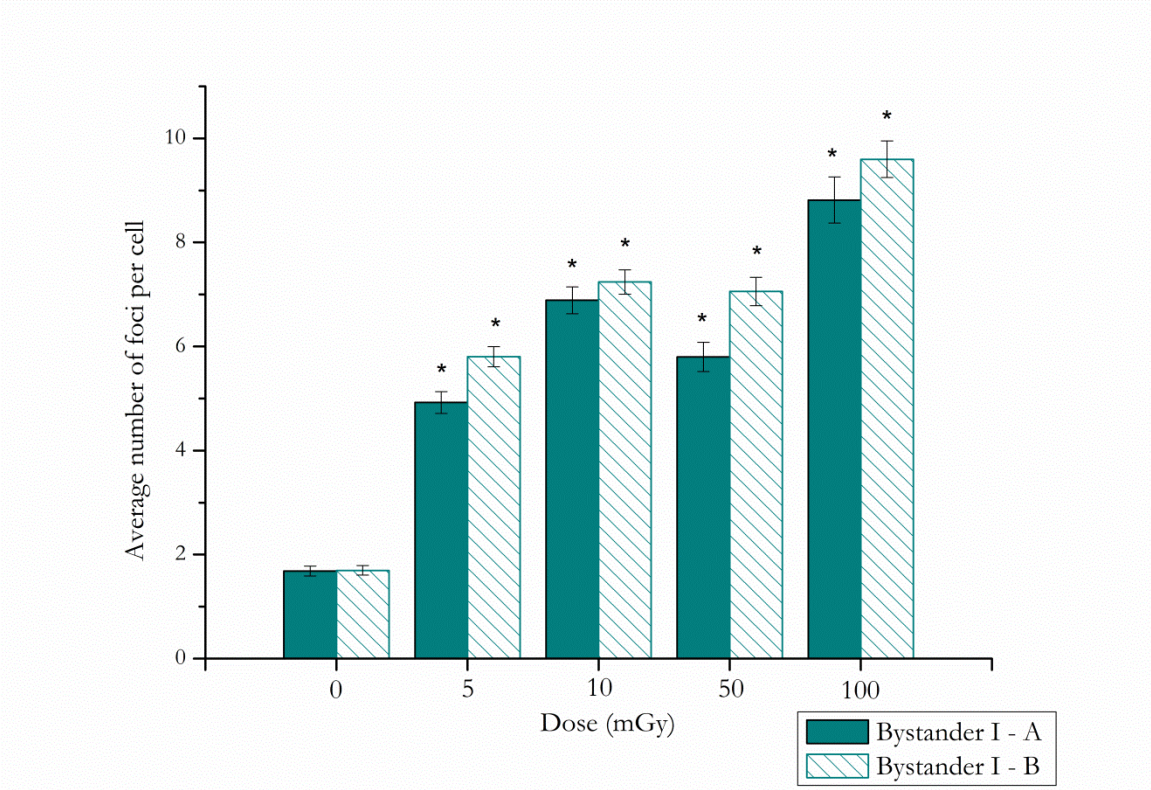

Figure 49: Induction of DSBs in the "Bbystander I-A" and "Bystander I-B" areas corresponding to non-irradiated cells in the areas nearest to the irradiated cells, in case of a lower and a higher number of irradiated cells, respectively. Data were collected from three independent experiments. Error bars represents the SEM. * $p < 0.005$ represents the statistically significance between each group and its own controls.

Comparing the number of foci in "Bystander I-A" and "Bystander I-B" areas (**Figure 49**), per dose values, a tendency is perceived for a lower number of DSBs in area I-A, being the statistical differences the following: 5 mGy ($p<0.2$), 10 mGy ($p=0.29$), 50 mGy ($p<0.2$) and 100 mGy ($p<0.1$). **Figure 50** shows the distribution of foci per cell, at both bystander areas I – A (and B), for all dose values.

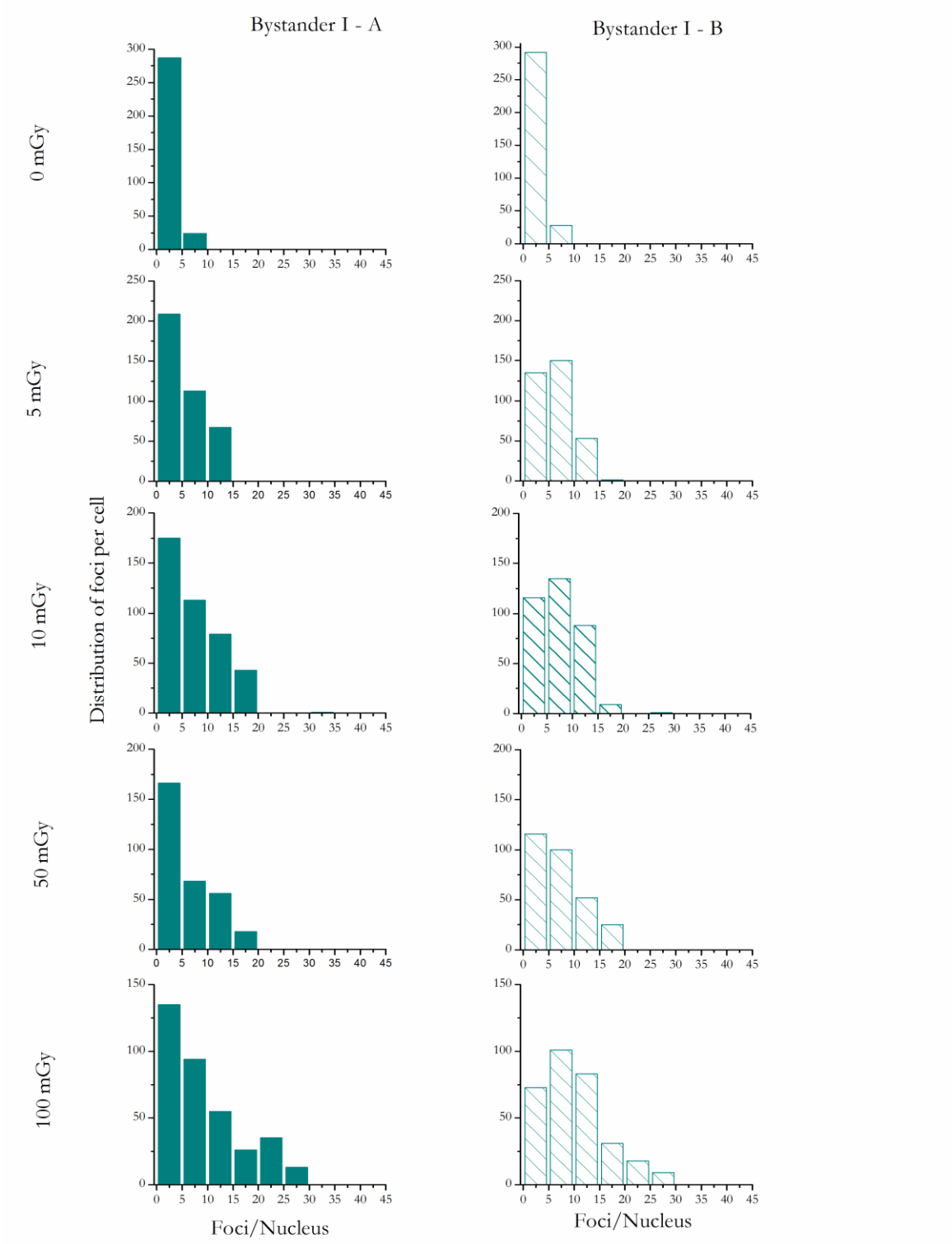

Figure 50: Distribution of foci number per cell for all dose values; left and right panels show the distribution of foci number in the Bystander I areas – A and B, respectively. The histograms show cells presenting 0 to 45 γ-H2AX foci per nucleus. Data were collected from three independent experiments. Different scales were used for a better visualization.

These results seem to indicate that the number of irradiated cells affects the bystander response near the irradiated area. Due to the largest possibility of cell-to-cell contact at the experiment I-B, as showed in **Figure 45**, and being the number of DSBs higher at this area, we investigate the role of gap-junctional intercellular communication to further understand the depicted results in **Figure 49**.

6.3.2.1.1 Role of the gap-junctional intercellular communication (GJIC)

Bystander effects are demonstrated in cells that are descendents of irradiated cells either directly or *via* media transfer or in cells that have communicated with irradiated cells. In this study both situations are allowed, i.e. the bystander signals can be propagated by the medium or the cells can communicate via GJIC. The irradiation of a higher number of cells (experiment B) involves a higher area of cell-to-cell contact between irradiated and non-irradiated cells. The results displayed in **Figure 49** demonstrated that the induced bystander effects are slightly higher in experiment-B. So, we investigate the role of GJIC in the areas closest to irradiation cells, using Lindane, a GJIC-suppressing agent. The results are displayed in **Figure 51** [1].

[1] As previously mentioned, DMSO is an effective scavenger of reactive oxygen species

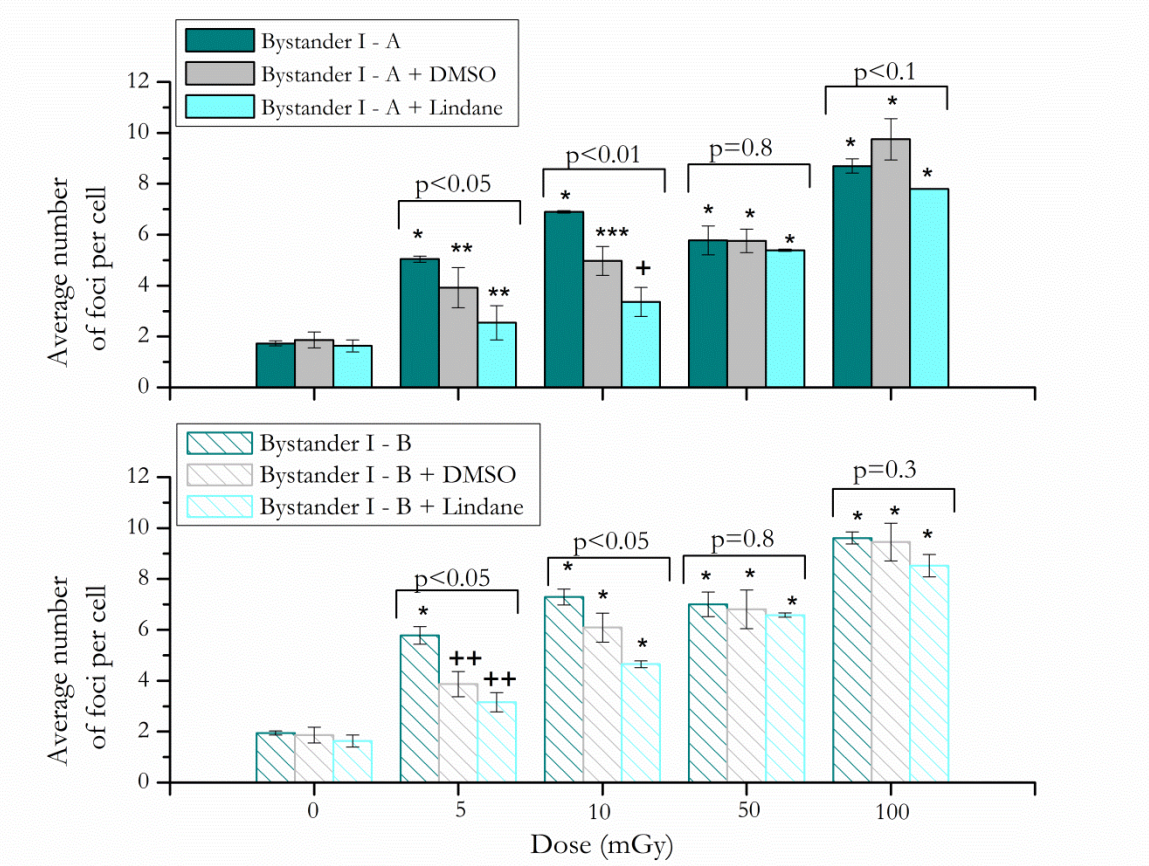

Figure 51: Average number of foci per cell of bystander cells with or without treatment with Lindane or DMSO. The data are plotted with the averaged values ± SEM of three independent experiments. * p< 0.005, ** p<0.02, *** p<0.01, $^{+}$ p<0.1 and $^{++}$ p<0.05 represents the statistically significance between each group and its own controls The statistical analysis, per dose value, of the data obtained for the three independent treatments was performed by ANOVA analysis.

As can be seen from the **Figure 51**, at lower doses (5 and 10 mGy), the number of DBSs was significantly different when cells treated with DMSO or lindane are compared with bystander cells without treatment;

- When the results obtained from the three experiments, i.e. Bystander I – A, Bystander I – A + DMSO and Bystander I – A + Lindane, where compared for 5 and 10 mGy, the statistical difference between them is significant with p< 0.05 and p<0.01, respectively.

- When the results obtained from the three experiments, i.e. Bystander I – B, Bystander I – B + DMSO and Bystander I – B + Lindane, where compared for 5 and 10 mGy, the statistical difference between them is significant with p< 0.05.

At 50 and 100 mGy, the number of DSBs is almost the same, in both experiments, with and without treatment.

6.3.2.2 Bystander II

Figure 52 displays the average number of foci per cell in the "Bystander II-A" and "Bystander II-B" areas for the different irradiation dose values.

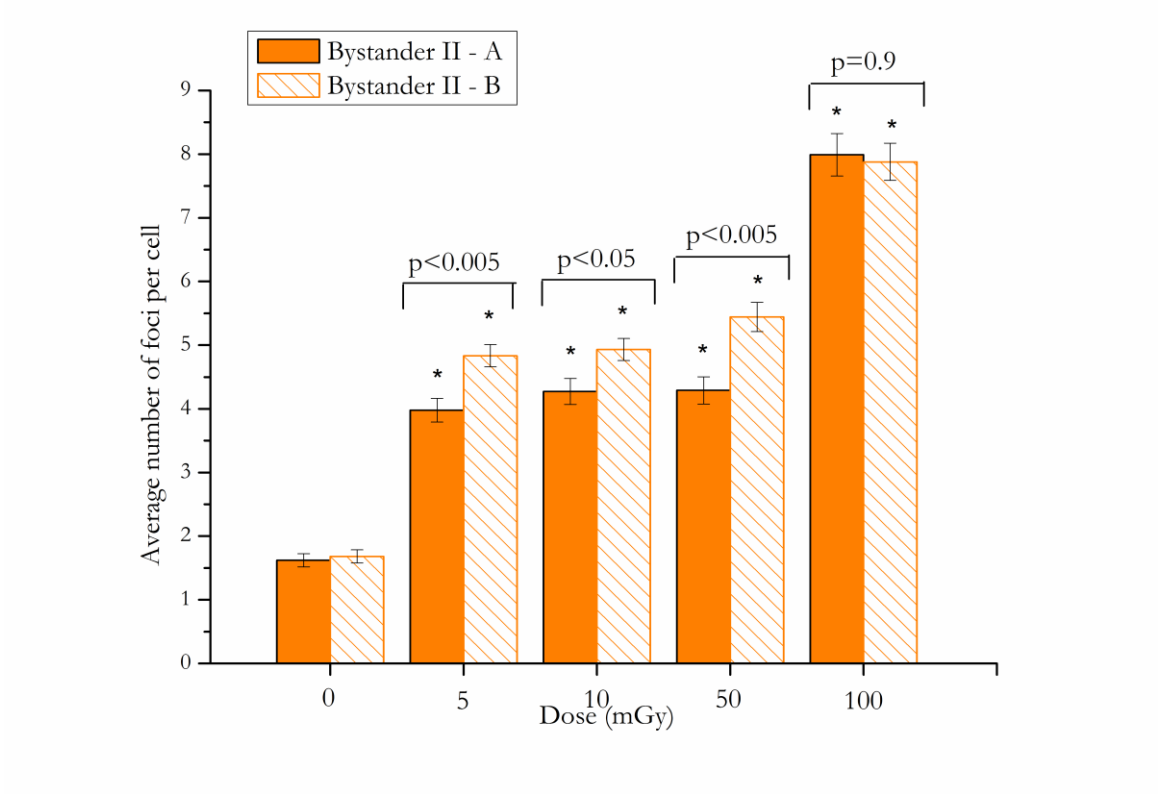

Figure 52: Induction of DSBs in the "Bystander II-A" and "Bystander II-B" areas, corresponding to non-irradiated cells in the areas more distant of the irradiated cells, in case of a lower (experiment A) and a higher number (experiment B) of irradiated cells, respectively. Data were collected from three independent experiments. Error bars represents the SEM and * p< 0.005.

From the analysis of the results from **Figure 52**, it can be concluded that the number of irradiated cells seems to influence the bystander response. As can be seen, the cellular damage induced, measured using the foci per cell, in cells located in bystander II-B is higher when compared with bystander II-A, except for 100 mGy.

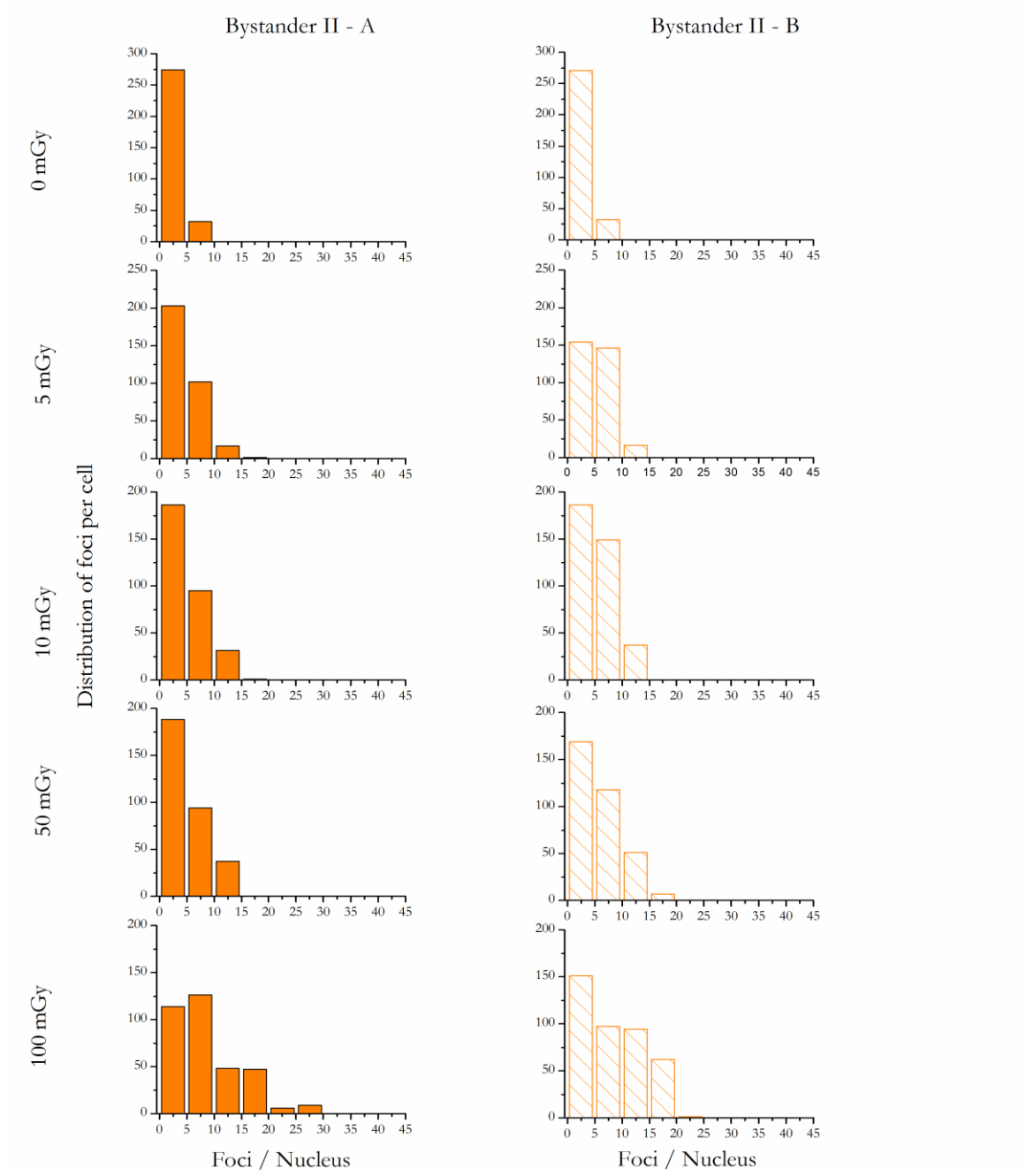

Figure 53: Distribution of foci number per cell for all dose values; left and right panels show the distribution of foci number in the Bystander II areas – A and B, respectively. The histograms show cells presenting 0 to 45 γ-H2AX foci per nucleus. Data were collected from three independent experiments. Different scales were used for a better visualization.

However, as previously mentioned, in order to maintain the same number of cells in non-irradiated areas, the distance between exposed and bystander cells is different in experiment A and B, i.e., the distance between irradiated areas and bystander II-A (or B) is 0.25 and 0.16 cm, respectively. For this reason, in order to verify that the number of irradiated cells

influences the bystander response, a third non-irradiated area, that will be referred to as "Bystander III-B" was considered, placed at 0.25 cm from irradiated area.

Figure 54 shows the comparison between non-irradiated cells considering the same distance between irradiated and non-irradiated cells at the position farther away from the exposed area. The comparison of the DSBs induced in non-irradiated areas, II-A and III-B, (both at the same distance from the irradiated cells) allows to conclude that the number of irradiated cells influences the bystander effects, since, as obtained in **Figure 52**, the number of DSBs induced in the "Bystander III-B" region is higher when compared with the one of region "Bystander II-A", except for 100 mGy.

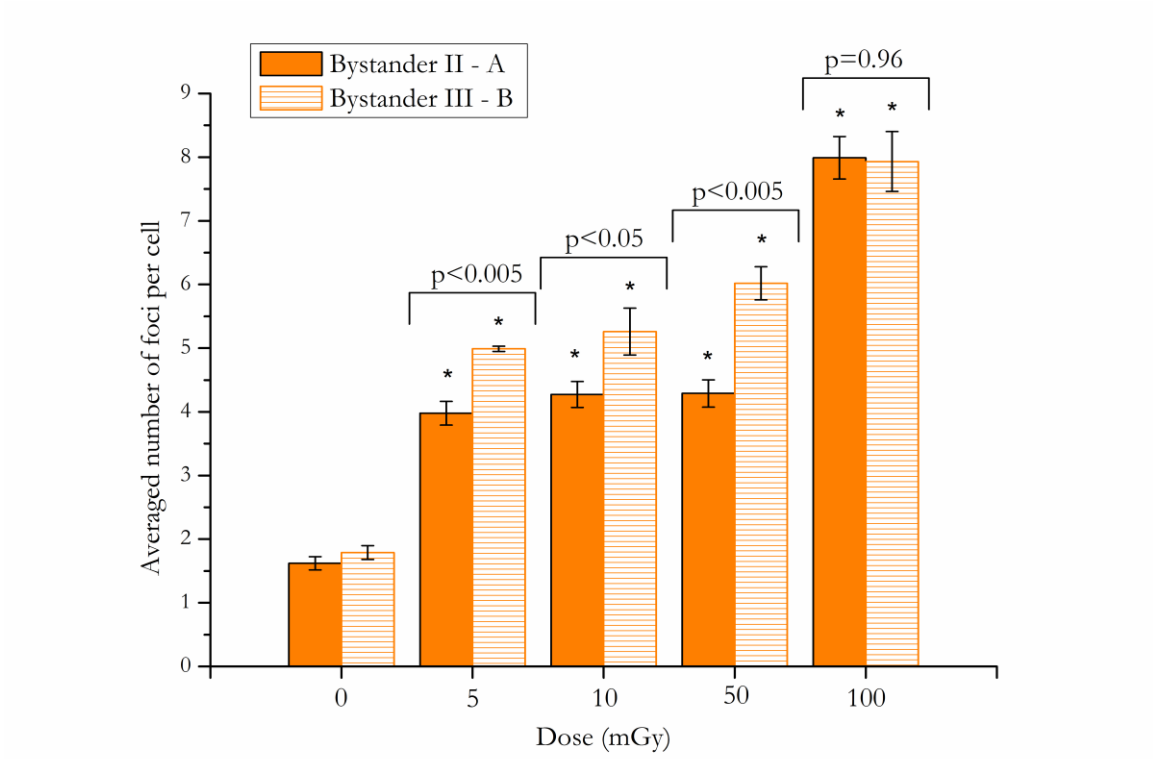

Figure 54: Induction of DSBs in "Bystander II – A" and "Bystander III – B" areas. "Bystander II – A" and "Bystander III – B" refers to non-irradiated cells, corresponding to a lower and a higher number of irradiated cells, respectively, but at the same distance from the irradiated cells. Data were collected from three independent experiments. Error bars represents the SEM and * $p < 0.005$.

6.4 Conclusions

Our results show evidence for bystander effects occurring in cells far away from the irradiated ones, meaning that *bystander signals* can easily spread throughout the cell culture. Additionally, our study highlights that the damage caused by radiation on the surrounding of irradiated areas could be different according to the number of irradiated cells, i.e., for the same dose value; the overall cellular damage could be different.

In our study we used two different irradiation apparatus design in order to investigate whether the bystander effect in A549 cells is influenced by the number of irradiated cells. For this purpose, the A549 cells were exposed to a set of low doses (5, 10, 50 and 100 mGy) of alpha-radiation. A strictly linear relationship between the dose and the DNA damage requires not only that the radiation induced damage in cells follows a mechanism which is independent of DNA damage initiation, but also that every lesion invokes the same trend for malignancy, being independent of cell type or type of radiation. In agreement with Aurengo [Aurengo *et al.*, 2005] who argues that the importance and contribution of each cellular mechanism varies with dose level, our work shows that the induced DSBs vary with dose and in a non-linear way below 100 mGy. In the dose range of 5 up to 50 mGy, a plateau seems to indicate that the level of cellular lesion is similar. Comparing the results obtained for 10 mGy and 5 mGy and for 10 mGy and 50 mGy, a higher number of DSBs is observed at 10 mGy ($p<0.2$). This effect known as low-dose hypersensitivity effect is described in several human cell lines using different types of radiation [Joiner *et al.*, 1996, Joiner *et al.*, 2001 and Marples *et al.*, 2004] and is explained mainly by DNA repair capacity. Studies led by Rothkamm [Rothkamm *et al.*, 2003] and Grudzenski [Grudzenski *et al.*, 2010] demonstrate the persistence of DSBs after very low doses of radiation, while lesions induced by higher doses can be rapidly repaired. They concluded that the DSBs repair after very low doses is substantially compromised indicating a total lack of repair below 1-2 mGy and extremely inefficient below 20 mGy. Our results seem to corroborate these studies, showing a similar response between 5 and 50 mGy that can be explained by the aforementioned inefficient repair mechanisms at these doses values. Moreover, in our studies we observed a higher sensitivity to radiation at 10 mGy showing that besides the inefficient repairing capacity of DNA, the cell irradiation itself might not be the unique process to induce cell damage/killing.

Nowadays, the bystander effects play an important role to quantify the low-dose effects and assessment of the radiological risk in the low dose region, being extensively reported in the literature. The ever increasing number of studies about these effects shows a lack of knowledge of risk assessment at low-doses, supporting the idea that the models used to estimate the population risk after exposure to low dose radiation must be revised. Following the studies [Nagasawa *et al.*, 2003] suggesting that different metabolic repair systems play an important role in bystander effects, depending on the cell line, we analyzed the behavior of A549 cells in terms of bystander response to α-radiation. Our results pointed out that the bystander effects at low doses are not negligible when compared to the matched controls

($p<0.05$). In addition, the bystander signals released after cell irradiation can spread easily by the cell culture, due to the DSBs appearance in the area farthest away of the irradiation culture. However, as one moves away from the area of irradiation, the bystander effects become less pronounced (see **Figure 48**). An important remark in **Figure 48**, is that the behavior of the curves is similar, leading us to hypothesize that the type of injury that occurs in cells that are directly irradiated is the same as occurs in bystander cells. The induction of bystander effects require that irradiated and non-irradiated cells communicate, which can occur via gap junction intercellular communication [Azzam *et al.*, 1998 and Azzam *et al.*, 2001] and/or via the release of various factors into cell culture medium [Iyer *et al.*, 2000 and Narayanan *et al.*, 1997].

Our results indicate that the bystander signals, initiated by very low doses of α-particles in irradiated cells, are dependent of the number of irradiated cells. This finding highlights a very important effect revealing, for the same dose value, a different cellular damage in the surrounding of irradiated cells. This finding may be very important to understand, for instance, the biological effects of radon exposure considering that the deposition of radon progenies' in lungs is non-homogeneous. Indeed, the dose is calculated taking into account the concentration of radon inhaled during a certain number of hours/days. But, if there are hot-spots, i.e. a higher number of particles deposited in a certain area, resulting from the energy deposition of particles onto bronchial epithelial cells, our results show evidences for a different overall cellular damage. When "Bystander I-A" and "Bystander I-B" were compared, as mentioned before, a lower number of DSBs was observed when a lower number of cells were irradiated. But, since a higher cell-to-cell contact was possible in the experiment "Bystander I–B", we study, making use of lindane, the role of gap junctional intercellular communication, in order to evaluate the relevance of both possible ways to induce a bystander response. When both experiments, "Bystander I-A" and "Bystander I-B", were compared for each dose value, using lindane as the treatment agent, the results pinpointed a higher number of DSBs in the area labeled as I-B. These results allow us to conclude that, when a higher number of cells are irradiated a higher cellular lesion can be induced in the surrounding areas.

The results obtained in this work emphasize that the risks attributable to low dose radiations encompass a complex variable cellular response and cannot simply be extrapolated from higher doses. Besides the evidences for bystander effects occurring in cells far away from the irradiated ones, there are also evidences for low-dose hypersensitivity, supporting the hypothesis that the shape of the curve to estimate the risks attributable to low dose exposure might be non linear.

CHAPTER 7

GENE-EXPRESSION IN DIRECTLY IRRADIATED AND BYSTANDER A549 CELLS AFTER EXPOSURE TO LOW DOSES OF α-RADIATION

7.1 Introduction

The existence of a bystander effect, in which cells not exposed directly to radiation express a cellular damage, was described in chapters 5 and 6 of this dissertation. As a step further, trying to better elucidate the signaling molecules involved in bystander effects, in the present study we have measured gene-expression in directly irradiated and bystander A549 cells at four hours after exposure to dose values of 5, 10, 50 and 100 mGy from α-particles. Ghandi [Ghandi et al., 2008] and Chauhan [Chauhan et al, 2012] showed, in a global gene expression, that a peak of gene expression is observed at four hours after exposure. For that reason in this work this time-point was also chosen.

Several studies regarding gene expression changes, induced by IR, gave important insights to elucidate signaling pathways which leads to cell cycle arrest, DNA repair, and apoptosis, among others. One of the main genes studied, which is a major contributor on understanding the stress response to IR, is the tumour suppressing gene (p53). Although not essential for normal development, it is the most commonly mutated gene in human cancer [Hollstein *et al.*, 1991].

The **gene GADD45A**, a common p53-regulated radiation response and DNA damage-inducible, has been found to play an important role in the G2-M checkpoint in response to several types of DNA damage [Jin *et al.,* 2000, Wang *et al.*, 1999 and Zhan *et al.*, 1999]. A study performed by Chauhan [Chauhan *et al.*, 2012], in directly irradiated A549 cells, showed, 4 hours after α-irradiation of 0.9 Gy, an up-regulation of this gene. In addition, other study performed by Ghandhi [Ghandhi *et al.*, 2008] also showed an up-regulation of this gene in both directly and bystander IMR-90 cells, being more expressive in directly irradiated ones. Due to the evidence of an expression of this gene related with IR, and due to its fundamental role on genome stability, in the present study we measured the gene expression of GADD45A in both irradiated (to dose values below 100 mGy) and bystander cells.

In contrast, to common p53-regulated radiation response genes like CDKN1A, which reveled high levels on directly irradiated cells but no changes in bystander, genes regulated by the nuclear factor-kappa B (NF-kB), such as **PTGS2**, IL8 and **BCL2A1**, respond nearly identically in directly irradiated and in bystander cells [Ghandhi *et al.*, 2008]. Several studies show that the transcription factor NF-kB plays an important role on anti-apoptotic mechanisms [Begg *et al.*, 1996, Liu *et al.*, 1996, Van Antwerp *et al.*, 1996]. Being the apoptosis mechanisms less exploited in the low dose range, in this thesis we studied the gene expression of PTGS2 and BCL2A1, in both irradiated (to dose value below 100 mGy) and in bystander cells. NF-kB is a protein complex that controls the transcription of DNA, i.e. is able to bind to a specific DNA sequence, thus controlling the transcription of genetic information from DNA to mRNA. In **Figure 55**, it is illustrated a cross-talking between NF-kB signaling and apoptosis. Several stress stimuli can induce apoptosis, such as IR, chemotherapeutic drugs, among others. Regarding, IR effects, NF-kB can be activated by the ROS released after irradiation. The anti-apoptotic effect can be carried out by NF-kB targeting genes including BCL-2 family, TRAF2, CIAP, FLIP and A-20, which has anti-apoptosis effect by either re-activating NF-kB signaling or blocking signal transduction as a negative feedback to activation of apoptosis.

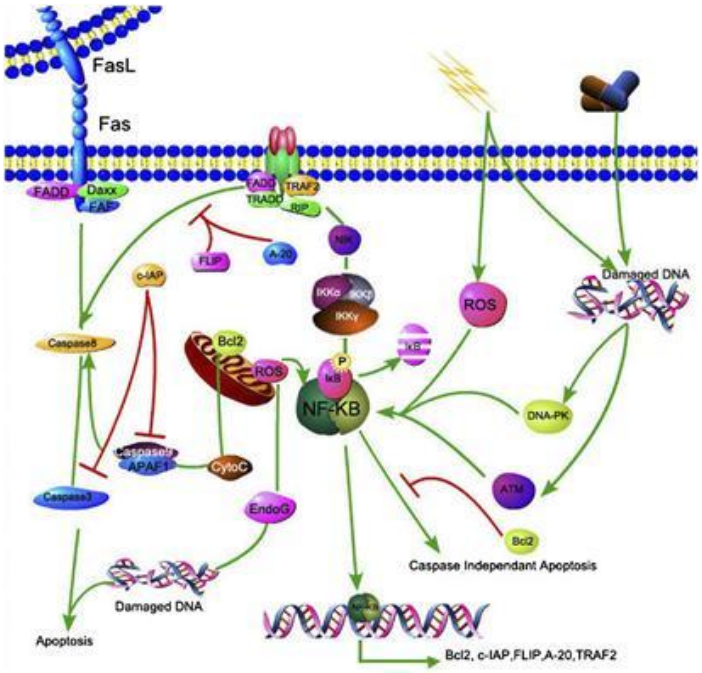

Figure 55: Cross-talking between apoptosis and NF-kB signaling. Figure extracted from Sun and Karin [Sun and Karin, 2008].

Apoptosis is a form of programmed cell death, executed by caspases, which are cysteinyl aspartate proteases that occurs in multicellular organisms being crucial for tissue homeostasis. Caspase is characterized for playing the central role in the transduction of apoptotic signals. Mitochondria are known to play a central role in cell death control [Susin *et al.*, 1998]. During programmed cell death, cytochrome *c* is released from mitochondria into the cytosol, where it binds with APAF1 to activate a series of caspase cascades [Cai *et al.*, 1998; Liu *et al.*, 1996].

Two pathways of cell death, i.e. apoptosis, can be distinguished: the **intrinsic** and **extrinsic** (see **Figure 56**). Under normal conditions, BH3-only proteins are either present in very low levels in the cytosol or in mitochondrial membrane, or remain inactive in the cytoplasm. It is known [Kelly *et al.*, 2010 and Willis and Adams, 2005] that IR impinging in cells initiates changes through the intrinsic pathway inducing a significant up-regulation of the BH3-only proteins. The BH3-only protein responds to a unique type of stress stimulus moving to the mitochondria and subsequently can be attached to pro-survival proteins (apoptosis inhibitors such as BCL2A1) or to pro-apoptotic proteins (apoptosis promoters, such as BAX, BAK) (see **Figure 56**).

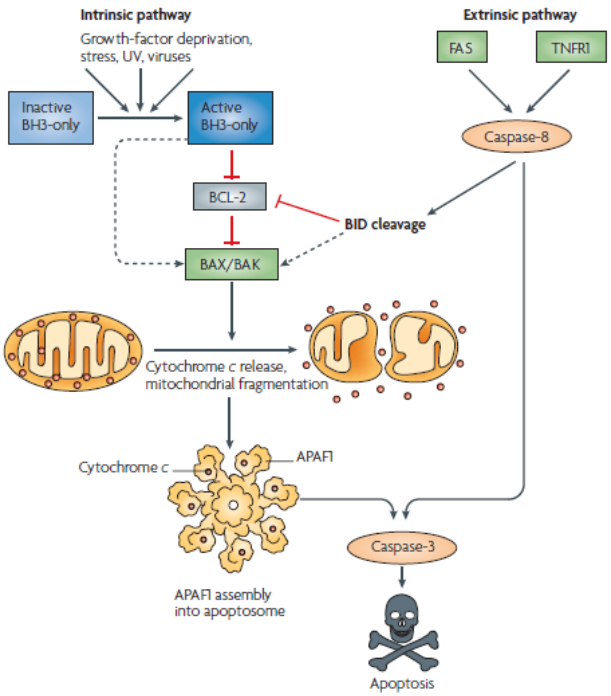

Figure 56: The intrinsic and extrinsic pathways in apoptosis. Apoptosis can be induced by cell surface receptors, extrinsic pathway, such as FAS and TNFR1 and by intrinsic pathway due to the exposure to various stress stimuli. Stress stimuli that induce apoptosis include DNA damage by IR, aberrant signals from cell surface receptors and production of ROS, among others. Figure extracted from Youle [Youle *et al.*, 2008].

As shown in the **Figure 56**, once activated, BAX and BAK promote cytochrome *c* release and mitochondrial fission, which leads to the activation of APAF1 into an apoptosome and activate caspase-9 to activate caspase-3. Under normal situations, caspase-3 activation induces cell demolition and removal. Taking into account the work made by Cai [Cai *et al.*, 1998], it is clear that a central and common pathway for signaling apoptosis involves release of cytochrome *c* from mitochondria and subsequent activation of the death protease caspase-3.

Cory [Cory *et al.*, 2003] stated that, whether a cell should live or die is largely determined by the BCL-2 family of anti-and pro-apoptotic regulators. Indeed, this vital process of interplay between opposing families, is a driving force to go deeply in the understanding of how this family of proteins integrates intracellular cues to arbitrate whether initiator caspases are unleashed.

The BCL-2 family members have been classified into three categories. One, which includes BCL-2, BCL-xL and BCL-A1, inhibits apoptosis, whereas the second category, the BAX family, promotes apoptosis. The third class of BH3-only proteins includes BAD and BID promotes apoptosis [Youle and Strasser, 2008]. The **gene BCL2A1**, the BCL2 related protein A1, has been reported as an apoptosis inhibitor. The protein encoded by this gene is able to reduce the release of pro-apoptotic cytochrome *c* from mitochondria and block

caspase activation. As previously described, the genes regulated by NF-kB are known to be crucial to elucidate the bystander effect. Bearing this in mind, in this thesis we studied the expression of BCL2A1 and PTGS2, genes regulated by NK-kB, both for directly irradiated and bystander cells.

7.1.1 The RNA isolation and cDNA synthesis

The mRNA transcribed, from the gene of interest, contains the information about its expression intensity. As a result, the first step, being crucial for the reliable information about gene-expression intensity, is the extraction of either the total RNA or an mRNA from biological sample. Bearing this in mind, Swift *et al.* [Swift *et al.*, 2000] claimed that the purity and integrity of the RNA extracted is an essential prerequisite for a good procedure. Namely, the RNA sample must be free of any DNA contamination, and well preserved from degradation by RNAses.

The RNA molecules are not recognized as a template for the polymerase chain reaction (PCR). So, a reverse-transcription of RNA into its complementary DNA copy must be performed. At this stage, the resulting is a single-stranded cDNA.

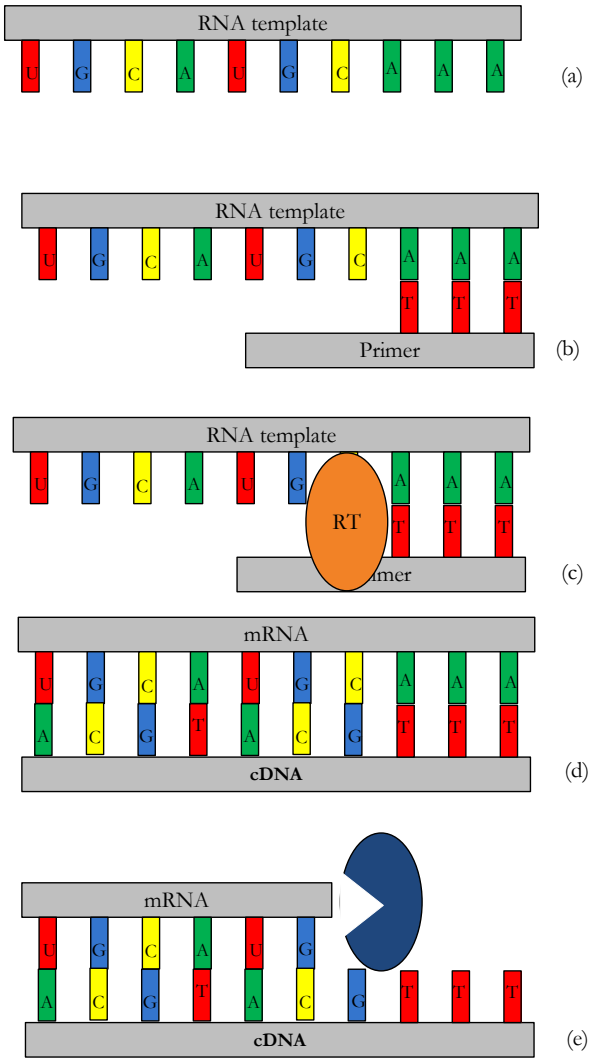

Figure 57: A schematic view of cDNA synthesis. (a) RNA template. Before the synthesis of cDNA, total or mRNA must be extracted from the biological sample. (b) To generate cDNA molecule by an enzyme reverse transcriptase (RT), a primer must be annealed to the template of RNA. This is the starting point for DNA synthesis. (c) The action of the enzyme RT beginning at the primer annealing site. (d) the first cDNA strand created. (e) Removal of RNA by RNAse H. After this step, the single-stranded cDNA is ready to be used for amplification by PCR. Figure adapted from Kendall and Riley [Kendall and Riley, 2000].

In this thesis, the Moloney Murine Leukemia Virus (M-MuLV, MMLV) reverse transcriptase enzyme was used. As can be seen in **Figure 57** a primer is needed to initiate the synthesis of CDNA by RT. The kit used in this work uses the oligo-dT as a primer.

7.1.2 Principle of the quantitative real-time PCR

The PCR is a polymerase chain reaction able to amplify a single piece of DNA generating several copies of a particular DNA sequence. During PCR, the cDNA is mixed with a master mix, containing a DNA polymerase and primers, which serve as recruitment sites for binding of the polymerase. During the PCR technique, the samples are exposed to a series of temperature cycles; so, to perform this technique a thermocylcer is used.

In the PCR technique, 3 well-defined steps can be described: **denaturation**, **annealing** and **extension**.

- **Denaturation**: engages the heating of the samples (94-98 °C) to cause denaturation of the template DNA, disrupting the hydrogen bonds and base interactions that, all together, maintain the DNA strands joined.
- **Annealing**: Once the strands are separated, the temperature is decreased (48 – 72 °C, depending on the melting temperature) to allow the primers to anneal to complementary regions of the template.
- **Extension**: in this, the temperature must be between 68-72 °C. The polymerase extends the primer to form a nascent DNA strand.

The three steps are illustrated in **Figure 58**. This process is repeated several times (typically 25-35 cycles with the 3 aforementioned steps each). At the end, the region of interest was largely amplified, because each new strand created can be used as a template for the primers.

In the work presented in this thesis, the selected chemistry to quantify the PCR products is the TaqMan probe; a based fluorogenic 5' nuclease chemistry (see **Figure 58**).

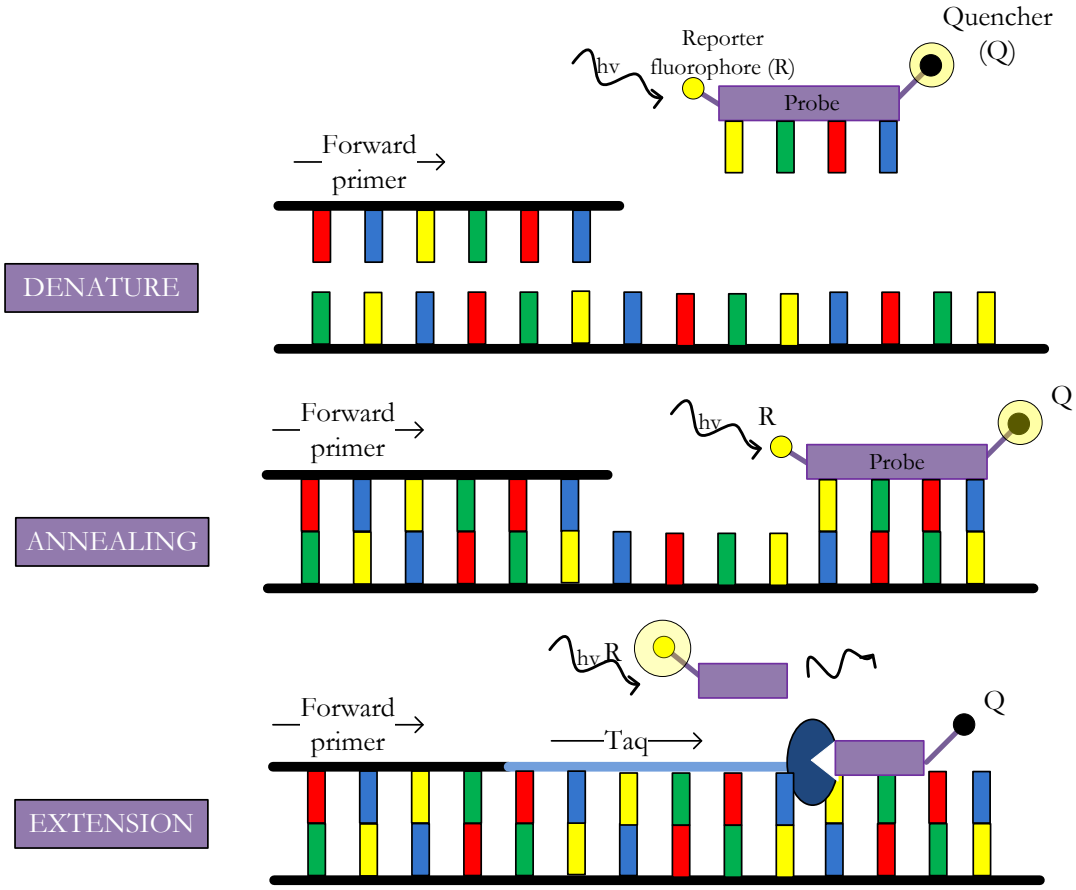

Figure 58: The 3 steps of PCR; denaturation, annealing and extension.

By analyzing **Figure 58**, denaturation (a), annealing (b) and extension (c) can be summarized as follows:

- (a) - A probe is constructed containing a reporter fluorescent (R) dye on the 5' end and a quencher (Q) dye on the 3' end. While the probe is intact, the proximity of the quencher dye greatly reduces the fluorescence emitted by the reporter dye by fluorescence resonance energy transfer (FRET).
- (b) - If the target sequence is present, the probe anneals downstream from one of the primer sites.
- (c) - The probe is cleaved by the 5´nuclease activity of Taq DNA polymerase as this primer is extended. At this stage, the reporter dye is separated from the quencher dye, being the reporter dye signal more intensive. Also, the probe is removed from the target strand, so, the primer can complete the strand replication. Additional reporter dye molecules are cleaved from their probes at each cycle, resulting in an increased intensity that is proportional to the amount of the amplicon (a short segment of DNA amplified during PCR) produced.

Figure 59 shows the characteristic amplification plot, commonly used in quantitative analysis.

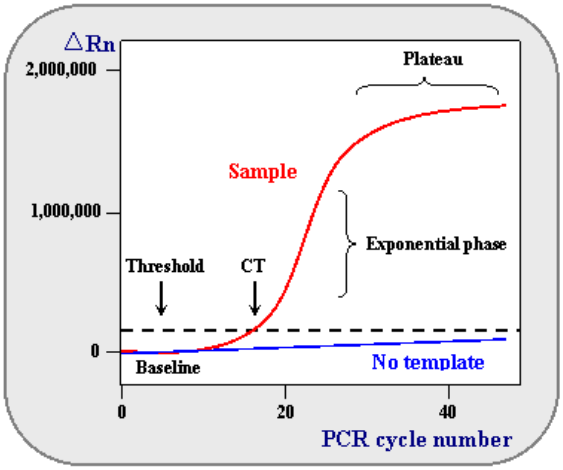

Figure 59: Model of a single-sample amplification plot, showing parameters used to a quantitative analysis.. Normalized reporter (Rn) is the ratio of the fluorescence emitted by the reporter dye and the passive reference dye. ΔRn is calculated by subtracting the baseline line value to the Rn values. All PCR measurements should have a No Template Control (NTC), without cDNA template, in order to verify the amplification quality. Figure extracted from: http://www.ncbi.nlm.nih.gov/projects/genome/probe/doc/TechQPCR.shtml

As displayed in **Figure 59**, three regions of the curve can be distinguished.

- Region I – *Baseline*: the initial cycles don't contain a significant difference of the fluorescence signal. This means that under the threshold line the increase of the fluorescence signal is mixed with the background fluorescence noise. At the end, this noise should be subtracted from the amplification curves.
- Region II – *Growth*: represents the increasing fluorescence acquisition. After reaching the threshold line, the fluorescence signal is considered to be a real signal, which can be used to established the threshold cycle (Ct) for a sample.
  The Ct is the intersection between the amplification curve and the baseline (see **Figure 59**).
  The threshold line has an arbitrary location; however there are some recommendations, such as, locate the line above the noise region, and in the region of the curve displaying an exponential growth.
- Region III – *Plateau*: in this region there is an attenuation of the fluorescence acquisition, mainly due to non-specific products generated. [Kainz, 2000].

7.2 Materials & Methods

7.2.1 Cell culture and exposure

A549 cells were cultured at 37°C with 5% CO_2 in DMEM medium containing 10% FBS and 1% penicillin-streptomycin solution. Log-phase cells were seeded onto 3.5 cm culture dishes with 6.3 µm of Mylar® base 24 hours before irradiation. Cells at exponential growth were exposed to 100, 50, 10 and 5 mGy using the monoenergetic ^{210}Po source described in the chapter IV. Control cultures were submitted to the same experimental conditions but not irradiated.

7.2.2 Medium transfer technique

In this study, the gene-expression quantification was performed in cells directly irradiated (Group I) and in cells in contact with the *irradiated medium* (Group II) (see **Figure 60**). The mentioned group, I and II, are the same described in chapter 5. The only exception is the elapsed time after irradiation to quantify the gene expression. At this experience, cells were harvested after 4h post-irradiation.

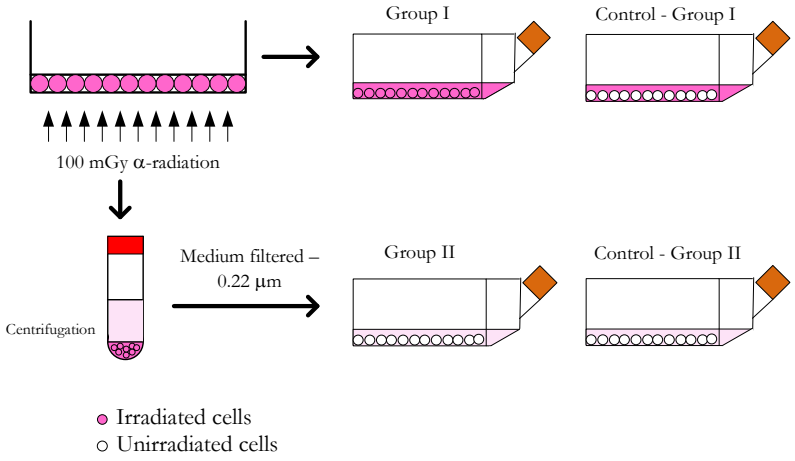

Figure 60: Medium transfer study for an exposure of 100 mGy; the same methodology was used for the others dose values. In group I irradiated cells were cultured with fresh medium after exposure to the aforementioned radiation doses. In group II, non-irradiated cells received irradiated medium.

7.2.3 RNA isolation and cDNA generation

The RNA isolation was performed using the PureLink® RNA Mini kit (Invitrogen), 4 hours post-irradiation, according to the manufacturer's instructions (see complete protocol in annexes-Protocol IV). Briefly, cells were lysated with Lysis Buffer with 2-mercaptoethanol, being the homogenization performed using a vortex. The cells homogenate were centrifuged, being the supernatant transferred to a clean RNase-free tube. One volume of 70% ethanol was added and mixed, by a vortex, to eliminate any precipitate. Then, 700 µl of the sample were transferred to a spin cartridge and centrifuged at room temperature. After

discard the flow-through, 700 µl of wash buffer I was added. Then, two washes were performed using 500 µl of wash buffer II. At the end, after drying the membrane by centrifugation, 50 µl of RNase-free water was added. After 1 minute of incubation the spin cartridge was centrifuged to elute the RNA from the membrane.

The concentration of the RNA sample isolation was determined through spectrophotometric method (see complete protocol in annexes-Protocol IV).At this, both OD_{260} and OD 2_{80} were measured to analyze the RNA quality. By the recommendations of the manufacturer, the total RNA isolated using the mentioned kit has an $OD_{260/280} > 1.8$ when samples are diluted in Tris-HCl (pH 7.5). As so, an $OD_{260/280} > 1.8$ indicates than RNA is clean of proteins or other UV chromophores that could either interfere with downstream applications or negatively affect the stability of the stored RNA.

The synthesis of cDNA from total RNA was performed using the High Capacity RNA-to-cDNA kit (Applied Biosystems), according to the manufacturer's instructions (see complete protocol in annexes-Protocol-V). The total amount of RNA used, at all samples, was determined to be 1 µg. For all samples, a +RT (with enzyme) and a –RT (without enzyme) reactions were done (see **Figure 61**).

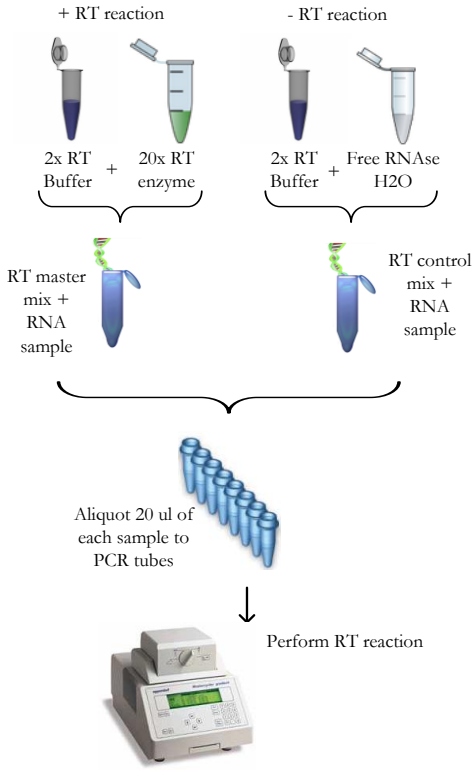

Figure 61: Illustration of the cDNA protocol.

7.2.4 Quantitative Real-Time PCR (qRT-PCR)

qRT-PCR reactions were performed with the ABI 7300 Real Time PCR system using TaqMan® Universal Master Mix II (Applied Biosystems) with initial activation at 50° for 120 seconds and 95° for 10 minutes followed by 40 cycles of 95° for 15 seconds and 60° for 60 seconds.
The TaqMan gene expression assays, GADD45A, BCL2A1, PTGS2 and GAPDH (endogenous control) were obtained from Applied biosystems. **Table 7** shows the volume used per reaction of each components of a PCR reaction.

Table 7: PCR reaction volume.

PCR reaction mix component	Volume per reaction (μL)
TaqMan® Universal Master Mix II	10
TaqMan Assay	1.0
cDNA template + RNase-free water	9.0
Total Volume	**20.0**

Reactions were prepared in 96-well plates and performed in triplicate. The relative expression of each gene was determined by using the comparative threshold (Ct) method [Livak and Schmittgen, 2001].

7.2.5 Statistical Analysis

Significance of variances between either for dose values and directly irradiated and bystander cells, for a specific target gene, was obtained by statistical one-way ANOVA test.

7.3 Results

The gene expression, in both directly and bystander cells, was obtained 4h after exposure to several doses of α-radiation. To analyze the expression of target genes, we applied the comparative Ct method. This allows normalizing to an endogenous reference using data generated during the PCR experiment. The expression level of the target gene, normalized to an endogenous control and relative to a calibrator, is calculated using the following equation:

$$\text{expression level} = 2^{-\delta Ct} \tag{25}$$

where:

$$\delta Ct = \Delta C_{T,q} - \Delta C_{T,cb} \tag{26}$$

Being $\Delta C_{T,q}$ the difference between the target gene and the endogenous control, and $\Delta C_{T,cb}$ refers to the calibrator, i.e. using the 0 mGy results as reference.

7.3.1 Directly irradiated cells

As previously explained, the gene expression was performed in directly irradiated and in bystander cells. In this section, the effects on directly irradiated cells will be discussed. Making use of the comparative Ct method, the fold difference in gene expression was obtained by **equation 25** with reference to 0 mGy. **Table 8, Table 9,** and **Table 10** display the results obtained for the three independent experiments.

Table 8: Ct values for the 1st independent experience. Using the GAPDH as the endogenous control, the $2^{-\delta Ct}$ values were obtained for both genes, GADD45A and BCL2A1, for different dose values.

Direct Irradiation – 1st experience						
	Dose values (mGy)					
GAPDH	**0**	**5**	**10**	**50**	**100**	**500**
Ct values	19.28	18.81	18.17	18	19	17.67
	19.23	18.73	18.21	18.03	18.89	17.58
	19.17	18.68	18.22	17.89	18.8	17.51
Mean Ct	19.22	18.74	18.2	17.97	18.89	17.58
Standard deviation	0.05	0.06	0.02	0.07	0.1	0.08
GADD45A						
Ct values	27.41	27.13	26.57	26.69	27.04	25.07
	27.3	27	26.75	26.61	27.01	25.16
	27.23	27.02	26.89	26.57	27	25.17
Mean Ct	27.31	27.05	26.73	26.62	27.01	25.13
Standard deviation	0.09	0.07	0.16	0.06	0.02	0.05
ΔCt	8.08	8.31	8.53	8.65	8.12	7.54
δCt	0	0.22	0.45	0.56	0.03	-0.54
$2^{-\delta Ct}$	1	0.85	0.73	0.67	0.97	1.45
BCL2A1						
Ct values	28.49	28.46	28.91	28.12	27.82	28.46
	28.41	28.42	28.8	28.05	28.04	28.44
	28.45	28.51	28.66	28.10	28.05	28.42
Mean Ct	28.45	28.46	28.79	8.09	27.97	28.44
Standard deviation	0.04	0.04	0.12	0.03	0.13	0.02
ΔCt	9.22	9.72	10.59	10.11	9.07	10.85
δCt	0	0.5	1.36	0.89	-0.15	1.63
$2^{-\delta Ct}$	1	0.70	0.38	0.53	1.10	0.32

Table 9: Ct values for the 2nd independent experience. Using the GAPDH as the endogenous control, the $2^{-\delta Ct}$ values were obtained for both genes, GADD45A and BCL2A1, for different dose values.

Direct Irradiation – 2nd experience						
	Dose values (mGy)					
GAPDH	**0**	**5**	**10**	**50**	**100**	**500**
Ct values	18.25	19.84	18.98	17.69	17.16	17.67
	19.17	19.21	18.93	17.69	17.1	17.58
	-	-	-	-	17.2	17.51
Mean Ct	18.71	19.52	18.95	17.69	17.15	17.58
Standard deviation	0.65	0.44	0.03	0	0.05	0.08
GADD45A						
Ct values	28.5	27.78	27.32	27.16	27.21	25.98
	28.39	27.52	27.38	27.09	27.23	25.97
	28.43	27.67	27.5	27.2	27.17	25.61
Mean Ct	28.44	27.65	27.4	27.15	27.20	25.85
Standard deviation	0.05	0.13	0.09	0.05	0.03	0.21
ΔCt	9.73	8.13	8.445	9.46	10.05	8.26
δCt	0	-1.59	-1.28	-0.27	0.32	-1.46
$2^{-\delta Ct}$	1	3.02	2.43	1.20	0.80	2.75
BCL2A1						
Ct values	30.61	28.8	29.02	28.54	28.16	28.46
	30.56	29.11	29.03	28.47	28.23	28.44
	30.62	29.13	28.79	28.43	28.26	28.42
Mean Ct	30.59	29.01	28.94	28.48	28.21	28.44
Standard deviation	0.03	0.18	0.13	0.05	0.05	0.02
ΔCt	11.88	9.48	9.99	10.79	11.06	10.85
δCt	0	-2.39	-1.89	-1.09	-0.82	-1.03
$2^{-\delta Ct}$	1	5.27	3.71	2.13	1.76	2.04

Table 10: Ct values for the 3rd independent experience. Using the GAPDH as the endogenous control, the $2^{-\delta Ct}$ values were obtained for both genes, GADD45A and BCL2A1, for different dose values.

Direct Irradiation – 3rd experience						
	Dose values (mGy)					
GAPDH	**0**	**5**	**10**	**50**	**100**	**500**
Ct values	17.6	17.51	17.63	17.81	-	17.96
	17.45	17.5	17.55	18.05	-	18.24
	17.55	17.58	-	-	-	-
Mean Ct	17.53	17.53	17.59	17.93	-	18.1
Standard deviation	0.07	0.04	0.05	0.16	-	0.19
GADD45A						
Ct values	25.35	26.08	26.21	27.4	-	26.25
	25.85	26.35	26.46	28	-	26.41
	25.42	-	26.08	-	-	-
Mean Ct	25.54	26.21	26.25	27.70	-	26.33
Standard deviation	0.27	0.019	0.19	0.42	-	0.11
ΔCt	8.00	8.68	8.66	9.77	-	8.23
δCt	0	0.67	0.65	1.76	-	0.22
$2^{-\delta Ct}$	1	0.62	0.63	0.29	-	0.85
BCL2A1						
Ct values	27.05	28.5	28.41	28.05	-	27.95
	26.93	28.75	28.51	28.18	-	28.10
	26.91	28.64	-	-	-	-
Mean Ct	26.96	28.63	28.46	28.11	-	28.02
Standard deviation	0.07	0.12	0.07	0.09	-	0.10
ΔCt	9.43	11.1	10.87	10.18	-	9.92
δCt	0	1.67	1.44	0.755	-	0.495
$2^{-\delta Ct}$	1	0.31	0.36	0.59	-	0.70

As can be evaluated from tables 9 to 11, there are discrepancies, for certain dose values, between the three independent experiments. Consequently, after performing a statistical evaluation, some values of $2^{-\delta(\Delta Ct)}$ were considered outliers. **Table 11** shows the values of $2^{-\delta\Delta Ct}$ which were retained and will be considered for further studies.

Table 11: Values of $2^{-\delta Ct}$ for both genes, considered for further studies, after take out the outliers.

GADD45A	**0**	**5**	**10**	**50**	**100**	**500**
$2^{-\delta Ct}$	1	0.85	0.73	0.67	0.97	1.45
	1	0.62	0.63	0.29	0.80	0.85
Mean	1	0.74	0.68	0.48	0.88	1.15
Standard deviation	0	0.16	0.06	0.27	0.12	0.42
BCL2A1						
$2^{-\delta Ct}$	1	0.70	0.38	0.53	1.10	0.32
	1	0.31	0.36	0.59	1.76	0.70
Mean	1	0.51	0.37	0.56	1.43	0.51
Standard deviation	0	0.27	0.01	0.03	0.46	0.27

Figure 62 shows the relative gene expression for both, GADD45A and BCL2A1 genes 4h after irradiation for cells directly irradiated.

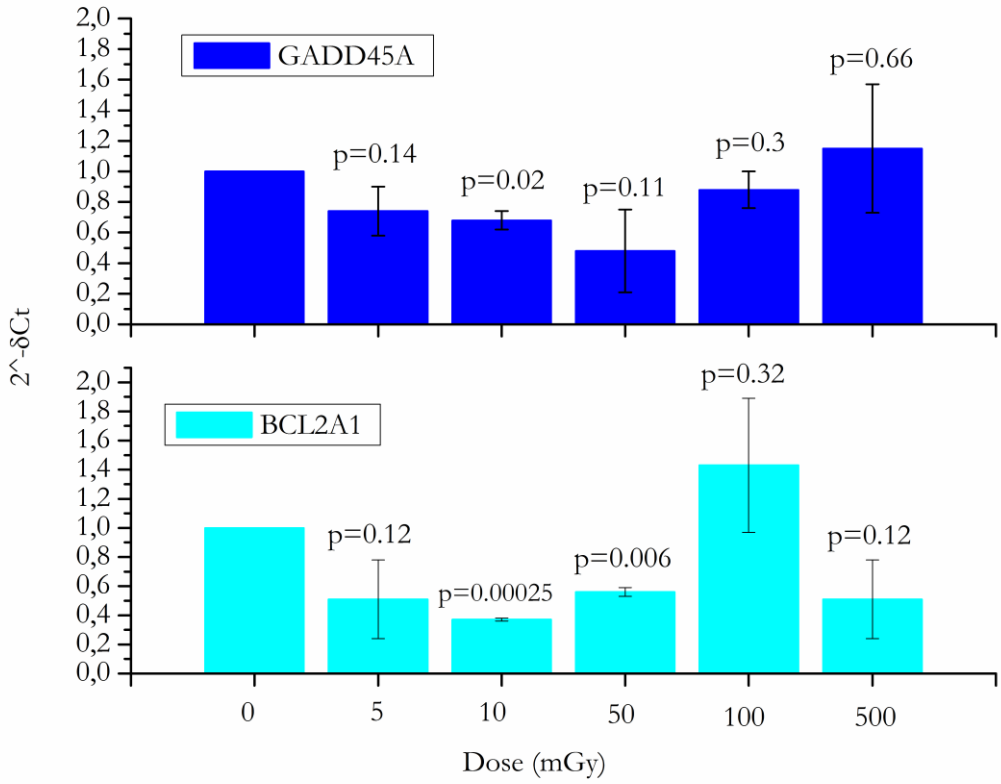

Figure 62: Relative gene expression levels after direct radiation. Quantitative real-time RT-PCR was used to quantify the expression of the GADD45A and BCL2A1 genes 4h after irradiation of A549 cells. Gene expression was normalized to GAPDH and is relative to the expression of 0 mGy. The presented data corresponds to the mean and the standard deviation of two independent experiences. The *p*-values represent the statistical analysis between each dose values and the control, i.e. 0 mGy.

As can be observed in **Figure 62, i**n directly irradiated cells, the gene expression level was almost similar, to the control, for all doses values studied. The exceptions belong to 10 mGy ($p<0.05$) for GADD45A and 10 ($p<0.0005$) and 50 mGy ($p<006$) for BCL2A1. It can be inferred, as well, that for very low doses (<50 mGy) both genes expressed a down-regulation. According to the results obtained by Chauhan [Chauhan et al, 2012] the gene GADD45A shows to be dose dependent. Being the same behavior observed for the BCL2A1 gene.

7.3.2 Bystander cells

Table 12, **Table 13**, and **Table 14** display the results obtained for the three independent experiments.

Table 12: Ct values for the 1st independent experience. Using the GAPDH as the endogenous control, the $2^{-\delta Ct}$ values were obtained for both genes, GADD45A and BCL2A1, for different dose values, for bystander cells.

Bystander Irradiation – 1st experience						
	Dose values (mGy)					
GAPDH	**0**	**5**	**10**	**50**	**100**	**500**
Ct values	17.51	18.02	17.92	18.01	19.4	18.23
	17.59	18	18.1	18.05	19.34	18.37
	27.4	17.97	18.16	18.01	19.25	18.15
Mean Ct	17.5	17.99	18.06	18.02	19.33	18.25
Standard deviation	0.09	0.02	0.12	0.02	0.07	0.11
GADD45A						
Ct values	27.16	27.39	27.65	27.57	29.14	26.79
	27.05	27.41	27.8	27.6	29.2	26.68
	26.96	27.43	27.93	27.64	29.22	26.55
Mean Ct	27.05	27.41	27.79	27.60	29.18	26.67
Standard deviation	0.10	0.02	0.14	0.03	0.04	0.12
ΔCt	9.55	9.41	9.73	9.58	9.85	8.42
δCt	0	-0.14	0.17	0.02	0.3	-1.13
$2^{-\delta Ct}$	1	1.10	0.88	0.98	0.81	2.19
BCL2A1						
Ct values	26.93	26.00	26.25	27.15	27.81	27.54
	26.84	26.02	26.25	27.12	27.79	27.65
	26.83	26.13	26.2	27.11	27.74	27.69
Mean Ct	26.86	26.05	26.23	27.12	27.78	27.62
Standard deviation	0.05	0.07	0.02	0.02	0.03	0.07
ΔCt	9.36	8.05	8.17	9.10	8.45	9.37
δCt	0	-1.31	-1.19	-0.26	-0.91	0.01
$2^{-\delta Ct}$	1	2.48	2.28	1.20	1.88	0.99

Table 13: : Ct values for the 2nd independent experience. Using the GAPDH as the endogenous control, the $2^{-\Delta\Delta Ct}$ values were obtained to both genes, GADD45A and BCL2A1, at different dose values, for bystander cells.

Bystander Irradiation – 2nd experience						
	Dose values (mGy)					
GAPDH	**0**	**5**	**10**	**50**	**100**	**500**
Ct values	18.48	18.08	18.5	18.41	18.59	18.23
	18.46	18.17	18.49	18.31	18.41	18.37
	18.63	18.01	18.57	18.31	18.33	18.15
Mean Ct	18.52	18.08	18.52	18.34	18.44	18.25
Standard deviation	0.09	0.08	0.04	0.05	0.13	0.11
GADD45A						
Ct values	26.73	26.69	26.65	26.65	26.74	26.79
	26.69	26.45	26.64	26.76	26.75	26.68
	26.58	26.57	26.85	26.75	26.72	26.55
Mean Ct	26.66	26.57	26.71	26.72	26.73	26.67
Standard deviation	0.07	0.12	0.11	0.06	0.01	0.12
ΔCt	8.14	8.48	8.19	8.37	8.29	8.42
δCt	0	0.34	0.05	0.233333	0.15	0.28
$2^{-\delta Ct}$	1	0.79	0.96	0.85	0.90	0.82
BCL2A1						
Ct values	27.75	27.73	27.69	27.35	27.17	27.54
	27.73	27.76	27.68	27.27	27.2	27.65
	27.72	-	27.62	27.54	27.22	27.69
Mean Ct	27.73	27.74	27.66	27.38	27.19	27.62
Standard deviation	0.01	0.02	0.03	0.13	0.02	0.07
ΔCt	9.21	9.65	9.14	9.04	8.75	9.37
δCt	0	0.44	-0.06	-0.16	-0.45	0.16
$2^{-\delta Ct}$	1	0.73	1.04	1.12	1.37	0.89

Table 14: Ct values for the 3rd independent experience. Using the GAPDH as the endogenous control, the $2^{-\delta Ct}$ values were obtained for both genes, GADD45A and BCL2A1, for different dose values, for bystander cells.

Bystander Irradiation – 3rd experience						
	Dose values (mGy)					
GAPDH	**0**	**5**	**10**	**50**	**100**	**500**
Ct values	18.73	17.93	17.76	-	18.44	17.02
	19.55	17.91	18.41	-	18.2	17.07
	-	-	-	-	-	-
Mean Ct	19.14	17.92	18.08	-	18.32	17.04
Standard deviation	0.57	0.01	0.45	-	0.16	0.03
GADD45A						
Ct values	27.91	26.33	25.94	-	25.34	24.83
	28	26.53	25.91	-	25.44	24.82
	-	-	25.89	-	25.38	24.89
Mean Ct	27.95	26.43	25.91	-	25.38	24.84
Standard deviation	0.06	0.14	0.02	-	0.05	0.03
ΔCt	8.81	8.51	7.82	-	7.06	7.80
δCt	0	-0.30	-0.98	-	-1.74	-1.01
$2^{-\delta Ct}$	1	1.23	1.98	-	3.35	2.01
BCL2A1						
Ct values	26.92	27.51	25.92	-	26.29	25.65
	27.69	26.76	25.93	-	26.33	25.58
	28.54	26.79	26.02	-	26.62	25.54
Mean Ct	27.71	27.02	25.95	-	26.41	25.59
Standard deviation	0.81	0.42	0.05	-	0.18	0.05
ΔCt	8.57	9.1	7.87	-	8.09	8.54
δCt	0	0.52	-0.70	-	-0.48	-0.03
$2^{-\delta Ct}$	1	0.69	1.63	-	1.39	1.02

Assuming the same methodology as for directly irradiated cells, and due to the same reasons, after performing a statistical evaluation, some values of $2^{-\delta Ct}$ were considered outliers. Table shows the final values of $2^{-\delta Ct}$ which were considered for further evaluation.

Table 15: Values of $2^{-\delta Ct}$ for both genes, considered for further studies, after take out the outliers.

GADD45A	0	5	10	50	100	500
$2^{-\delta Ct}$	1	1.10	0.88	0.98	0.81	2.19
	1	1.23	0.96	0.85	0.90	2.01
Mean	1	1.16	0.92	0.91	0.85	2.10
Standard deviation	0	0.09	0.05	0.09	0.06	0.12
BCL2A1						
$2^{-\delta Ct}$	1	0.73	2.28	1.20	1.37	0.99
	1	0.69	1.63	1.12	1.39	1.02
Mean	1	0.71	1.95	1.16	1.38	1.00
Standard deviation	0	0.02	0.46	0.05	0.01	0.02

Figure 63 shows the relative gene expression for both, GADD45A and BCL2A1 genes, after 4h of irradiation for bystander cells.

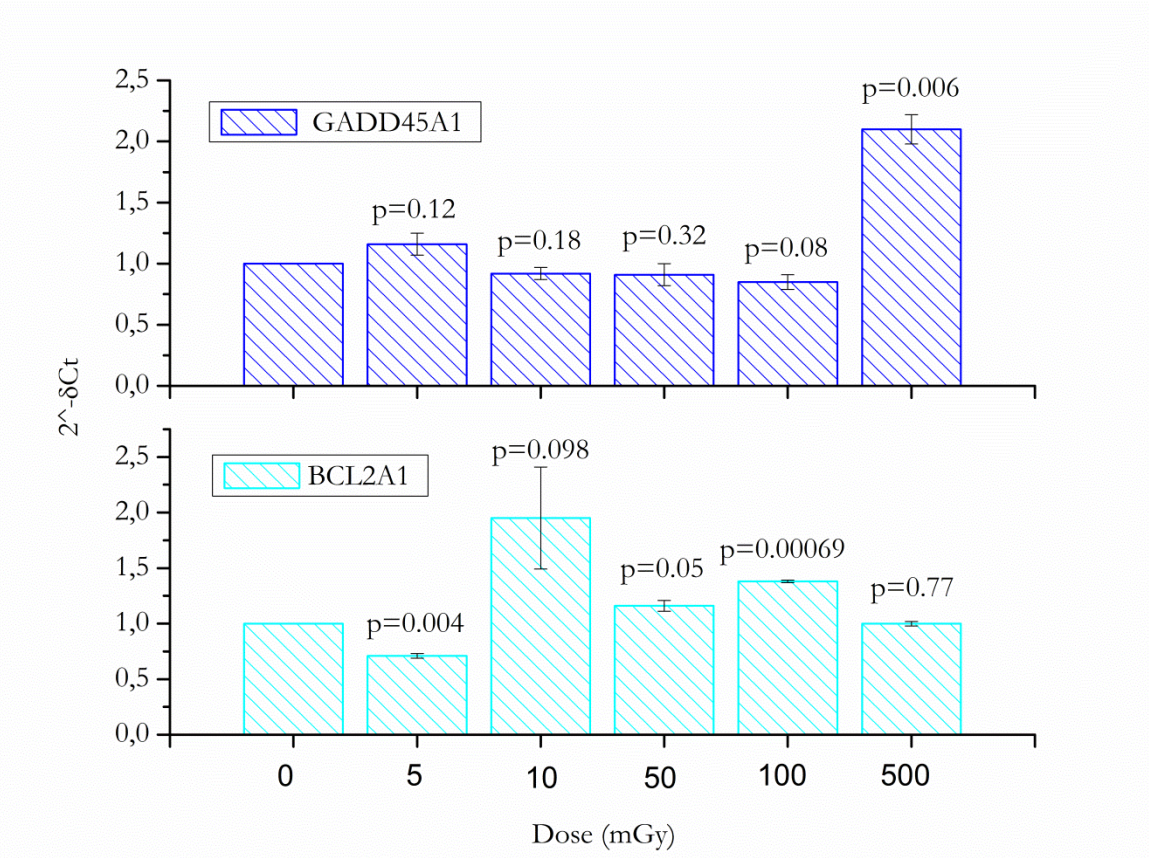

Figure 63: Relative gene expression levels for bystander cells. Quantitative real-time RT-PCR was used to quantify the expression of GADD45A and BCL2A1 genes 4h after irradiation of A549 cells. Gene expression was normalized to GAPDH and is relative to the expression of 0 mGy. The presented data is the mean and the standard deviation of two independent experiences. The *p*-values represent the statistical analysis between each dose values and the control, i.e. 0 mGy.

The relative gene expression in bystander cells is almost similar for GADD45A gene, irrespective of the dose value, however a significantly up-regulation of this gene was observed for 500 mGy ($p<0.01$). It seems that the dose-dependence in bystander cells doesn't exist for doses lower than 100 mGy, contrary to what was observed for directly irradiated cells. The gene BCL2A1 revealed different relative gene expression, comparing with 0 mGy, for doses lower than 100 mGy. In this case, it is observable that the pattern of gene expression, below 100 mGy, is not strictly linear, showing down- and up-regulations over this range.

7.3.3 Directly irradiated and Bystander cells

The existence of a radiation bystander effect in the low dose range when A549 cells are exposed to several doses of α-radiation was described in the previous chapters. The relative gene expression of each gene seems to indicate, as seen in sections 7.3.1 and 7.3.2., a pattern of up-and down-regulation when both directly irradiated and bystander cells are exposed to low doses of α-radiation. To provide some insight about the signaling pathways in bystander responses, the comparison between directly irradiated and bystander cells will be performed in the following sub-sub-section.

7.3.3.1 GADD45A gene profile expression

Figure 64 shows the relative gene expression for the GADD45A gene, in directly irradiated and in bystander cells. To investigate whether the responses of directly and bystander irradiated A549 cells differ, and the dose dependence of such difference of responses, the gene expression levels for a each dose value (0 mGy, 5 mGy, 10 mGy, 50 mGy, 100 mGy and 500 mGy) are compared in **Figure 64**.

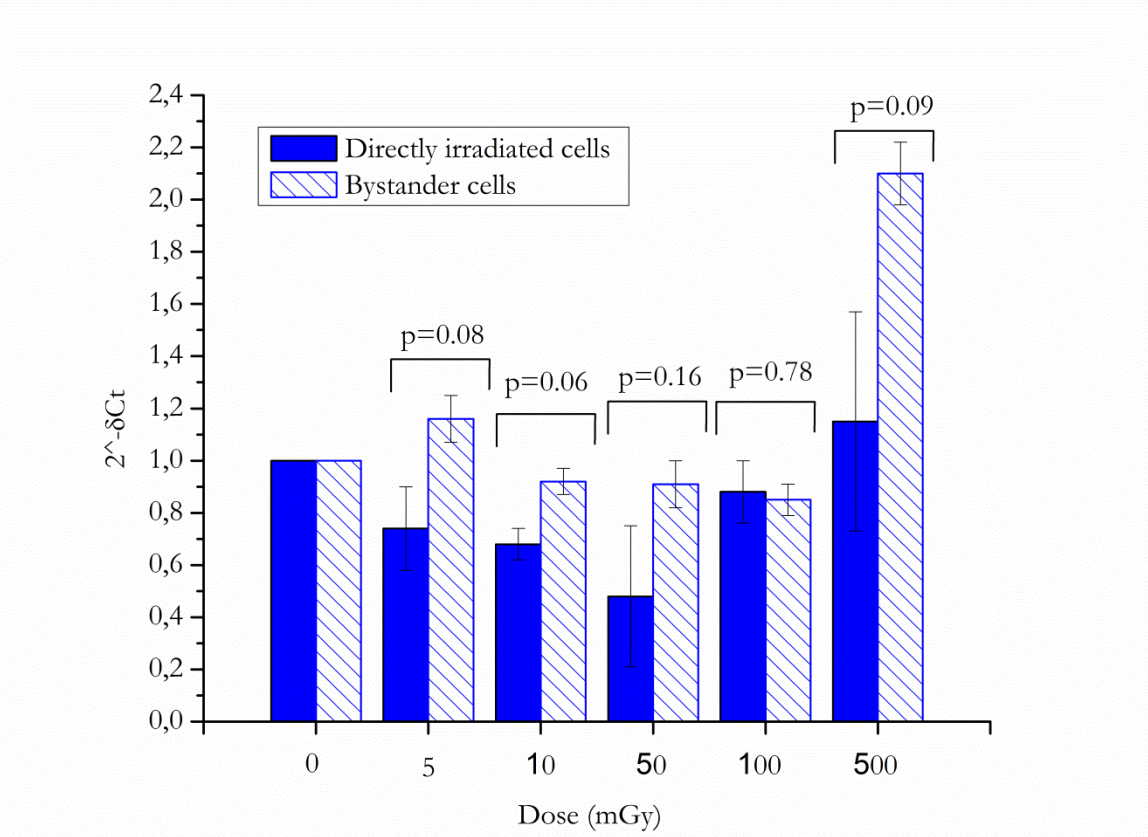

Figure 64: Relative gene expression of GADD45A in directly irradiated and bystander cells, 4h after irradiation of A549 cells for different dose values. The gene expression was normalized to GAPDH and is relative to the expression of 0 mGy. The data displayed corresponds to the mean and the standard deviation of two independent experiences.

In **Figure 64** it is observed that the relative gene expression in directly and bystander cells is different, being however almost similar for 100 mGy (p=0.78). For both directly and bystander effects, the relative gene expression decreases with increasing dose up to 100 mGy. After this dose value, 100 mGy, the gene expression levels increase, being this increased more evident for bystander cells.

7.3.3.2 BCL2A1 gene profile expression

Figure 65 shows the relative gene expression for the BCL2A1 gene, in directly irradiated and in bystander cells. As previously performed for the GADD45A gene, in order to investigate whether the responses of directly and bystander irradiated A549 cells differ and the dose dependence of such difference of responses, the gene expression levels for each dose value (0 mGy, 5 mGy, 10 mGy, 50 mGy, 100 mGy and 500 mGy) are compared in **Figure 65**.

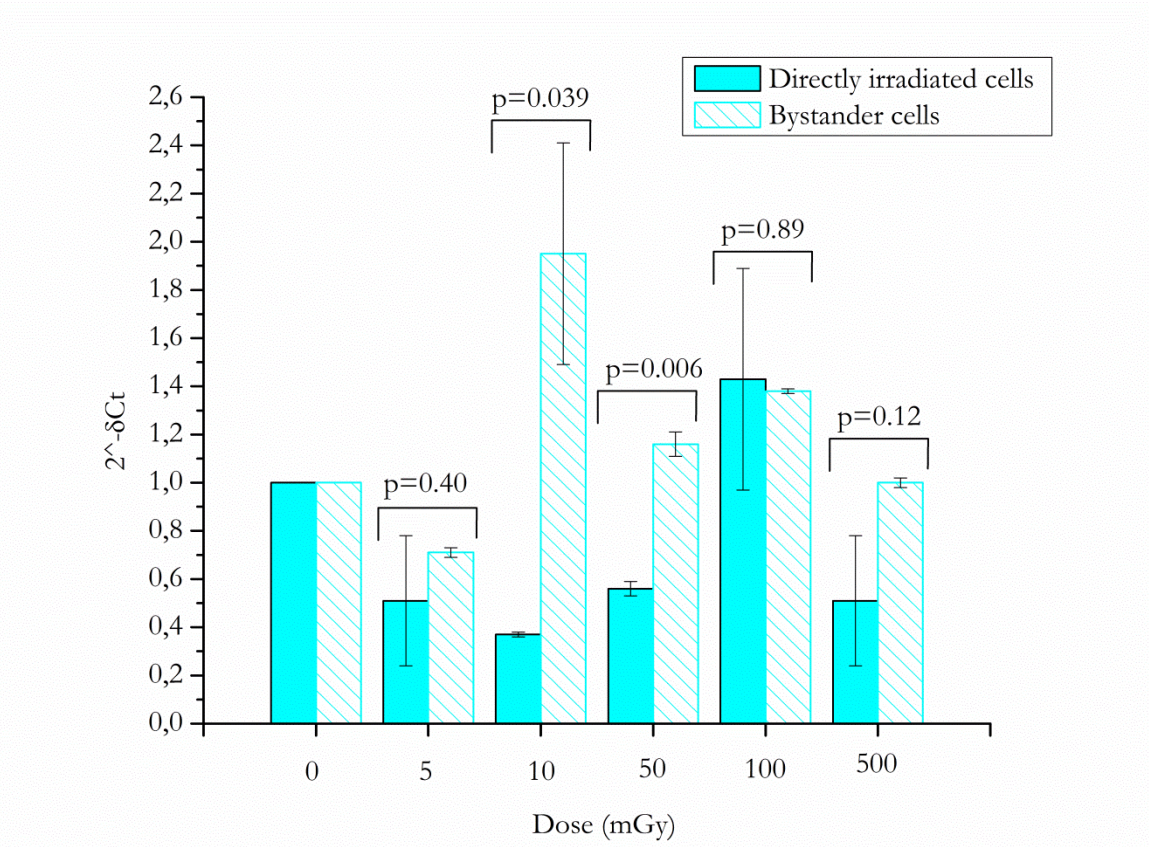

Figure 65: Relative gene expression of BCL2A1 in directly irradiated and bystander cells, 4h after irradiation of A549 cells. The gene expression was normalized to GAPDH and is relative to the expression of 0 mGy. The data displayed corresponds to the mean and the standard deviation of two independent experiences

As seen in **Figure 65**, the relative gene expression of BCL2A1 is higher for bystander cells when compared to directly irradiate ones. For bystander cells an over expression is clearly observed, for 10 and 50 mGy. Being this gene an apoptosis-inhibitor, these results seem to indicate that contrary to what is commonly anticipated, the mechanisms of apoptosis are also important at low doses. Moreover, our results seem to indicate that 100 mGy is a kind of threshold, not meaning that the gene-expression becomes different before and after this value, but in terms of the fold difference in gene expression.

7.4 Discussion and Conclusions

The possibility, through PCR reactions, of amplifying a single or few copies of a DNA segment, generating millions of copies, opens the possibility to study gene regulation even in a single cell [Liss, 2002].

Over the years, some improvements were observed in gene-expression techniques, being the quantitative real-time PCR (qRT-PCR) a single technique, using fluorescence, which allows documenting the amplification process in real-time. This technique allows not only to detect if such a gene is expressed but also to detect the fold-difference in the gene-expression.

In this thesis, we have measured the gene expression, by qRT-PCR, in directly and bystander cells after exposure to dose values of 5, 10, 50, 100 and 500 mGy of α-particles.
The GADD45A gene is involved in stress signaling responding to physiological and/or environmental stress inductors, leading to cell cycle arrest, DNA repair, cell survival and senescence or apoptosis [Liebermann and Hoffman, 2007]. Moreover, these authors [Liebermann and Hoffman, 2007] claim that this stress sensor is mediated by a complex interplay of physical interactions with other cellular proteins that are implicated in cell cycle regulation, such as PCNA, p21, cdc2/cyclinB1, and the p38.

Main findings for the GADD45A gene

Our results seem to indicate that, for directly irradiated cells, the GADD45A gene show a down-regulation for doses lower than 100 mGy, and an up-regulation for 500 mGy, when compared to 0 mGy. The canonical pathway associated with this gene is the G2/M DNA damage checkpoint, which is important to prevent cells from undergoing a malignant transformation and therefore maintain the genome integrity. Bearing this in mind, it seems that for doses lower than 100 mGy this gene is not activated, so i) the cellular damage is not enough to create a fold-difference in this gene expression, or ii) because GADD45A was not activated at low-doses the cells exposed over this range of doses could experience a malignant transformation, jeopardizing the genome stability.
For bystander cells, the results seem to indicate that the response of GADD45A is almost similar up to 100 mGy, being up-regulated for 500 mGy.
Our previous studies showed that the cellular lesion - observed either using the MN or γ-H2AX assays - induced in bystander response was lower when compared to directly irradiated cells. The results obtained in this chapter, a down-regulation of GADD45A, represent a driving force to deeply understand what happen with low-doses exposure. It can be hypothesized that the down-regulation of this gene at low doses (<100 mGy) can imply a non-efficient repair of cells and therefore imply a cellular lesion higher than those expected by using the extrapolation model for higher doses.

Main findings for the BCL2A1 gene

The gene BCL2A1 encoded a protein that decreases the release of cytochrome c from the mitochondria and blocks the activation of caspases. In this study a down-regulation of this gene in cells directly exposed to radiation, suggested that for doses lower than 100 mGy, the activation of caspases is not compromised and the apoptosis mechanism could be initiated. These results suggest that low level exposure to radiation may modify the mitochondria-dependent apoptosis pathway. For 10 mGy, in directly irradiated cells, there is an evident down-regulation of BCL2A1, which lead us to think that cells could experience apoptosis and therefore the survival fraction will be decreased in this dose range.

However, in our previous studies was demonstrated that for directly irradiated cells, the survival fraction for 10 mGy at 2 days post-irradiation was almost similar to the survival fraction for 5 mGy, i.e. no significant decrease on survival fraction at 10 mGy could be observed. Furlong *et al* [Furlong et al., 2013] demonstrated that BCL2A1 in directly irradiated cells is down-regulated for a 50 mGy dose, after 1h and 24h and up-regulated with 500 mGy after 1h and down-regulated after a further 24h. These results may pinpoint that this gene expression is time- and dose-dependent and thus our survival fractions results could not be used to elucidate what caused the significant down-regulation of this gene at 10 mGy.

For bystander cells, the behavior of this BCL2A1 gene is completely different when directly irradiated and bystander cells are compared. In this, at 10 mGy an over-expression of this gene is observed.

CHAPTER 8

CONCLUSIONS AND FUTURE WORK

8.1 Conclusions

The robustness of the international system of Radiological Protection and its underlying LNT hypothesis are being challenged to take into account scientific information on the effects arising from exposure to low radiation doses. Significant breakthroughs in low dose radiation-related topics such as the dependence of the individual sensitivity on factors such as genetics, gender, age, lifestyle, amongst others and non-cancer effects (circulatory diseases, cognitive functions, lens opacities, etc.) will pave the way to developments of the system of Radiological Protection. In order to achieve such breakthroughs, new scientific findings and a more detailed and accurate understanding of the mechanisms of response of cells to ionizing radiation are necessary.

Whether low doses of radiation trigger biological protective mechanisms or an enhancement of carcinogenesis and/or cell death is, as of today, unclear. The behavior of low-dose radiation-induced genomic instability, adaptive responses, and bystander effects is the driving force to develop models for predicting the response of *in vivo* low dose radiation exposures. Some studies [Morgan, 2003 and Kadhim *et al.*, 2004] show some characteristics in common to all three, such as the difficulty to obtain a reliable dose-response curve, the use of multiple endpoints, and some characteristics that distinguish one from the other such as, LET

response, and DNA repair-mechanisms. Schwartz [Schwartz, 2006] claims that the *in vitro* studies strongly suggest that modeling low-dose responses is a complex process, suggesting that each phenomena should be studied separately over a high range of cell lines.

Part of the complexity associated to the modeling of low-dose exposures is related to bystander effects, in which cells not directly irradiated respond to a stress signal from nearby irradiated cells. As shown in **Figure 66**, what invokes a response in cells not directly irradiated is still unknown. Indeed the cause is not well established; the effects are documented in the literature and are related to those observed in directly irradiated cells (see **Figure 66**).

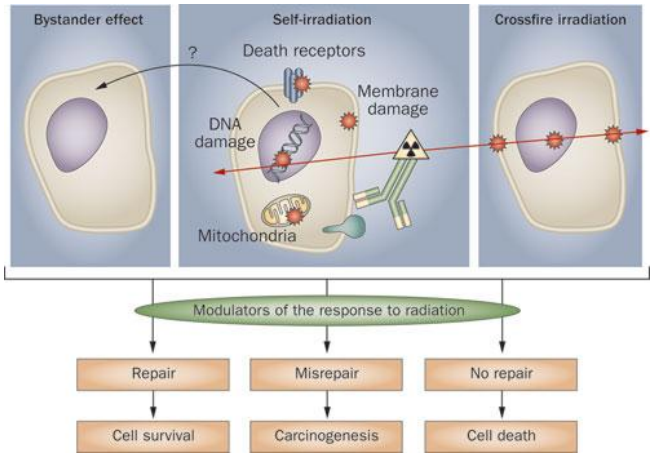

Figure 66: Different effects that can be observable when a single cell is irradiated.

The protective or detrimental nature of bystander effects arising from low-dose radiation exposure is unknown. One possible explanation of the protective one consists on assuming that the directly irradiated cells emit a signal to neighboring cells in order to make them aware about a possible damage and to prepare the neighboring cells to initiate some repair or death processes. As for the detrimental nature, it assumes that the bystander signal is itself toxic inducing a cellular damage in non-irradiated cells.

The driving force to deeply understand the mechanisms underlying bystander effects are related to the enhancement of genomic instability, mutations, among others, which represent a concern for radiation protection. As mentioned in the Introduction section of this document, a High Level European group was recently formed in order to establish sizable research programs on low dose risk assessment, in order to verify if the aforementioned mechanisms question the acceptability of the LNT model currently used to assess the risks of low dose exposures,.
The results obtained in this thesis reinforce the concerns about radiation protection. Our results seem to indicate that the early cellular lesions induced in bystander cells cannot be negligible, even when compared to those obtain in directly irradiated cells. Some authors

[Streffer 2004 and Dugan and Bedford, 2003] state that not all cell types are susceptible to instability induction. Our results show that radiation-induced genomic instability was induced in both directly irradiated and bystander A549 cells when exposed to several dose values of α-radiation.

The emerging applications of ionizing radiation in medicine, both for diagnostic and therapy, stand for an actual concern. And, also in these applications the bystander effects have an important role. In terms of radiation therapy, bystander effects could be related with; i) an increase of tumor cell death and ii) an increase in cell death or mutation in cells nearby the tumor. The way to understand the *in vivo* effects of these two *vias* is very complex and requires further studies. Our results show evidences that the bystander signal could be easily spread over the cell culture. And, the bystander effects are dependent on the number of irradiated cells. Although these results were obtained *in vitro* they may call for the need for further studies trying to elucidate if this behavior is also observed *in vivo*. If this hypothesis would be corroborated by such studies these results might be used to create a beneficial/harmful mechanism to enhance tumor cell death.

In addition to the medical applications, other area of concern for the protective or detrimental effects of low-dose is the exposure to natural sources. The worldwide annual exposures to natural radiation sources is estimated to be in the range 1 to 10 mSv/year, with 2.4 mSv being the present estimate of the central dose (UNSCEAR, 2000). About half of this dose, to which the average person is exposed, came from exposure to radon and its progenies. These data reinforce several studies trying to elucidate the correlation between radon inhalation and lung cancer. Some published studies have shown that there is a measurable risk of lung cancer for radon levels of about 100 Bq/m^3 [Darby and Hill, 2003 and Krewski *et al.*, 2005]. Additionally, some microdosimetry-related studies demonstrated that the spatial distribution of the energy deposited by the alpha particles, on the bronchial epithelial cells after inhalation, is non-homogeneous (Balásházy *et al*, 2002, Balásházy *et al*, 2009 and Farkas *et al.* 2008).Our results highlight that the pattern of cellular damage in bystander areas is directly related to the number of irradiated cells. Our observations could be related with the microdosimetry-related studies by linking the hot spots created by deposited particles in bronchial epithelial cells and the number of inhaled particles. That is, if a different number of radiation particles are inhaled, then different number of particles will be deposited in bronchial cells, and thus the spatial distribution of bystander effects will be different. According to our results if a higher number of cells are exposed the cellular damage induced in bystander areas will be increased.

During the last decades, and also in this thesis, the studies performed using high-LET radiation is related with its ability to induce genomic instability in directly and bystander cells. However, an extended study related to the transcription level has not yet been done. Recently, Chauhan [Chauhan et al., 2012] published an extended study on gene expression

changes induced in A549 cells after exposure to α-radiation. However, this study focused on directly irradiated cells using 30, 300 and 900 mGy. In this thesis, we have measured the gene expression, by qRT-PCR, in directly and bystander cells after exposure to 5, 10, 50, 100 and 500 mGy of α-particles. Our results seem to indicate that, for directly irradiated cells, the GADD45A gene show a down-regulation for doses lower than 100 mGy, and an up-regulation for 500 mGy, when compared to 0 mGy. The canonical pathway associated with this gene is the G2/M DNA damage checkpoint that is important to prevent cells to undergo a malignant transformation and therefore maintain the genome integrity. Bearing this, it seems that for doses lower than 100 mGy this gene is not activated, because; i) the cellular damage is not enough to create a fold-difference in this gene expression, or ii) GADD45A was not activated at low-doses, the cells exposed over this range of doses could experience a malignant transformation, jeopardizing the genome stability.

For bystander cells, the results seem to indicate that the response of GADD45A is almost similar up to 100 mGy, being up-regulated for 500 mGy. The gene BCL2A1 encoded a protein that decreases the release of cytochrome c from the mitochondria and blocks the activation of caspases. In this study a down-regulation of this gene, in cells directly exposed to radiation, suggested that, for doses lower than 100 mGy, the activation of caspases is not compromised and the apoptosis mechanism could be initiated. These results suggest that low level exposure to radiation may modify the mitochondria-dependent apoptosis pathway. For 10 mGy, in directly irradiated cells, there is an evident down-regulation of BCL2A1, which lead us to think that cells could experience apoptosis and therefore the survival fraction will be decreased for this dose value. However, in our previous studies, we demonstrate that for directly irradiated cells, the survival fraction for 10 mGy, at 2 days post-irradiation, was almost similar to 5 mGy, e.g. a significant decrease on survival fraction at 10 mGy was not observed. Furlong *et al* [Furlong et al., 2013] demonstrated that BCL2A1 in directly irradiated cells is down-regulated with 50 mGy after 1h and 24h and up-regulated with 500 mGy after 1h and down-regulated after a further 24h. This results show that this gene is time- and dose-dependent and thus our survival fractions results could not be used to elucidate what caused the significant down-regulation of this gene at 10 mGy.

For bystander cells, the behavior of this BCL2A1 gene is completely different when directly irradiated and bystander cells are compared. At 10 mGy an over-expression of this gene is observed.

In summary, the results presented in this thesis indicate that:

i) The cellular damage, induced in A549 cells by low doses of α-radiation, seems to be not linear with respect to dose, up to 100 mGy, for both directly irradiated and bystander cells.
ii) A radiation-induced genomic instability was observed in A549 cells in both directly irradiated and bystander cells.
iii) The bystander effects induced in A549 cells by low doses of α-radiation, are not negligible for doses up to 100 mGy.
iv) The bystander signal disperses easily over the cellular culture.
v) The cellular damage on bystander areas has a dependence on the number of irradiated cells.

8.2 Future work

Motivated by the obtained results on radiation-induced bystander effects, we plan to further expand the obtained *in vitro* results to *in vivo* models. Taking into account that epithelial cells are the first line of organism defense against toxic substances in the air, we intend to perform a 3-D tissue model, incorporating A549 cells into a cellular matrix. Sedelnikova [Sedelnikova *et al.*, 2007] developed a study to quantify the DNA double-strand breaks in a 3-D tissue model, preserving the three-dimensional geometric arrangement and communication of cells present in tissue *in vivo*. In the study of Sedelnikova et al., the irradiation was done using a microbeam; however, it is our intention to use the same Po-210 source that was used during this thesis. Using the same methodology, as described in chapter 4, we plant to irradiate the 3-D tissue model from the bottom and analyze the bystander effects using either the γ-H2AX or the MN assay. As said before, the role of bystander effects in radiation carcinogenesis is the driving motivation to several ongoing studies. Bearing this in consideration, in order to deeply understand the role of bystander signal propagation it is our intention to use the same methodology, as used in chapter 6, to understand the role of GJIC in tissue models.

In chapter 6, we demonstrated that the number of irradiated cells plays an important role in the spatial distribution of bystander effects. We observed that in bystander areas nearest to the irradiated area the cellular lesions are increased. Moreover, we also observed that the bystander signal could be easily spread onto the cellular culture which means that in the bystander areas more distant to irradiate ones the cellular lesion could not be negligible. These results highlight that the damage caused by radiation in the areas surrounding the irradiated areas could be different according to the number of irradiated cells, i.e., for the same dose value; the overall cellular damage could be different. This raises an important question: is this observable *in vivo*? Although we are not able yet to model mechanisms on the level of the whole organism in a sophisticated way, studying the radiation response on tissue level instead of the level of individual cells can help us to gain more insight into the mechanisms associated with radiation exposure and to better estimate health risks.

A number of dosimetric models have been developed to estimate the particle tracks and consequently absorbed doses in different organs/tissues or cells. In terms of natural sources exposures, one of the most studied models, due to its high relevance in terms of radiation protection, relates the pattern of α-particle emitters' deposition, e.g. radon, onto the airways and the biological effects related to such exposure. Szoke and co-authors [Szoke, *et al.*, 2009 and Szoke *et al.*, 2007] developed a model that strongly suggests an inhomogeneity of particles deposition within the central respiratory passages which results in non-uniform local distribution of radiation dose along the epithelium of the bronchi. As a future work, and continuing the ongoing collaboration with Doctor Istvan Szoke and its colleagues, it is intended to use our experimental results to validate and/or improve the aforementioned model.

BIBIOLOGRAPHY

Agostinelli, S. et al. 2003. GEANT4 – a simulation toolkit. Nucl. Instr. and Meth. A, 506:250–303.

Amundson, S. A., Bittner, M., Meltzer, P., Trent, J., and Fornace, A. J. 2001. Induction of gene expression as a monitor of exposure to ionizing radiation. *Radiat Res*, 133: 41-51.

Averbeck, D. 2009. Does scientific evidence support a change from the LNT model for low-dose radiation risk extrapolation? *Health Phys.,* 97, 493-504.

Azzam, E. I., Toledo, S. M., and Little, J. B. 2001. Direct evidence for the participation of gap junction-mediated intercellular communication in the transmission of damage signals from alpha-particle irradiated to nonirradiated cells. *Proc Natl Acad Sci*, USA 98: 473-478.

Azzam, E. I., Toledo, S. M., and Little, J. B. 2003. Oxidative metabolism, gap junctions and the ionizing radiation-induced bystander effect. *Oncogene* 22: 7050-7057.

Balásházy, I., Hofmann, W., Farkas, A., Szoke, I. 2002. Modelling carcinogenic effects of low doses of inhaled radon progenies. *J. Radiol. Prot.*, 22, A89-A93.

Balásházy, I, Farkas, A., Madas, B., Hofmann, W. 2009. Non-linear relationship of cell hit and transformation probabilities in a low dose of inhaled radon progenies. *J. Radiol. Prot.*, 29, 147-162.

Bayram, H., Devalia, J. L., Sapsford, R. J., Ohtoshi, T., Miyabara, Y., Sagai, M., and Davies, R.J. 1998. The effect of diesel exhaust particles on cell function and release of inflammatory madiators from human bronchial epithelial cells in vitro. *Am. J. Respir. Cell Mol. Biol.*, 18: 441-448.

Belchior, A., Botelho, M. L., Peralta, L., and Vaz, P. 2008. Dose mapping of a ^{60}Co irradiation facility using PENELOPE and MCNPX and its validation by chemical dosimetry. *Applied Radiation and Isotopes*, vol. 66, no. 4, pp 435-440.

Belchior, A., Peralta, L., Almeida, P., and Vaz, P. 2010. Calibration of an alpha particle irradiator for in vitro cells irradiation. *International Journal of Low Radiation*, vol.7, no.6, pp. 500-510.

Belchior, A., Monteiro Gil, O., Almeida, P. and Vaz, P. 2011. Evaluation of the cytotoxicity and the genotoxicity induced by α-particle radiation in an A549 cell line. *Radiation Measurements*, 46, 958-961.

Belchior, A., Monteiro Gil, O., Almeida, P. and Vaz, P. 2013. Dose and time dependence of targeted and untargeted effects after very low doses of α-particle irradiation of human lung cancer cells. *Dose Response*, vol. 1, issue 1, 431-446.

Belyakov, O. V, Malcolmson, A.M., Folkard, M., Prise, K. M., and Michael, B. D. 2001. Direct evidence for a bystander effect of ionizing radiation in primary human fibroblasts. *Br J Cancer*, 2; 84(5): 674-9.

Berger, M. J. and Seltzer, S. M. 1964. Tables of energy losses and ranges of electrons and positrons. NASA Report SP-3012.

Berger, M. J., Coursey, J. S., Zucker, M. A., and Chang, J. 2005. Stopping-Power and Range Tables for Electrons, protons, and helium Ions – NIST Standard Reference Database (ASTAR), National Institute of Standards and Tecnology, 2005.

Bertini, B.W. 1963. Low-energy intranuclear cascade calculation. *Phys. Rev*. 131, 1801-1821.

Bonner, W., Redon, C., Dickey, J., Nakamura, A., Sedelnikova, O., Solier, S., and Pommier, Y. 2008. γH2AX and cancer. *Nat. Rev. Cancer*, 8(12) 957-967.

Bowler, D., Moore, S., Macdonald, D., Smyth, S., and Clapman, P. 2006. Bystander-mediated genomic instability after high LET radiation in murine primary haemopoietic stem cells. *Mutation Research,* 597: 50-61.

Brenner, D., and Sachs, R. 2010. Estimating radiation-induced cancer risks at very low doses: rationale for using a linear no-threshold approach. *Radiat. Environ Biophys*, 44: 253-256.

Bressan, D.A., Baxter, B.K., Petrini, J.H. 1999. The Mre11-Rad50-Xrs2 protein complex facilitates homologous recombination-based double-strand-break in repair in *Saccharomyces cerevisiae*. *Mol Cell Biol* 19: 7681-7687.

Briesmeister, J. F. 2000. MCNP™—A General Monte Carlo N-Particle Transport Code, Version 4C, Los Alamos National Laboratory report LA-13709-M

Bushberg, J., Seibert, J., Leidholdt, E., Boone, J. 2012. The essential physics of medical imaging. 3rd Edition, ISBN-0781780578.

Cai, J., Yang, J. and Jones, D. P. 1998. Mitochondrial control of apoptosis: the role of cytochrome *c*. *Biochim. Biophys. Acta* 1366, 139-149.

Charlton, D. E. and Sephton, R. 1991. A relationship between microdosimetry spectra and cell survival for high LET irradiation. *Int. J. Radiat. Biol.*, 8, 453-466.

Cory S., Huang D., Adams J. 2003. The Bcl-2 family: roles in cell survival and oncogenesis. *Oncogene*, 22, 8590-8607.

Cugnon, J., Volant, C. and Vuillier, S. 1997. Improved intranuclear cascade model for nucleon-nucleus interactions. *Nuclear Physics A* 620, 475 – 509.

Darby, S., Hill, D., Doll, R. 2001. Radon: a likely carcinogen at all exposures. *Annuals of Oncology*, vol. 12, no. 10, pp. 1341-1351.

Darby, S.C. and Hill, D.C. 2003. European collaborative group on residential radon and lung cancer. Health effects of residential radon:a European perspective at the end of 2002. *Radiat. Prot. Dosim*. 104 (4), 321-329.

Dugan, L. C., and Bedford, J. S. 2003. Are chromosomal instabilities induced by exposure of cultured normal human cells to low-or high-LET radiation? *Radiat. Res.*, 159: 301-311.

Edwards, A. A., Lloyd, D. C., and Purrott, R. J.1979. Radiation induced chromossome aberrations and the poisson distribution. *Rad. And Environm. Biophys.*, 16: 89-100.

Farkas, Á. et al. 2008 Quantification of particle deposition in asymmetrical tracheobronchial model geometry. *Comput. Biol. Med.*, 38, 508-518.

Fenech, M. 2000. The in vitro micronucleus technique. *Mutat. Res.* 455: 81-95.

Ferrari, A., Sala, P., Fasso, A. and Ranft, J. 2011. FLUKA: a Multiparticle Transport Code. CERN, 2005-10, INFN/TC 05/11, SLAC-R-773.

Folkard, M., Vojnovic, B., Prise, K. M., Bowey, A. G., Locke, R. J., Schettino, G., and Michael, B. D. 1997. A charged-particle microbeam. I. Development of an experimental system for targeting cells individually with counted particles. *Int. J. Radiat. Biol.*, 72: 375-385.

Franken, N., Rodermond, H., Stap, J., Haveman, J., and van Bree, C. 2006. Clonogenic assay of cells *in vitro*. *Nature Protocols*, Vol. 1, 5: 2315-2319.

Fujii, T., Hayashi, S., Hogg, J. C., Vincent, R., and Vincent, S. F. 2001. Particulate matter induces cytokine expression in human bronchial epithelial cells. *Am. J. Respir. Cell Mol. Biol.*, 25: 265-271.

Ghandhi SA, Yaghoubian B, Amundson SA. 2008. Global gene expression analyses of bystander and alpha particle irradiated normal human lung fibroblasts: synchronous and differential responses. *BMC Med Genomic*, 1: 63.

Grifalconi, M., Celloti, L., and Mognato, M. 2007. Bystander response in human lymphoblastoid TK6 cells. *Mutat Res*, 625: 102-111.

Hei, T. K., Wu, L., Liu, S., Vannais, D., Waldren, C. A., and Randers – person, G. 1997. Mutagenic effects of a single and an exact number of α particles in mammalian cells. *Proc Natl Acad Sci*, USA 94: 3765-3770.

Hoeijmakers, J. H. 2001. Genome maintenance for preventing cancer. *Nature*, 411, 366-374.

Hu, B., Wu, L., Han, W., Zhang, L., and Chen S. 2006. The time and spatial effects of bystander response in mammalian cells induced by low dose radiation. *Carcinogenesis* , 27: 245-251.

ICRU Stopping Powers for Electrons and Positrons, 1984. International Commision on Radiation Units and Measurements, ICRU Report 37.

ICRU Stopping Powers and Ranges for protons and Alpha Particles. 1993. International Commision on Radiation Units and Measurements, ICRU Report 49.

Inkret, W. C., Eisen, Y., Harvey, W. F., Koehler, A. M., and Raju, M. R. 1990. Radiobiology of α particles, exposure system and dosimetry. *J. Radiat. Res.* 123, 304-310.

Ishigure, N., Nakano, T., and Enomoto, H. 1991.A device for in vitro irradiation with α-particles using an α–emitting radioactive source. *J. Radiat. Res.*, 32, 404-416.

Iyer, R., Lehnert, B. E., and Svensson, R. 2000. Factors underlying the cell growth-related bystander responses to alpha particles. *Cancer Res*, 60:1290 – 1298.

Janni, J.F. 1982. Proton range-energy tables, 1 keV – 10 GeV. *Atomic Data and Nuclear data Tables* 27, Nos 2 – 5.

Jenkins, G., Zair, Z., Johnson, G., and Doak, S. 2010. Genotoxic thresholds, DNA repair, and susceptibility in human populations. *Toxicology,* 10: 305-310.

Joiner, M. C., Marples, B., Lambin, P., Short, S. C., and Turesson, I. 2001. Low-dose hypersensivity: current status and possible mechanisms. *Int J Radiat Oncol Biol Phys*, 49:379-389.

Kadhim, M. A., Lorimore, S. A., Townsend, K. M., Goodhead, D. T., Buckle, V. J., and Wright, E. G. 1995. Radiation-induced genomic instability: delayed cytogenetic aberrations and apoptosis in primary human bone narrow cells. *Int. J. Radiat. Biol.*, 76: 31-42.

Kadhim, M. A., Moore S.R., Goodwin, E.H. 2004. Interrelationships amongst radiation-induced genomic instability, bystander effects, and the adaptive reponse. Mutat. Res. 568, 21-32.

Kainz, P. 2000. The PCR plateau phase-towards an understanding of its limitations. *Biochim biophys Acta*, 1494 (1-2): 23-7.

Kamali-Asl, A., Mohanmmad Hassan, M., and Aghamiri, S. M. 2010. Assessment of absorbed dose in digital and MIRD phantoms by MCNP in thorax area. *International Journal of Low Radiation*, vol. 7, no.2, pp. 110 – 120.

Kastan, M. 2007. DNA damage responses: mechanisms and roles in human disease. *Mol Cancer Res*, 6:517:524.

Kelly, P.N., White, M.J., Goschnick, M.W., Fairfax, K.A., Tarlinton, D.M., Kinkel, S.A., Bouillet, P., Adams, J.M., Kile, B.T., Strasser, A. 2010. Individual and overlapping roles of BH3-only proteins Bim and Bad in apoptosis of lymphocytes and platelets and in suppression of thymic lymphoma development. *Cell Death Differ*, 10, 1655-64.

Kendall, L. V., and Riley, L. K. 2000. Reverse transcriptase polymerase reaction chain (RT_PCR). Poster presentation on the *American Assiciation for Laboratory Animal Science*, vol. 39, no. 1.

Krewski, D., Lubin, J.H., Zielinski, J.M., Alavanja, M., Catalan, V.S., Field, R.W., Klotz, J.B., Létourneau, E.G., Lynch, C.F., Lyon, J.I., Sandler, D.P., Schoenberg, J.B., Steck, D.J., Stolwijk, J.A., Weinberg, C., Wilcox, H.B. 2005. Residential radon and risk of lung cancer: a combined analysis of 7 North American case–control studies. *Epidemiology* 16 (2), 137–145.

Liebermann D. A. and Hoffman B. 2007. Gadd45 in the response of hematopoietic cells to genotoxic stress. *Blood cells molecules and Diseases* 39, 329-335.

Little, M. 2010. Do non-targeted effects increase or decrease low dose risk in relation to the linear-non-threshold (LNT) model? *Mutation Research*, 687: 17-27.

Lorimore, S. A., Kadhim, M. A., Pocock, D. A., Papworth, D., Stevens, D. L., Goodhead, D. T., and Wright, E. G. 1998. Chromossomal instability in the descendents of unirradiated surviving cells after alpha-particle irradiation. *Proc. Natl. Acad. Sci.*, USA 95, 5730-5733.

Liss, B. 2002. Improved quantitative real-time RT–PCR for expression profiling of individual cells. *Nucleic Acids Res* 30, e89.

Liu, X., Kim, C. N., Yang, J., Jemmerson, R. and Wang, X. 1996. Induction of apoptotic program in cell-free extracts: requirement for dATP and cytochrome *c*. *Cell* 86, 147-157.

Luis, R., Bento, J., Carvalhal, G., Nogueira, P., Silva, L., Teles, P., and Vaz, P. 2010. Parameter optimization of a planar BEGe detector using Monte Carlo simulations. *Nuclear Instruments and Methods in Physics Research A*, 623, 1014-1019.

MacFarlene, R.E., Muir, D.W. and Boicourt, R.M. 1982a. The NJOY nuclear data processing system, volume I: User's Manual. Os Alamos National Laboratory report LA-9303-M, Vol. I (ENDF-324).

MacFarlene, R.E., Muir, D.W. and Boicourt, R.M. 1982b. The NJOY nuclear data processing system, volume II: The NJOY, RECONR, BROADR, HEATR, and THERMR Modules. Os Alamos National Laboratory report LA-9303-M, Vol. II (ENDF-324).

Mashnik, S.G., Sierk, A.J., Gudima, K.K. and Baznat, M.I. 2006. Cem03 and laqgsm03 – new modeling tools for nuclear applications. Journal of Physics: Conference Series 41, 340.

McGowan, C. and Russell, P. 2004. The DNA damage response: sensing and signaling. *Current Opinion in Cell Biology*, 16:629-633.

Metting, N. F., Koehler, A. M., Nagasawa, H., Nelson, J. M. and Little, J. B. 1995.Design of a benchtop alpha particle irradiator. *Health Phys*, 68: 710-715.

Morgan, W.F. 2003. Is there a common mechanism underlying genomic instability, bystander effects and other nontargeted effects of exposure to ionizing radiation? *Oncogene,* 22, 7094-7099.

Mothersill, C., and Seymour, C. B. 1998a. Mechanisms and implications of genomic instability and other delayed effects of ionizing radiation exposure. *Mutagenesis*, 13:421-426.

Mothersill, C., and Seymour, C. B. 1998b. Cell-cell contact during gamma irradiation is not required to induce a bystander effect in normal human kerotinocytes: evidence for release during irradiation of a signal controlling survival into the medium. *Radiat Res*, 149: 256-262.

Mothersill, C., and Seymour, C. B. 2000. Genomic instability, bystander effects and radiation risks: implications for development of protection strategies for man and the environment. *Radiats Biol Radioecol*, 40: 615-620.

Mothersill, C., Rea, D., Wright, E. G., Lorimore, S. A., and Murphy, D. 2001.Individual variation in the production of a 'bystander signal' following irradiation of primary cultures of normal human urothelium. *Carcinogenesis*, 22: 1465-1471.

Mothersill, C., Seymour, C. B., and Joiner, M. C. 2002. Relationship between radiation-induced low-dose hypersensitivity and the bystander effect. *Radiat Res*, 157: 526-532.

Murakami, H. and Okayama, H. 1995. A kinase from fission yeast responsible for blocking mitosis is S phase. *Nature*, 374, 817-819.

Nagasawa, H., Huo, L., and Little, J. B. 2003. Increased bystander mutagenic effect in DNA double-strand break repair-deficient mammalian cells. *Int. J. Radiat. Biol*, 79: 35-41.

National Research Council. 1999. Health Effects of Exposure to Radon (BEIR VI). National Academy Press, Washington, DC.

Neti, P. V., Toledo, S. M., Perumal, V., Azzam, E. I. and Howell, R. W. 2004. A multi-port low fluence alpha particle irradiator: fabrication, testing and benchmark radiobiological studies. *Radit. Res*, 161: 732-738.

Nogueira, P., Silva, L., Teles, P., Fernandes, E., Oliveira, A. D., and Vaz, P. 2009. A Monte Carlo simulation of a whole body counter. *International Journal of Low Radiation*, vol. 6, no. 4 pp. 312 – 324.

Nuta, O., and Darroudi, F. 2008. The impact of the bystander effect on the low-dose hypersensitivity phenomenon. *Radiat Environ Biophys*, 47:265-274.

Ohtoshi, T., Takizawa, H., Okazaki, H., Kawasaki, S., Takeuchi, N., Ohta, K., and Ito, K. 1998. Diesel exhaust particles stimulate human airway epithelial cells to produce cytokines relevant to airway inflammation in vitro. *J. Allergy Clin. Immunol.*, 101: 778-785.

Ojima, M., Ban, N., and Kai, M. 2008. DNA double-strand breaks induced by very low X-ray doses are largely due to bystander effects. *Radiat Res*, 170 (3): 365-71.

Pelowitz D. B. 2005. MCNPX user's manual version 2.5.0. Los Alamos National Laboratory (LANL), LA-CP-05-0369.

Pouget J.P., Navarro-Teulon, I., Bardiès, M., Chouin, N., Cartron, G., Pèlegrin, A., Azria, D. 2011. Clinical radioimmunotherapy—the role of radiobiology. *Nat. Rev. Clin. Oncol.* 8; 8(12): 720-34.

Prael, R.E. 2000. Proposed modification to the charged hadron tracking algorithm in MCNPX. Los Alamos Research note X-5-RN(U), LA-UR-00-4027.

Report of High Level and Expert Group on European Low Dose Risk Assessment, January 2009. http://ec.europa.eu/research/energy/pdf/hleg_report_-_january_2009.pdf

Rogakou, E. P., and Pilch, D.R. 1999. Magabase chromatin domains involved in DNA double-strand breaks *in vivo*. *J. Cell. Biol.,* 146, 9.5-915.

Rothkamm, K., Kruger, I., Thompson, L.H., Lobrich, M. 2003. Pathways of DNA double strand break repair during the mammalian cell cycle. *Mol Cell Biol* 23, 5706-15.

RSICC. 2006. Computer Code Collection, Report CCC-715, LANL, Los Alamos

Sawant, S. G., Randers-Pehrson, G., Geard, C. R., Brenner, D. J., and Hall, E. J. 2001. The bystander effect in radiation oncogenesis: I. Transformation in C3H 10T1/2 cells in vitro can be initiated in the unirradiated neighbors of irradiated cells. *Radiat. Res.* 155, 397-401.

Schettino, G., Folkard, M., Prise, K. M., Vojnovic, B., Held, K. D., and Michael, B. D. 2003. Low dose studies of bystander cell killing with targeted soft X-rays. *Radiat. Res.* 160, 505-511.

Schwartz, J.L. 2006. Variability: The common factor linking low dose-induced genomic instability, adaptation and bystander effects. *Mut. Res.* 616, 196-200.

Sedelnikova, O., Nakamura, A., Kovalchuck, O., *et al.* 2007. DNA Double-Strand Breaks Form in Bystander Cells after Microbeam Irradiation of Three-dimensional Human Tissue Models. *Cancer Res* 67: 4295-4302.

Seymour, C., and Mothersill, C. 2000. Relative contribution of bystander and targeted cell killing to the low-dose region of the radiation dose-response curve. *Radiat Res*, 153:508-511.

Shao, C., Furusawa, Y., Kobayashi, Y., and Funayam, T. 2006. Involvement of gap junctional intercellular communication in the bystander effect induced by broad-beam or microbeam heavy ions. *Nuclear Instruments and Methods in Physics Research B*, 251: 177-181.

Soyland, C., and Hassfjell, S. P. 2000. A novel ^{210}Po-based α-particle irradiator for radiobiological experiments with retrospective α-particle hit per cell determination. *Radiat. Environ. Biophys*. 39, 125-130.

Sternheimer, R.M., Seltzer, S.M. and Berger, M.J. 1982. Density effect for the ionization loss of charged particles in various substances. *Phys. Rev*., B26:6067.

Streffer C. 2004. Bystander effects, adaptive response and genomic instability induced by prenatal irradiation. *Mutat. Res*. 568, 79-87.

Stringer, B., and Kobzik, L. 1998. Environmental particulate-mediated cytokine production in lung epithelial cells (A549): role of preexisting inflammation and oxidant stress. *J. Toxicol. Environ*., 55: 31-44.

Sun, B. and Karin, M. 2008. NF-kB signaling, liver disease and hepatoprotective agents. *Oncogene*, 27, 6228-6244.

Susin, S. A., Zamzami, N. and Kroemer, G. 1998. Mitochondria as regulators of apoptosis: doubt no more. *Biochim. Biophys. Acta* 1366, 151-165.

Sutherland, B. M., Bennett, P. V., Sutherland, J. C., and Laval, J.2002. Clustered DNA damages induced by x rays in human cells. *Radiat Res*, 157 (6): 611-6.

Suzuki, M., Zhou, H., Geard, C. R., Hei, T. K. 2004. Effect of medium on chromatin damage in bystander mammalian cells. *Radiat Res,* 162: 264-269.

Swift, G. H., Peyton, M. J., MacDonald, R. J. 2000. Assessment of RNA quality by semi-quantitative RT-PCR of multiple regions of a long ubiquitous mRNA. *Biotechniques*, 28 (3): 524, 526, 528, 530-1.

Szabó, J., Fehér, J., Pálfalvi, J., Balásházy, I., Dám, A. M., Polonyi, I., and Bogdándi, E. N. 2002. In vitro cell irradiation systems based on ^{210}Po alpha source: construction and characterization. *Radiation Measurements* 35, 575 – 578.

Szoke,I., Farkas, A., Balashazy, I., Hofmann, W. 2007. Modelling of cell deaths and cell transformations of inhaled radon in homes and mines based on a biophysical and microdosimetric model. *International Journal of Radiation Biology*, 84:2, 127-138.

Szoke,I., Farkas, A., Balashazy, I., Hofmann, W. 2009. Stochastic Aspects of Primary Cellular Consequences of radon inhalation. *Radiation Research*, 171, 96-106.

Tauchi, H., Kobayashi, J., Morishima, K., van Gent, D.C., Shiraishi, T., Verkaik, N.S., vanHeems, D., Ito, E., Nakamura, A., Sonoda, E., Takata, M., Takeda, S., Matsuura, S., Komatsu, K., 2002. Nbs1 is essential for DNA repair by homologous recombination in higher vertebrate cells. *Nature*, 420: 93-98.

Trauner, M and Jansen, P. 2003. Molecular Pathogenesis of cholestasis. Kluwer academic/ Plenum publishers.

Tubiana, M., Aurengo, A., Averbeck, D., and Masse, R. 2006. The debate on the use of a linear no threshold for assessing the effects of low doses. *J. Radiol. Prot*., 26:317-324.

UNSCEAR (United Nations Scientific Committee on the Effects of Atomic Radiation). 2000. Sources and effects of ionizing radiation. Report to the General Assembly with scientific annexes. New York, United Nations.

Wakeford, R. 2009. Radiation in the workplace – a review of studies of the risks of occupational exposure to ionizing radiation. *Journal of radiological Protection*, vol.29, no. 2, pp. A61-A79.

Walmorth, N., Davey, S. and Beach, D. 1993. Fission yeast chk1 protein kinase links the rad checkpoint pathway to cdc2. *Nature*, 363, 368-371.

Waters, L.S. 2002. MCNPX™ User's Manual, ECI, Version 2.4.0, Los Alamos National Laboratory report LA-CP-02-408.

Waters, L.S., McKinney, G.W., Durkee. J.W., Fensin, M.L., Hendricks, J.S., James, M.R., Johns, R.C. and Pelowitz, D.B. 2007. *AIP conference proceedings* 896, 81.

Whitehouse, C. A., and Tawn, E. J. 2001. No evidence for chromosomal instability in radiation workers with in vivo exposure to plutonium. *Radiat. Res*., 156: 467-475.

Willis, S., Adams, J. 2005. Life in the balance: how BH3-only proteins induce apoptosis. Current opinion in Cell Biology, volume 17, issue 6, 617-625.

Wykes, S. M., Piasentin, E., Joiner, M. C., Wilson, G. D., and Marples, B. 2006. Low-dose hyper-sensitivity is not caused by a failure to recognize DNA double-strand breaks. *Radiat Res*, 165:516-524.

Wolff, S. 1998. The adaptive response in radiobiology: evolving insights and implications. *Environ Health Perspect*, 106 (Suppl 1): 277-283.

Yang, H., Assad, N., and Held, K. D. 2005. Medium-mediated intercellular communication is involved in bystander responses of X-ray – irradiated normal human fibroblasts. *Oncogene*, 24: 2096-2103.

Yariv, Y. and Fraenkel, Z. 1979. Intranuclear cascade calculation of high-energy heavy-ion Interactions. *Phys. Rev*. C 20, 2227- 2243.

Yariv, Y. and Fraenkel, Z. 1981. Intranuclear cascade calculation of high energy heavy ion collisions: Effect of interactions between cascade particles. *Phys. Rev*. C 24, 488-494.

Youle, R. and Strasser, A., 2008. The BCL-2 protein family: opposing activities that mediate cell death. *Nat. Rev. Mol. Cell Biol*. 9, 47-59.

Zhou H, Ivanov VN, Gillespie J, Geard CR, Amundson SA, Brenner DJ, Yu Z, Lieberman HB, Hei TK. 2005. Mechanism of radiation-induced bystander effect: role of the cyclooxygene-2 signaling pathway. *Proc Natl Acad Sci USA*, 102 (41): 14641 – 14646.

Ziegler, J. F., Biersack, J. P., and Ziegler, M.D. 2008. SRIM - The Stopping and Range of Ions in Matter, SRIM Co., USA, 398p.

RESEARCH PROTOCOLS

Protocol I - Cytokinesis-blocked Micronuclei Assay

Cell culture

i. Add $1x10^5$ cells to the Mylar® discs, DMEM medium supplemented with 10% fetal bonive serum (F7524, Sigma, St Louis, MO, USA) and 1% Penicillin Streptomycin Solution (P0781, Sigma, St Louis, MO, USA) in order to achieve 3 ml of total volume.

ii. Incubate at 37% of temperature and 5% of CO_2.

iii. Irradiate cells 24h after the culture and remove the medium after irradiation. Incubate at 37% of temperature and 5% of CO_2.

iv. At 44h of incubation, add cytochalasin-B (Sigma, St Louis, MO, USA) to a final concentration of 2μg/ml.

Preparation of slides

i. After a total of 72h of culture, harvest cells by centrifugation 800 r.p.m., 10 minutes, at room temperature.

ii. Wash twice with 5ml of RPMI 1640 medium (Sigma, St Louis, MO, USA), supplemented with 2% fetal bovine serum.

iii. Centrifuge for 7 minutes at 700 r. p.m., at room temperature.

iv. Remove supernatant and subject cells to a mild hypotonic treatment, consisting of a mixture (pH 7.2) of RPMI 1640: deionised water 1:4, supplemented with 2% fetal bovine serum.

v. Remove supernatant and loosen pellet.

vi. Place small drops of cell pellet in clean dry slides, and perform smears.

vii. Air dry slides overnight.

viii. Fix with freshly prepared ice-cold methanol/acetic acid (3:1) for 20 minutes.

ix. Allow to dry and stain with 4% Giemsa in 0.01 M phosphate buffer pH 6.8 for 8 minutes.

x. Close the slides with Entellan® (Merck, Darmstadt, Germany).

Scoring of slides

i. Code the slides and score 1000 binucleated cells with well-preserved cytoplasm for micronuclei, identified according to the criteria described by Fenech and Morley (1985).

ii. Score 500 cells for the cytokinesis blocked proliferation index (CBPI), calculated according to [Surrallés et al., 1995]: CBPI = [MI+2MII+3(MII+MIV]/total number of cells, where MI – MIV are the number of cells with one to four nuclei.

Protocol II – γ – H2AX Assay

Cell culture

i. Add $1x10^5$ cells to the Mylar® discs, DMEM medium supplemented with 10% fetal bonive serum (F7524, Sigma, St Louis, MO, USA) and 1% Penicillin Streptomycin Solution (P0781, Sigma, St Louis, MO, USA) in order to achieve 3 ml of total volume.

ii. Incubate at 37% of temperature and 5% of CO_2.

iii. Irradiate cells 24h after the culture procedure.

Preparation of slides

i. Immediately after irradiation, remove the medium culture.

ii. Add 1ml of 4% formaldehyde in PBS for 15 min.

iii. Wash 1x with PBS and permeabilize using Triton X-100 (0.5 %) at room temperature for 5 min.

iv. Wash 2x with 1% Bovine Serum Albumin (BSA). and block for 1 h with a solution of 4% BSA.

v. Incubate cells with the γ-H2AX primary antibody at 2 μg/ml for 2 h.

vi. Wash 2x with BSA 1%

vii. Incubate with a FITC-conjugated goat anti-mouse second antibody at 1 μg/ml for 1 h.

viii. Wash 3x with BSA 1%

ix. Incubate with Hoechst (1 μg/ml) for 5 min.

x. Finally, wash 3x with PBS and mount with anti-fade.

Scoring of slides

i. Cells were analyzed at 64x magnification in a fluorescence microscope.

ii. Images were randomly obtained in each slide. Image analysis of γ-H2AX foci was performed by the freeware Cellprofiler.

iii. At least 100 nuclei were analyzed per experiment per dose.

Protocol III – Clonogenic Assay

Cell culture

i. Add $1x10^5$ cells to the Mylar® discs, DMEM medium supplemented with 10% fetal bonive serum (F7524, Sigma, St Louis, MO, USA) and 1% Penicillin Streptomycin Solution (P0781, Sigma, St Louis, MO, USA) in order to achieve 3 ml of total volume.

ii. Incubate at 37% of temperature and 5% of CO_2.

iii. Irradiate cells 24h after the culture procedure.

Preparation of plates

i. Remove the culture medium from cells and wash 1x with PBS.

ii. Trypsinize cells (cells in a monolayer) to produce a suspension.

iii. Homogenize cells and count them.

iv. Dilute the cell suspension into the desired concentration and seed into plates.

v. Place the dishes in an incubator them until cells in control plates formed large clones.

Fixation and staining of colonies

i. Remove the culture medium from the plates.

ii. Rinse carefully with PBS

iii. Remove the PBS and add 3 mL of methanol: acid acetic (3:1) for 10 min.

iv. Add 3 mL of 0.5 % crystal violet for 30 min

v. Remove the crystal violet and rinse with tap water.

vi. Leave the plates to dry at room temperature.

Counting the colonies

i. Count the number of colonies after treatment and in control plates.

Platting efficiency and surviving fractions

To determine the plating efficiency the following equation is used:

$$PE = \frac{\text{no.of colonies formed}}{\text{no.of cells seeded}} \times 100\%$$

The number of colonies that arise after treatment of cells (in this study after IR), expressed in terms of PE, are called the surviving fraction and can be calculated as follows:

$$SF = \frac{\text{no.of colonies formed after treatment}}{\text{no.of cells seeded} \times PE}$$

Protocol IV - RNA isolation

The following protocol encompasses the recommendations specified in the manual of the **PureLink® RNA Mini Kit** used in this work.

Cell lysates

i. Remove the growth medium from the cells, then add 0.3 mL Lysis buffer with 1% 2-mercaptoethanol (see **Table 16**)

Table 16: Required volume of Lysis buffer (Extracted from the PureLink® RNA Mini Kit manual)

Cell number	Lysis Buffer required for each sample
$\leq 1 \times 10^6$	0.3 mL
1×10^6 - 5×10^6	0.6 mL
5×10^6 - 5×10^7	0.6 mL per 5×10^6 cells (e.g., use 1.2 mL for 1×10^7 cells)

ii. Vortex until the cell pellet is dispersed and the cells appear lysated.

Cell homogenization

i. Transfer the lysate into a clean homogenization tube, and perform manual homogenization. Centrifuge the homogenate at 12,000 x *g* for 2 minutes.

RNA purification

i. Add one volume 70% ethanol to each volume of cell homogenate. Note: The ethanol 70% must be prepared in RNase-Free Water.

ii. Vortex to mix thoroughly and to disperse any visible precipitate that may form after adding ethanol.

iii. Transfer up to 700 µL of the sample to the spin cartridge with the collection tube.

iv. Centrifuge at 12,000 x *g* for 15 seconds at room temperature. Discard the flow-through and the collection tube. Place the spin cartridge into a new collection tube.

v. Add 700 µL Wash Buffer I to the spin cartridge.

vi. Centrifuge at 12,000 x *g* for 15 seconds at room temperature. Discard the flow-through and the collection tube. Place the spin cartridge into a new collection tube.

vii. Add 500 µL Wash Buffer II with ethanol to the spin cartridge.

Wash Buffer II: for the first time, add 60 mL of ethanol. p.a.

viii. Centrifuge at 12,000 x *g* for 15 seconds at room temperature. Discard the flow-through.

ix. Repeat steps vii and viii.

x. Centrifuge the spin cartridge at 12,000 x *g* for 2 minutes to dry the membrane with bound RNA. Discard the collection tube and insert the spin cartridge into a recovery tube.

xi. Add 50 µL RNase-free water to the center of the spin cartridge.

xii. Incubate at room temperature for 1 minute.

xiii. Store the purified RNA at -80 °C.

RNA quantification

The RNA quantification was performed by UV absorbance, as follows:

i. An aliquot of the total RNA was diluted in 10 mM Tris-HCl, pH7.5.

ii. The OD260 of the solution was determined

iii. The amount of RNA was calculated by the following formula:

Total RNA (µg) = OD_{260} x [40 µg/ ($1OD_{260}$ x 1 mL)] x dilution factor x total sample volume (mL)

Protocol V – cDNA synthesis

The following protocol encompasses the recommendations specified in the manual of the **High Capacity RNA-to-cDNA kit** used in this work.

Procedure:

Note: The following procedure must be dose on ice.

i. Use, at least, 1 µl of total RNA sample per 20 µl reaction.

ii. After the determination of the quantity of total RNA, in µl, corresponding to the referred 1 µg, refer to the following table to calculate the volume of components needed to prepare the required number of reactions.

Table 17: Volume required per reaction of each components. * Quantity Sufficient

Component	Component Volume/Reaction (µl)	
	+RT reaction	-RT reaction
2X RT Buffer	10	10
20X Enzyme Mix	1	-
RNA sample	Up to 9 µl	Up to 9 µl
Nuclease-free H_2O	Q.S. to 20 µl	Q.S. to 20 µl
Total per reaction	20 µl	20 µl

iii. Aliquot the RT mix into tubes and cap them.

iv. Briefly centrifuge the tubes to spin down the contents and to eliminate any air bubbles.

v. Incubate the reaction for 37°C for 60 minutes. Stop reaction by heating to 95°C for 5 minutes and hold at 4°C.

vi. The cDNA is ready for use in real time- PCR application or long term storage in freezer (-15°C to -25°C).